Development of a New Atmospheric Correction Algorithm for Turbid Inland Waters

A Dissertation Submitted to
the Graduate School of Life and Environmental Sciences,
the University of Tsukuba
in Partial Fulfillment of the Requirements
for the Degree of Doctor of Philosophy in Science
(Doctoral Program in Integrative Environmental Sciences)

Lalu Muhamad Jaelani

Table of Contents

List of Tables

List of Figures

List of Symbols

$\rho_{toa}(\lambda)$	=	reflectance that recorded by satellite sensor
$\rho_r(\lambda)$	=	reflectance from Rayleigh scattering
$\rho_a(\lambda) + \rho_{ra}(\lambda)$=		reflectance from the sum of aerosol scattering and the interaction between Rayleigh and aerosol scattering; aerosol multiple scattering
$\rho_A(\lambda)$	=	aerosol multiple scattering reflectance
$\rho_{as}(\lambda)$	=	aerosol single scattering reflectance
$\rho_w(\lambda)$	=	water leaving reflectance
$t(\lambda)$	=	diffuse transmittance of atmospheric column
$R_{rs}(\lambda)$	=	above-remote sensing reflectance
$L_u(\lambda)$	=	water leaving radiance
$E_d(\lambda)$	=	downward irradiance
$L_{sky}(\lambda)$	=	downward radiance of skylight
$\varepsilon(\lambda, 865)$	=	epsilons value at all wavelength with reference of 865 nm
α	=	ratio of aerosol multiple scattering reflectance (in MUMM algorithm)
ε	=	ratio of water leaving reflectance normalized by sun-sea atmospheric transmittance at two NIR reference bands (in MUMM algorithm)
$b_{bp}(\lambda)$	=	backscattering coefficient of particles
$b_{bw}(\lambda)$	=	backscattering coefficient of pure water
$b_b(\lambda)$	=	total backscattering coefficient
$a_t(\lambda)$	=	total absorption coefficient

$a_w(\lambda)$	=	absorption coefficient of pure water
$\mu(\lambda)$	=	inherent optical property
Y	=	spectral slope of particle backscattering
$a_{CDOM}(440)$	=	absorption coefficient of CDOM at 440 nm
$Chl-a$	=	chlorophyll-a concentration
N	=	sample size
R^2	=	determination coefficient

List of Abbreviations

AC	=	Atmospheric Correction
AOT	=	Aerosol Optical Thickness
BEAM	=	Basic ERS & ENVISAT AATSR and MERIS
BOA	=	Bottom of Atmosphere
C2WP	=	Case 2 Water Processor
CDOM	=	Colored Dissolved Organic Matter
CEBES	=	Center for Environmental Biology and Ecosystem Studies
COD	=	Chemical Oxygen Demand
CV	=	Coefficients of Variation
DOC	=	Dissolved Organic Carbon
ESA-EOLi	=	European Space Agency –Earth Observation Link
GW94	=	Gordon and Wang 1994 (atmospheric correction algorithm)
GWI	=	the standard Gordon and Wang algorithm with an iterative process and a bio-optical model
IOCCG	=	International Ocean Colour Coordinating Group
IOP	=	Inherent Optical Property
LUT	=	Look-up Table
MERIS	=	Medium Resolution Imaging Spectrometer
MNAE	=	Mean Normalized Absolute Error
MODIS	=	Moderate Resolution Imaging Spectroradiometer
NAP	=	Non-Algal Particles
N-GWI	=	New-GWI
NIES	=	National Institute of Environmental Sciences
NIR	=	Near-Infrared

NN = Neural Network

NOMAD = NASA bio-Optical Marine Algorithm Dataset

NPP = Net Primary Productivity

RE = Relative Error

RH = Relative Humidity

RMSE= Root Mean Square Error

RT = Radiative Transfer

SAMO-LUT=Semi-Analytical Model Optimizing and Look-up Tables

SCAPE-M= Self-Contained Atmospheric Parameters Estimation for MERIS data

SD = Standard Deviation

SeaBASS = the SeaWIFS Bio-optical Archive and Storage System

SeaDAS = SeaWIFS Data Analysis System

SNR = Signal to Noise Ratio

SWIR = Shortwave infrared

TOA = Top of Atmosphere

TSM = Total Suspended Mater

TSS = Total Suspended Solids

Acknowledgments

I would like to gratefully acknowledge my academic advisor, Prof. Bunkei Matsushita, for his help since my study in University of Tsukuba was initiated three years ago. His teaching, guidance and motivation are greatly useful for accomplishing my research and study in this university.

It is a pleasure to thank those who made this research possible: Prof. Takehiko Fukushima, Dr. Wei Yang and Dr. Youichi Oyama for their guidance and useful knowledge sharing during my research in University of Tsukuba.

I would like to show my gratitude to the ESA Earth Observation Missions Helpdesk Team for helping us ordering and providing MERIS L1B data; the SeaBASS database contributors and NASA Ocean Biology Processing Group for maintaining and distributing the SeaBASS database; the CEBES–NIES team for collecting and managing a long-term Lake Kasumigaura Database; Environmental Modeling and Creation (EMC) laboratory for providing *in situ* data of Lake Kasumigaura, Japan and Lake Dianchi, China; Dr. L. Guanter who developed SCAPE-M algorithm and performed atmospheric correction of SCAPE-M on the MERIS images used in this study; and Dr. Wei Yang who developed SAMO-LUT algorithm and performed Chl-a estimation based on the result of developed atmospheric correction algorithms proposed in this study.

I dedicate my thesis to my wife Hesti Wahyuni Afidiana and my parents in Lombok and Banyuwangi, also my little daughter Baiq Hasna Qurratu Aini for their encouragement, understanding and endless patience.

This study was funded by the Directorate General of Higher Education, Ministry of Education and Culture, Republic of Indonesia under Higher Education (DIKTI) Scholarship Program.

Chapter I General Introduction

Lakes play important roles as freshwater resources for drinking water, agriculture, industry, fishing, recreation, eco-tourism, power generation, and habitat for plants and animals. Lakes are also applicable as an important media for transportation in some regions (Giardino *et al.* 2001). However, the condition of some lakes are suffering from increasing of water pollution, excessive water withdrawals and accelerated eutrophication that become a significant environmental issue around the world (Ayres *et al.* 1996). Water quality monitoring is thus a critical requirement for water resource management in order to support the sustainable use of freshwater ecosystems. In light of the spatial and temporal heterogeneities of water bodies, remote sensing techniques can be an effective approach for the routine monitoring of water quality (Liu, Islam, and Gao 2003).

The optical signal received by remote sensing sensor, which is called top of atmosphere (TOA) reflectance, is generally a mixture of signals from surface reflectance (i.e., waters or land target), atmosphere and their interaction before reaching the sensor (Gordon and Wang 1994; Santer et al. 1999). Under favorable condition, only 10% of signal recorded by sensor originates from water, the remaining ones come from atmosphere in the visible spectrum (Huot et al. 2001). In order to retrieve pure signal from water, removing atmospheric effect that contaminate TOA reflectance could be done by atmospheric correction. Thus, estimating of water quality in inland waters using remote sensing highly depends on accurate atmospheric correction.

Most of atmospheric correction (AC) methods in water remote sensing originated from basic scheme proposed by Gordon and Wang (1994), as follows :

$$\rho_{toa}(\lambda) = \rho_r(\lambda) + [\rho_a(\lambda) + \rho_{ra}(\lambda)] + t(\lambda)\rho_w(\lambda) \quad (1.1)$$

Where, $\rho_{toa}(\lambda)$ is reflectance that recorded by satellite sensor, $\rho_r(\lambda)$ is reflectance from Rayleigh scattering that is the dominant contributor to $\rho_{toa}(\lambda)$, $[\rho_a(\lambda)+ \rho_{ra}(\lambda)]$ is aerosol and aerosol-Rayleigh scattering reflectance, $t(\lambda)$ is diffuse transmittance of atmosphere and $\rho_w(\lambda)$ is water leaving reflectance. In Equation 1.1, $\rho_r(\lambda)$ and $t(\lambda)$ can be accurately estimated from radiative transfer model *a priori*, while variables $[\rho_a (\lambda) +\rho_{ra} (\lambda)]$ remains as the largest uncertainty which needs to be solved in retrieval of $\rho_w(\lambda)$ (Selby et al. 1978; Gordon et al. 1988; Gordon and Wang 1994).

A widely used AC algorithms proposed by Gordon & Wang (1994) (denote as GW94 hereafter) exploit the fact of very low signal from water in near infra red (NIR) regions (Figure 1.1). GW94 assumes that signal can be neglected to make Equation 1.1 simpler. The water leaving reflectances ($\rho_w(\lambda)$) at two NIR reference bands (i.e. 779 nm and 865 nm in MERIS spectral band) are set to 0.0 sr^{-1}, thus the only unknown variable in Equation 1.1 is $[\rho_a (\lambda) +\rho_{ra}(\lambda)]$ that can be estimated for NIR band.

$$\rho_{toa}(779) - \rho_r(779) = \rho_a(779) + \rho_{ra}(779) = \rho_A(779) \quad (1.2a)$$

$$\rho_{toa}(865) - \rho_r(865) = \rho_a(865) + \rho_{ra}(865) = \rho_A(865) \quad (1.2b)$$

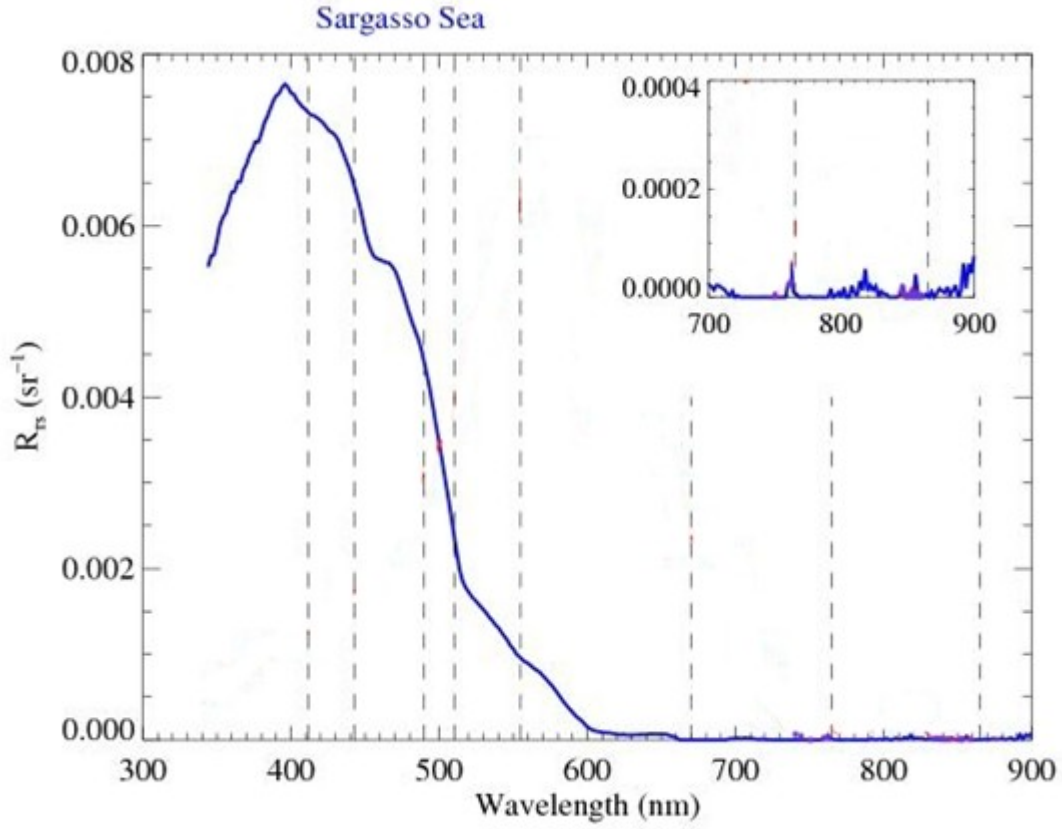

Figure 1.1. Above remote-sensing reflectance over clear water

(Taken from NASA Ocean Biology Processing Group)

In order to extrapolate aerosol scattering from longer to shorter wavelengths, I need to convert multiple scattering aerosols ($\rho_A(\lambda)$) to single scattering aerosol ($\rho_{as}(\lambda)$) as follow:

$$\rho_A(779);\ \rho_A(865) \underset{LUT}{\longrightarrow} \rho_{as}(779);\ \rho_{as}(865) \tag{1.3}$$

Then, estimate epsilon (ε) by rationing two aerosol reflectances in NIR, this ε is used for selecting the aerosol models:

$$\varepsilon(779,865) = \frac{\rho_{as}(779)}{\rho_{as}(865)} \tag{1.4}$$

$$\varepsilon(\lambda,865) = \exp[\frac{\ln(\varepsilon(779,865))}{(865-779)}(865-\lambda)] \tag{1.5}$$

$$\rho_{as}(\lambda) = \rho_{as}(865)\varepsilon(\lambda,865) \tag{1.6}$$

$$\rho_{as}(779);\ \rho_{as}(865) \underset{LUT}{\longrightarrow} \rho_A(779);\ \rho_A(865) \tag{1.7}$$

Extrapolating ε to shorter wavelength based on ε(779,865) as in Equation 1.5 to retrieve epsilon at shorter wavelength (ε(λ,865)). This epsilon is used to estimate single scattering aerosol at shorter wavelengths (Equation 1.6). Then, convert back the single scattering aerosol (ρ_a (λ)) into multiple scattering (ρ_A (λ)) using Equation 1.7. The final goal of this atmospheric correction scheme is to estimate $R_{rs}(\lambda)$ at shorter wavelengths by removing ρ_A (λ) and ρ_r (λ) from TOA signal as follow:

$$\rho_w(\lambda) = \frac{\rho_{toa}(\lambda)-\rho_r(\lambda)-\rho_A(\lambda)}{t(\lambda)} \tag{1.8}$$

$$R_{rs}(\lambda) = \frac{\rho_w(\lambda)}{\pi} \tag{1.9}$$

Note, this method is only applicable in clear water when the assumption of negligible $R_{rs}(\lambda_{NIR})$ is valid.

Due to high water turbidity in most inland waters, reflectances at NIR wavelengths are more significant than in clear water (Figure 1.2). Over this kind of water, the assumption of negligible water leaving reflectance at NIR wavelengths becomes invalid (Hu, Carder, and Muller-Karger 2000; Shi and Wang 2007; Shi and Wang 2009; Wang, Son, and Shi 2009). Several efforts have been made to solve this problem by estimating water leaving reflectance, directly estimating aerosol scattering, and estimating aerosol and water leaving reflectance simultaneously (Guanter et al. 2010; Guanter, Sanpedro, and Moreno 2007; Hu, Carder, and Muller-Karger 2000; Ruddick, Ovidio, and Rijkeboer 2000; Wang and Shi 2007; Bailey, Franz, and Werdell 2010; Stumpf et al. 2003; Wang, Shi, and Jiang 2012; Doerffer and Schiller 2007; Doerffer and Schiller 2008; Kuchinke, Gordon, and Franz 2009; Schroeder et al. 2007)

In order to understand the applicability of existing algorithm in inland turbid waters (e.g, Lake Kasumigaura), I evaluated four existing atmospheric correction algorithms (GWI, Stumpf et al. [2003]; Bailey, Franz, and Werdell [2010]; MUMM, Ruddick, Ovidio, and Rijkeboer [2000]; C2WP, Doerffer and Schiller [2007]; Doerffer and Schiller [2008] and SCAPE-M, Guanter et al. [2010]) using *in situ* water-leaving reflectance and concurrently acquired MERIS images collected from Lake Kasumigaura, Japan). The validity of the assumptions in the four atmospheric correction algorithms was also investigated to understand the advantages as well as limitations of each algorithm.

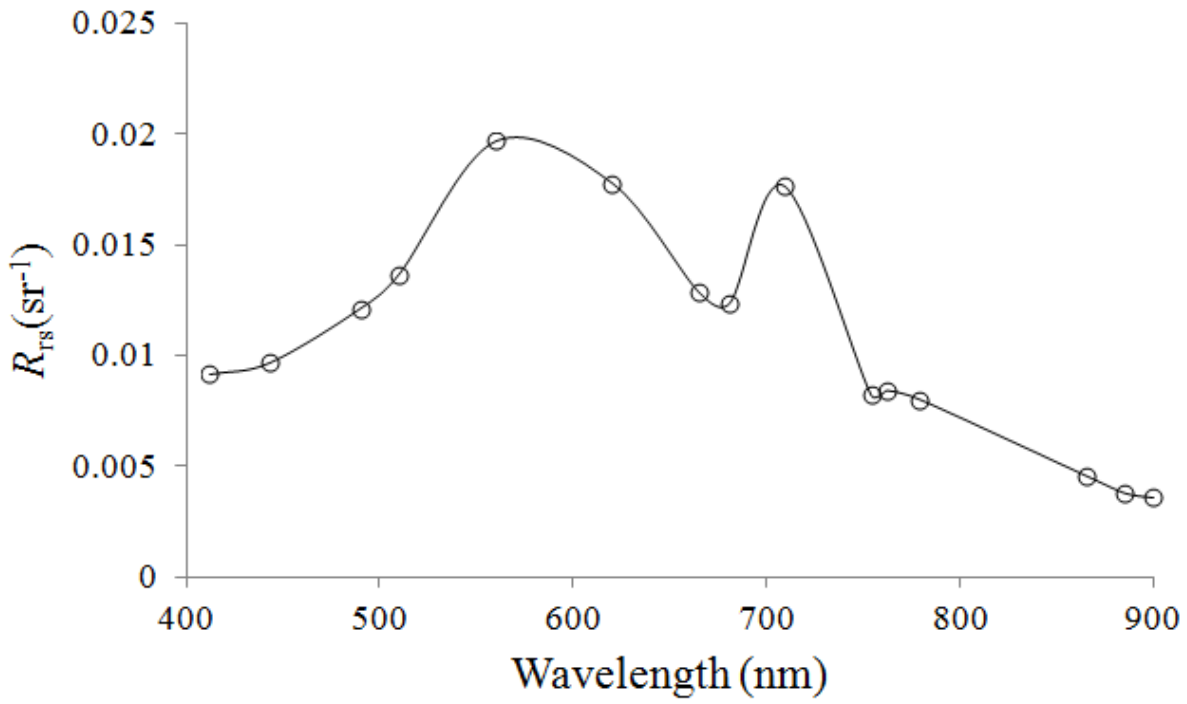

Figure 1.2. Average above remote-sensing reflectance in Lake Kasumigaura (acquired on February 18, 2006). Significant $R_{rs}(\lambda)$ at NIR wavelengths.

The results show that all evaluated atmospheric correction algorithms have limitations in Lake Kasumigaura, although the SCAPE-M and MUMM algorithms had acceptable accuracy for atmospheric correction in several cases. The performances of all four algorithms strongly depended on their assumptions (atmospheric state and/or turbidity of water body), and each algorithm failed when its assumptions became invalid.

These results indicate that further improvements are necessary to address the issue of atmospheric correction for turbid inland waters such as Lake Kasumigaura. By considering the features of atmosphere and water quality over/in Lake Kasumigaura, the NN technique with more suitable training data and the estimation of water-leaving reflectance at two NIR reference wavelengths using a more appropriate method may improve the existing atmospheric correction algorithms in the lake. Unfortunately, the lack of inherent optical properties (IOPs) data collected in Lake Kasumigaura make the improvement of atmospheric correction algorithms based on NN technique becomes difficult. Meanwhile, there is a possibility for improving the algorithms by using more appropriate method in water-leaving reflectance estimation (i.e., following GWI scheme).

I developed a new atmospheric corrected algorithms (namely N-GWI) which was based on the idea of GWI algorithm (the standard Gordon and Wang algorithm with an iterative process and a bio-optical model, Stumpf *et al.* [2003]; Bailey, Franz, and Werdell [2010]), in order to avoid spatial homogeneity assumption (e.g, atmospheric and water condition) that limited the performance of some existing atmospheric correction for turbid coastal and inland waters (e.g, MUMM and SCAPE-M). The developed algorithm proposed three improvements to overcome the limitation of existing algorithms by *(1)*

using a fixed aerosol model; *(2)* shifting the reference band from visible to NIR; *(3)* generating a semi-analytical model for the estimation of spectral slope of particle backscattering. To test the performance of developed algorithms, I validate the algorithm using 92 sites *in situ*-measured remote-sensing reflectance collected in two Asian turbid lakes: Lake Kasumigaura, Japan and Lake Dianchi, China as well as four American sea waters. Further investigation of N-GWI applicability in Lake Kasumigaura was carried out by using a long-term MERIS data and *in situ* chlorophyll-*a* concentration obtained in 2003 to 2012. Two-hundred-fifteen MERIS images covering Lake Kasumigaura were ordered and obtained from ESA-EOLi client. MERIS data were atmospherically corrected by my developed algorithm (N-GWI) and other existing algorithms (GWI, MUMM, C2WP and SCAPE-M) with an output of above remote-sensing reflectance. The outputs were then converted to estimated chlorophyll-*a* concentration through a semi-analytical model optimizing and look-up tables (SAMO-LUT) model (Yang et al. 2011). Two set of data were used to validate the MERIS-derived chlorophyll-*a* concentration, they were Lake Kasumigaura *in situ* dataset which was collected by the team of University of Tsukuba and Lake Kasumigaura database which was collected and managed by CEBES-NIES, Japan.

Chapter II Evaluation of four existing atmospheric correction algorithms in turbid waters

2.1 Introduction

Lakes play important roles as freshwater resources for drinking water, agriculture, industry, fishing, recreation, and tourism (Giardino et al. 2001). However, accelerated eutrophication in lakes is becoming a significant environmental issue around the world (Ayres et al. 1996). Water quality monitoring is thus a critical requirement for water resource management in order to support the sustainable development of freshwater ecosystems. In light of the spatial and temporal heterogeneities of water bodies, remote sensing techniques can be an effective approach for the routine monitoring of water quality (Liu, Islam, and Gao 2003).

The first key step for water colour remote sensing is atmospheric correction. A widely used atmospheric correction algorithm with sufficient accuracy was developed by Gordon and Wang (1994) for clear waters (e.g. open oceans). However, this algorithm has often been reported to fail in coastal and inland waters because its assumption of negligible water-leaving reflectance at near-infrared (NIR) wavelengths becomes invalid in these turbid waters (Hu, Carder, and Muller-Karger 2000; Shi and Wang 2007; Shi and Wang 2009; Wang, Son, and Shi 2009). Several efforts have been made to solve this

problem. Currently, there are five types of approach for atmospheric correction over turbid waters (inland or coastal waters, Table 2.1).

The first type of approach is based on the estimation of water-leaving reflectance (or radiance) at two NIR reference wavelengths rather than neglecting the water-leaving reflectance (or radiance) at these two wavelengths (Hu, Carder, and Muller-Karger 2000; Stumpf et al. 2003; Bailey, Franz, and Werdell 2010; Wang, Shi, and Jiang 2012). For example, Stumpf et al. (2003) and Bailey, Franz, and Werdell (2010) suggested the use of a bio-optical model to estimate water-leaving reflectance at two NIR reference wavelengths through an iterative procedure. This approach is now widely used for atmospheric correction over turbid waters.

The second type of approach is based on the direct prediction of atmospheric parameters over water pixels (Ruddick, Ovidio, and Rijkeboer 2000; Guanter et al. 2010). For example, Ruddick, Ovidio, and Rijkeboer (2000) proposed the use of two new assumptions rather than the assumption in Gordon and Wang (1994) to estimate multiple-scattering aerosols and aerosol- Rayleigh reflectances at two reference NIR wavelengths. Guanter, Sanpedro, and Moreno (2007) and Guanter et al. (2010) proposed the use of atmospheric parameters derived over neighbouring land pixels to predict atmospheric parameters over close-to-land water pixels through a spatial extension method; this can avoid assumptions on water composition and its spectral response.

The third type of approach is based on neural network (NN) techniques (Doerffer and Schiller 2007, 2008; Schroeder, Schaale, and Fischer 2007; Schroeder et al. 2007). For example, Doerffer and Schiller (2008) designed an algorithm to directly estimate

remote-sensing reflectance at the bottom-of-atmosphere (BOA) from that at the top-of atmosphere (TOA) based on separate NNs. The fourth type of approach still keeps the assumption of zero water-leaving reflectance but extends the reference wavelengths from NIR to shortwave infrared (SWIR) for turbid water pixels (Wang and Shi 2007). The fifth type of approach is based on spectral optimization (Kuchinke, Gordon, and Franz 2009; Kuchinke et al. 2009). In this approach, absorbing aerosol models and a bio-optical reflectance model were combined to provide the TOA reflectance; the modelled TOA reflectance was then fitted to the observed TOA reflectance through non-linear optimization to determine the parameters of both models. These parameters were then gradually improved through an iterative procedure to accomplish atmospheric correction.

Medium resolution imaging spectrometer (MERIS) has 15 narrow spectral bands in the visible and NIR spectral ranges (most bandwidths are around 10 nm) and a medium spatial scale (about 300 m for full spatial resolution data). Regarding spectral configuration and spatial resolution, MERIS offers the best compromise between spatial, spectral, and temporal resolution for many inland water studies (although since April 2012 MERIS has no longer been providing data, the next-generation sensors will be launched in 2014; Aschbacher and Milagro-Pérez [2012]). In addition, the availability of an atmospheric correction algorithm for public use is also expected.

Table 2.1. Summary of existing atmospheric correction algorithms for turbid waters.

Type	Approach descriptions	References for example
1	Estimation of water-leaving reflectance at two NIR reference wavelengths; subtraction of the estimated water-leaving reflectance from TOA remote-sensing reflectance at two NIR reference wavelengths; application to Gordon and Wang's (1994) scheme for atmospheric correction.	Hu, Carder, and Muller-karger (2000); Stumpf et al. (2003); Bailey, Franz, and Werdell (2010) and Wang, Shi, and Jiang (2012)
2	Direct prediction of atmospheric parameters over water pixels; application to Gordon and Wang's (1994) scheme or other methods for atmospheric correction.	Ruddick, Ovidio, and Rijkeboer (2000); Guanter et al. (2010)
3	Neural network (NN) techniques	Schroeder, Schaale, and Fischer (2007); Schroeder et al. (2007); Doerffer and Schiller (2007, 2008)
4	Keep the assumption of zero water-leaving reflectance but extend the reference wavelengths from NIR to SWIR for turbid water pixels; application to Gordon and Wang's (1994) scheme for atmospheric correction.	Wang and Shi (2007)
5	Spectral optimization techniques	Kuchinke et al. (2009); Kuchinke, Gordon, and Franz (2009)

Note: NIR: near infrared; TOA: top-of-atmosphere; SWIR: shortwave infrared.

Therefore, I used two criteria for selecting the algorithms: (*1*) applicability to MERIS data; and (*2*) current or expected future implementation into the widely used processing software packages SeaDAS (SeaWiFS Data Analysis System; http://seadas.gsfc.nasa.gov) and BEAM (Basic ERS & ENVISAT AATSR and MERIS; http://www.brockmann-consult.de/cms/web/beam). Based on these two criteria, I selected four existing atmospheric correction algorithms for an evaluation of their performance in this study. I selected one atmospheric correction algorithm from the first type of approach and another from the second type. Both are currently available in SeaDAS software for processing level-1b data from satellite sensors such as SeaWiFS (Sea-viewing Wide Field of-view Sensor), MODIS (Moderate Resolution Imaging Spectroradiometer), and MERIS.

Another atmospheric correction algorithm was chosen from the third type of approach, which is currently available in the BEAM toolbox. I selected the fourth atmospheric correction algorithm from the second type of approach, which will be available in the BEAM toolbox in the near future. Although the fourth and fifth types of approach are available in SeaDAS software, they can only be applied to MODIS and SeaWiFS data (not available for MERIS), respectively, and thus they were not used in this study. More details about the four selected atmospheric correction algorithms can be found in Section 2.2.1.

Although several of the above-mentioned algorithms have been evaluated using a simulated testing dataset (e.g. IOCCG, 2010) or *in situ* measurements from coastal waters (e.g. Jamet et al., 2011) or European lakes (e.g. Guanter et al., 2010), few studies have been designed to evaluate for turbid Asian lakes to show the applicability of these

algorithms (Wang, Shi, and Tang 2011; Duan et al. 2012). The objectives of the present study were thus: (*1*) to evaluate the four selected atmospheric correction algorithms by comparing the atmospherically corrected remote-sensing reflectance from three MERIS images using the algorithms with concurrent *in situ* remote-sensing reflectance obtained from three data collection campaigns in Lake Kasumigaura, Japan; and (*2*) to investigate the validity of the assumptions in the four atmospheric correction algorithms to understand the advantages as well as the limitations of each algorithm.

2.2 Methods

2.2.1 Four Atmospheric Correction Algorithms

The first selected atmospheric algorithm was developed by Stumpf et al. (2003) and updated by Bailey, Franz, and Werdell (2010). This algorithm is based on the original atmospheric correction scheme proposed by Gordon and Wang (1994), denoted as GW94 hereafter, which is based on the assumption of negligible water-leaving radiance at an NIR band, but the algorithm can avoid the over-correction of the atmospheric signal for waters where the assumption in the GW94 is not valid (Bailey, Franz, and Werdell 2010).

In the algorithm, water-leaving reflectance at two NIR reference bands was first estimated by a bio-optical model. Then the two estimated water-leaving reflectance values were removed from corresponding remote-sensing reflectance at the TOA, and inputted into the GW94 algorithm. The iterative procedure makes the estimated water-leaving reflectance by the bio-optical model gradually close to the actual water-leaving reflectance (the algorithm allows up to 10 iterations, but it will converge after 3–4 in

most cases; Bailey, Franz, and Werdell [2010]). Therefore, this algorithm is hereafter called the GWI algorithm (standard Gordon and Wang's algorithm with an iterative process and a bio-optical model). The new assumption in the GWI algorithm is that the bio-optical model used can provide accurate estimates of water-leaving reflectance at two NIR reference wavelengths.

The second selected atmospheric correction algorithm is MUMM (Management Unit of the North Sea Mathematical Models), which was proposed by Ruddick, Ovidio, and Rijkeboer (2000). This algorithm is also based on the original atmospheric correction scheme in GW94. The MUMM algorithm uses two different assumptions as a replacement for the original assumption in GW94 (i.e. zero water-leaving reflectance at NIR bands), according to the stable spectral shapes of aerosol and water-leaving reflectances at two NIR reference bands.

Ruddick et al. (2006) assumed that the ratios of (*1*) multiple-scattering aerosols and aerosol-Rayleigh reflectances and (*2*) water-leaving reflectance normalized by the sun–sea atmospheric transmittance at two NIR reference bands are spatially homogeneous over the sub-scene of interest (the former was named ε and the latter, α; Ruddick, Ovidio, and Rijkeboer [2000]). These two new assumptions allow the estimates of multiple-scattering aerosols and aerosol-Rayleigh reflectances at two NIR reference bands even for waters where water-leaving reflectance cannot be ignored. The estimated multiple-scattering aerosols and aerosol-Rayleigh reflectance at two NIR reference bands are then inputted into the original GW94 algorithm for atmospheric correction in turbid waters. Thus, the performance of the MUMM algorithm depends not only on water

composition and its spectral response (this is the definition of α), but also on the atmosphere status over the target waters (the definition of ε).

The third atmospheric correction algorithm selected for comparison is the SCAPE-M (Self-Contained Atmospheric Parameters Estimation for MERIS Data) algorithm (Guanter, Sanpedro, and Moreno 2007; Guanter et al. 2010). Unlike the traditional atmospheric correction algorithms for waters, which are 'water-based' methods, the SCAPE-M is a 'land-based' method for the retrieval of aerosol and water-leaving reflectances. Therefore, the SCAPE-M algorithm requires neither a priori assumptions about water composition and its spectral response nor the use of bio-optical models. It uses atmospheric parameters derived over neighbouring land pixels to predict atmospheric parameters over close-to-land water pixels through a spatial extension method.

In the SCAPE-M algorithm, aerosol retrieval is performed at the macro-pixel scale. First, a MERIS Level-1b image is divided into a series of macro-pixels (30 km × 30 km). For each macro-pixel, a maximum AOT550 (aerosol optical thickness at 550 nm) is estimated from dark pixels in the area to avoid negative reflectance after atmospheric correction. This value is then refined by the exploitation of those macro-pixels with sufficient green vegetation and bare soil pixels (generally, five land pixels that show mixed vegetation and bare soil with as much spectral contrast as possible are needed). By assuming that surface reflectance can be provided by a linear combination of two endmembers (i.e. pure vegetation and bare soil), the abundance of each endmember and the AOT550 are retrieved concurrently for each macro-pixel.

Finally, the obtained AOT550 is applied to water pixels for atmospheric correction by assuming that the atmospheric state is laterally homogeneous within each macro-pixel. Because of the above assumptions, the SCAPE-M algorithm can only be used for small and medium-sized water bodies. In addition, only a rural aerosol model is used in the SCAPE-M algorithm because less information is available for the reliable retrieval of aerosol type over land from MERIS (Santer, Vidot, and Aznay 2005; Ramon and Santer 2005). The SCAPE-M algorithm will be available in the BEAM toolbox in the near future (L. Guanter, personal communication).

The last selected atmospheric correction algorithm is the Case-2 Water Processor (C2WP), which is available in the BEAM toolbox (Doerffer and Schiller 2008). The C2WP algorithm contains three different processors: the *Case-2 Regional* water processor, the *Eutrophic Lakes* processor, and the *Boreal Lakes* processor. The three processors share the same architecture, but the bio-optical models were optimized for different concentrations of chlorophyll-*a*, total suspended mater (TSM), and yellow substance. The NNs for atmospheric correction were trained based on the radiative transfer (RT)-simulated water-leaving reflectance at both the BOA and the TOA by taking into account various atmospheric and oceanic conditions.

To generate water-leaving reflectance from RT simulations at the BOA, the inherent optical properties (IOPs) were taken from European coastal waters, Spanish lakes, and Finnish lakes. By considering the water quality parameters in Lake Kasumigaura, Japan, the *Eutrophic Lakes* processor (version 1.5.7) was selected for atmospheric correction in the present study. The concentration ranges covered in the

simulations for the *Eutrophic Lakes* processor were 1–120 mg m^{-3} for chlorophyll-*a*, 0.433–51.9 g m^{-3} for TSM, and 0.1–3.0 m^{-1} (at 443 nm) for yellow substance. The C2WP algorithm was designed for European waters, and it is worthwhile to evaluate the performance of this algorithm in Asian waters.

2.2.2 Data

To evaluate the above-mentioned atmospheric correction algorithms in turbid inland waters, I collected concurrent *in situ* and MERIS data from Lake Kasumigaura, Japan. The lake is located in the eastern part of Japan's Kanto plain and has a surface area of 171 km^2 (western part only), an average depth of 4.0 m, and a maximum depth of 7.3 m. It is the second largest lake in Japan (Lake Biwa is the largest) and it is a eutrophic-turbid lake due to high loading of nutrients and resuspension of bottom sediments by wind (Fukushima et al. 1996; Oyama et al. 2009). During the previous two or three decades, Lake Kasumigaura's average TSM concentration has increased from 14.1 to 26.4 g m^{-3} (mainly due to the resuspension of bottom sediments by wind); chlorophyll-*a* concentration decreased from 87 to 61 mg m^{-3} (owing to watershed management by the local government); and Secchi disk depth has decreased from 70 to 52 cm (CEBES 2011).

Three full-resolution MERIS images (level-1b) covering Lake Kasumigaura were acquired on 18 February 2006 (denoted as K06 hereafter), 7 August 2008 (denoted as K08 hereafter), and 18 May 2010 (denoted as K10 hereafter). The orbital information for the three MERIS images is summarized in Table 2.2. These satellite images were processed using the SeaDAS (version 6.4) and BEAM (version 4.10.03) software

packages to obtain atmospherically corrected water-leaving reflectance images by the GWI, MUMM, and C2WP algorithms. Since the SCAPE-M is not yet available for public use, I asked the algorithm's author (Dr Luis Guanter) to process the MERIS data using the SCAPE-M algorithm.

Three data collection campaigns were undertaken in 2006 (February 18, 10 sites), 2008 (August 7, 14 sites), and 2010 (May 18, 26 sites) in Lake Kasumigaura, and the campaigns were timed to coincide with acquisition of MERIS images. The spatial distribution of the sampling sites is shown in Figure 2.1. All reflectance measurements and water sample collections were performed between 10:00 and 14:00 h local time over optically deep waters. The water-leaving radiance ($L_u(\lambda)$), downward irradiance ($E_d(\lambda)$), and downward radiance of skylight ($L_{sky}(\lambda)$) were measured at each site using a FieldSpec HandHeld (or Pro VNIR) spectroradiometer (Analytical Spectral Devices, Boulder, CO, USA) in the range of 325–1075 nm at 1 nm intervals. The above-water remote-sensing reflectance ($R_{rs}(\lambda)$) was approximated using the following equation (Mobley 1999):

$$R_{\mathrm{rs}}(\lambda) = \left(\frac{L_{\mathrm{u}}(\lambda)}{E_{\mathrm{d}}(\lambda)} - \frac{rL_{\mathrm{sky}}(\lambda)}{E_d(\lambda)}\right) \times Cal\,(\lambda) \qquad (2.1)$$

where *Cal(λ)* is the spectral reflectance of the grey reference panel that has been accurately calibrated, and *r* represents a weighted surface reflectance for the correction of surface-reflected skylight and is determined as a function of wind speed (Mobley 1999).

Table 2.2. Orbital information for three MERIS images used in this study (UTC: Coordinated Universal Time).

MERIS Data	K06	K08	K10
Orbit	20755	33652	42942
Acquisition date	18 February 2006	7 August 2008	18 May 2010
Starting time (UTC)	1:13:47	0:56:48	0:59:28
Ending time (UTC)	1:15:26	0:58:26	1:01:06
Sun Zenith (°)	53.04696	31.16381	27.08951
Sun Azimuth (°)	149.56363	122.01693	121.66913
View Zenith (°)	19.64261	14.39096	10.24573
View Azimuth (°)	285.36258	102.55517	102.91293

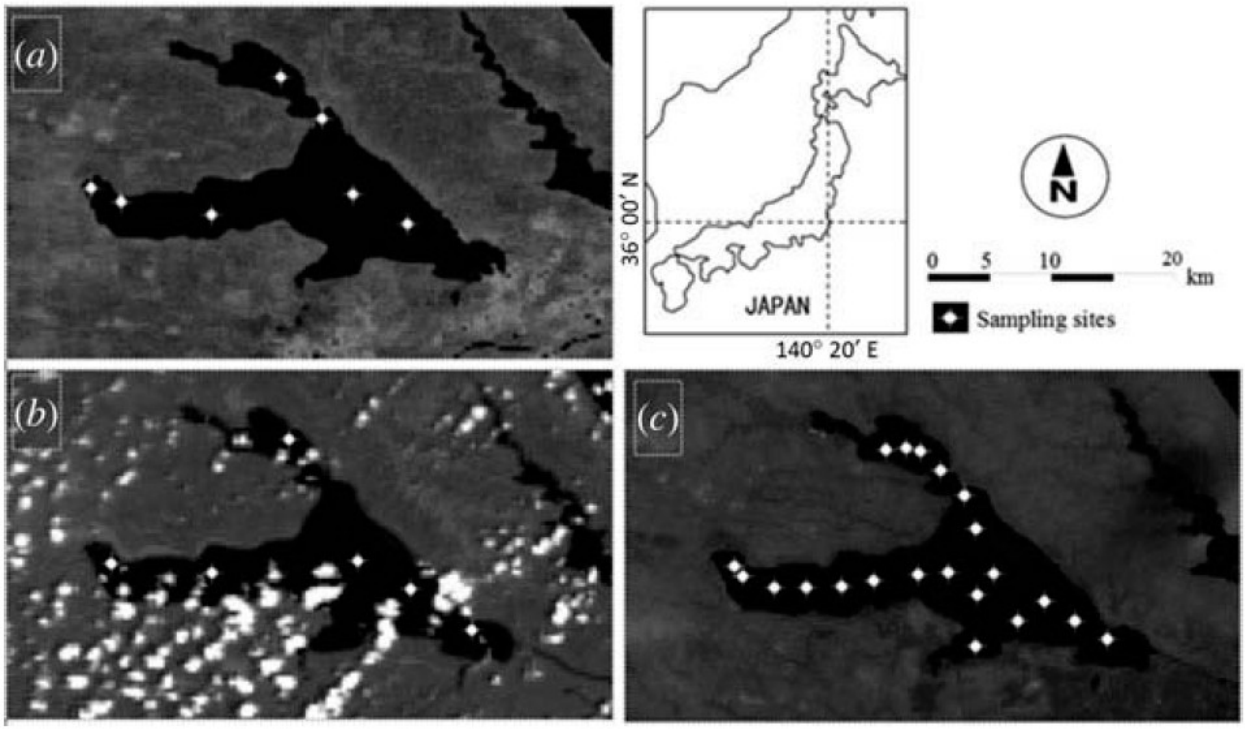

Figure 2.1. MERIS images and sampling sites at Lake Kasumigaura, Japan on (*a*) 18 February 2006, (*b*) 7 August 2008, and (*c*) 18 May 2010

Water samples were kept in ice boxes and taken to the laboratory within approx. 0.5 h after the whole data collections. Chlorophyll-*a* was extracted using methanol (100%) at 4°C under dark conditions for 24 h. The optical density of the extracted chlorophyll-*a* was measured at four wavelengths (750, 663, 645 and 630 nm), and the concentration was calculated according to SCOR-UNESCO equations (SCOR-UNESCO 1966). The total suspended solids (TSS) were determined gravimetrically. Samples were filtered through a filter pre-combusted at 500°C for 4 h to remove dissolved organic matter in suspension, and the filter was then dried at 105°C for 4 h and weighed to obtain the TSS. The absorption of coloured dissolved organic matter (CDOM) was measured using a spectrophotometer (UV–1700, Shimadzu, Kyoto, Japan) with filtered water. Descriptive statistics of the optical water quality parameters are summarized in Table 2.3, in which it can be seen that the turbidity of Lake Kasumigaura is very high.

To evaluate the performance of the four atmospheric correction algorithms, I extracted the average water-leaving reflectance of the pixels nearest the sampling locations along with the eight surrounding pixels (3 × 3 window) from the atmospherically corrected MERIS images, and I compared reflectance with the corresponding *in situ* measurements. The use of the 3 × 3 window rather than a single pixel can reduce the potential error in the geometric correction and dynamics of water bodies, as well as potential error in spatial variability (Han and Jordan 2005). Pixels contaminated by clouds and corresponding sampling sites located less than one pixel away from the banks were then excluded. Accordingly, 7, 6, and 21 sites remained for comparison in February 2006, August 2008, and May 2010, respectively.

Table 2.3. Descriptive statistics of optical water quality parameters measured in Lake Kasumigaura, Japan.

	Min.	Max.	Median	Average	SD	CV (%)	*N*
18 February 2006							
Chl-a (mg m^{-3})	69.65	95.02	84.54	83.99	9.69	11.54	7
TSS (g m^{-3})	22.00	46.10	32.80	33.71	8.11	24.05	7
$^{a}_{CDOM}$ (440) (m^{-1})	no data	no data	no data	no data	no data	no data	0
7 August 2008							
Chl-a (mg m^{-3})	44.40	76.90	62.90	62.18	11.92	19.17	6
TSS (g m^{-3})	11.70	21.10	16.40	16.73	3.18	19.02	6
$^{a}_{CDOM}$ (440) (m^{-1})	1.15	1.36	1.15	1.20	0.09	7.23	6
18 May 2010							
Chl-a (mg m^{-3})	36.60	83.40	44.80	53.70	17.61	32.80	21
TSS (g m^{-3})	18.00	27.73	21.17	22.13	3.59	16.22	21
$^{a}_{CDOM}$ (440) (m^{-1})	0.51	0.94	0.62	0.71	0.16	22.23	21

Notes: Chl-a, chlorophyll-a concentration; TSS, total suspended solids;
$^{a}_{CDOM}$ (440), absorption coefficient of CDOM at 440 nm;
SD, standard deviation; CV, coefficient of variation (= SD/average of parameter);
N, number of samples.

2.2.3 Accuracies Assessment

Two indices, root mean square error (RMSE) and relative error (RE), were used to assess the accuracy of atmospheric correction. These indices were defined as follows:

$$RMSE = \sqrt{\frac{\sum_{i=1}^{N}\left(x_{\mathrm{esti,i}} - x_{\mathrm{meas,i}}\right)^2}{N}} \tag{2.2}$$

$$RE = \frac{1}{N}\sum_{i=1}^{N}\left(\sqrt{\left(\frac{x_{\mathrm{esti,i}} - x_{\mathrm{meas},i}}{x_{\mathrm{meas}}}\right)^2}\right) 100\% \tag{2.3}$$

where $x_{\mathrm{meas,i}}$ and $x_{\mathrm{esti,i}}$ are the measured and estimated values, respectively, and N is the sample size. The RMSE gives the absolute scattering of the retrieved water-leaving reflectance, and the RE represents the uncertainty associated with satellite-derived distribution. The determination coefficient (R^2) between *in situ* measured $R_{\mathrm{rs}}(\lambda)$ and estimated $R_{\mathrm{rs}}(\lambda)$ from atmospherically corrected MERIS data was also calculated.

2.3 Results

2.3.1 Performance of the four atmospheric correction algorithms for MERIS single bands

Figure 2.2 provides the overall comparisons between the measured (*x*-axis) and retrieved (*y*-axis) water-leaving remote-sensing reflectance values obtained by the four atmospheric correction algorithms at MERIS bands 1–10 for the three dates. Generally, the SCAPE-M algorithm overestimated the values of water-leaving reflectance at all MERIS bands (except for several bands in 2006), whereas the other three algorithms gave

underestimation of water-leaving reflectance (except for bands 1, 2, and 10 for MUMM in 2008).

From the data collected in 2006 (K06), the results show that the SCAPE-M algorithm with an RMSE of 0.002, RE of 17.1% and determination coefficient (R^2) of 0.746 achieved the best performance, followed by the MUMM algorithm (RMSE=0.004, RE=18.1%, R^2=0.646), C2WP (RMSE=0.005, RE=33.9%, R^2=0.590), and GWI (RMSE=0.010, RE=70.5%, R^2=0.444). For the 2008 results (K08), the MUMM algorithm showed the best performance (RMSE=0.002, RE=16.9%, R^2=0.778), followed by SCAPE-M (RMSE=0.002, RE=29.9%, R^2=0.722), C2WP (RMSE=0.004, RE=50.5%, R^2=0.647), and GWI (RMSE=0.006, RE=69.9%, R^2=0.541).

Although the GWI algorithm gave the poorest performance for both the 2006 and 2008 data, it gave the best performance for the 2010 data (K10; RMSE=0.005, RE= 42.0%, R^2=0.599). The next-best performances were by MUMM (RMSE=0.006, RE=49.6%, R^2=0.487) and C2WP (RMSE=0.007, RE=62.3%, R^2=0.478). The SCAPE-M algorithm showed the poorest performance for the 2010 data (RMSE=0.008, RE=82.7%, R^2=0.221). It is notable that all four atmospheric correction algorithms showed poorer performance for the 2010 data compared with those of 2006 and 2008.

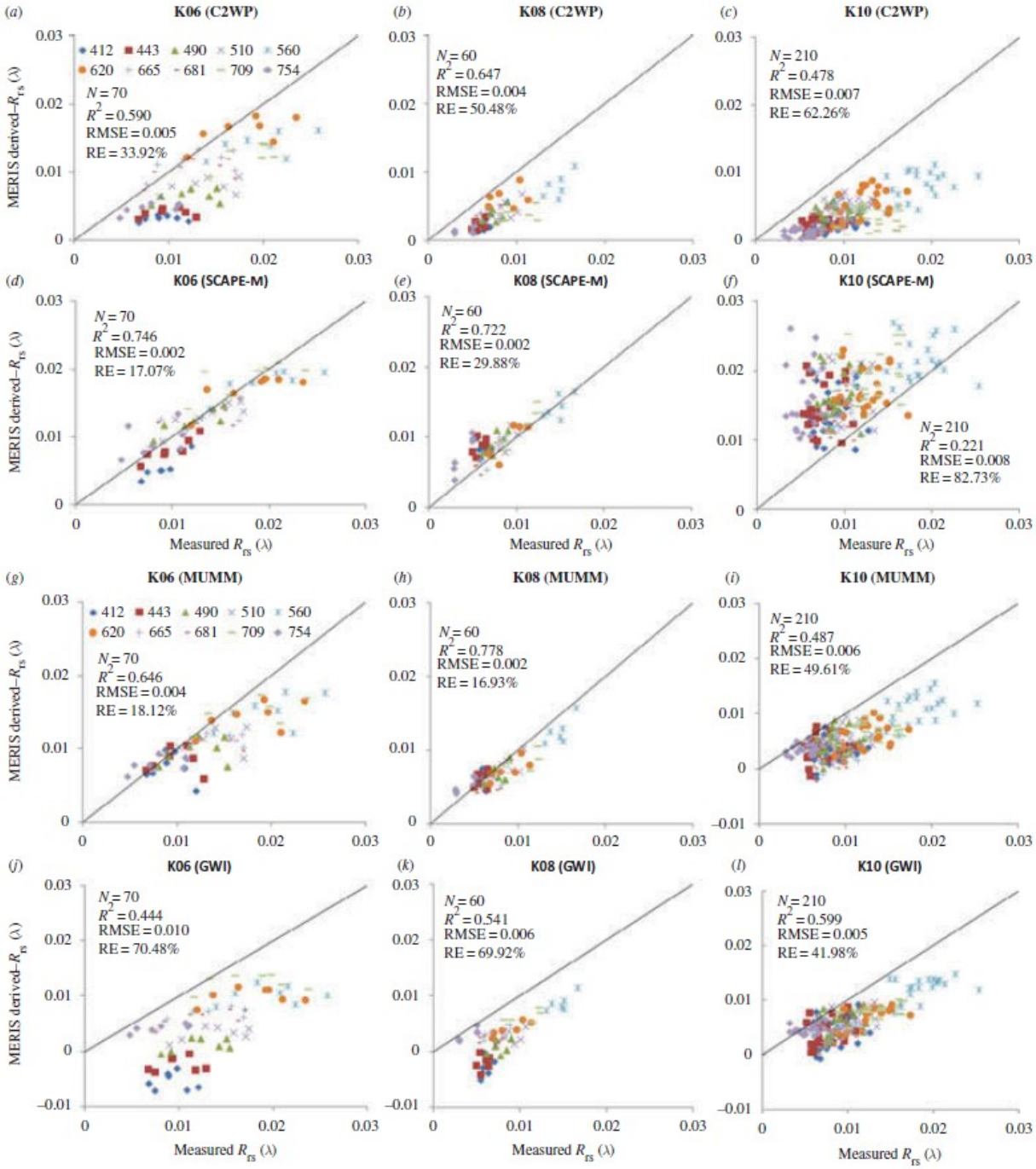

Figure 2.2. Comparisons between *in situ*-measured and MERIS-derived water-leaving remote-sensing reflectance by the four atmospheric correction algorithms (C2WP, SCAPE-M, MUMM, and GWI) in Lake Kasumigaura, Japan, for MERIS bands 1–10. The centre wavelength at each band is shown in the legend. The black line represents the 1:1 line. Left column, 18 February 2006; middle, 7 August 2008; right, 18 May 2010.

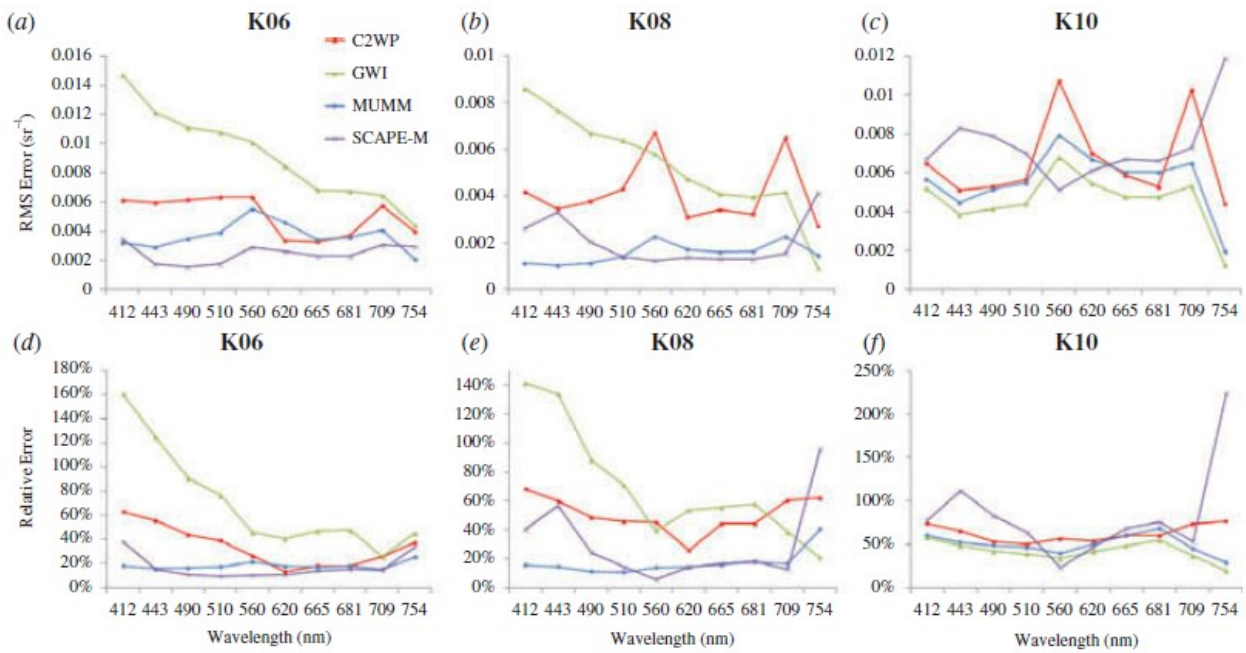

Figure 2.3. Variation in root mean square error (RMSE, top) and relative error (RE, bottom) as a function of wavelength.

The C2WP algorithm showed relatively large retrieval errors for all three dates. In addition, the GWI algorithm showed variations in RMSE and RE as a function of wavelength, while the other three algorithms showed relatively constant RMSE and RE values for all bands, especially for the MUMM algorithm.

2.3.2 Performances of four atmospheric correction algorithms for NIR-Red indices

One of the most important applications of water colour remote sensing is to estimate chlorophyll-*a* concentration, which is a key parameter for assessing water quality, the primary production of phytoplankton, and more. To develop chlorophyll-*a* estimation algorithms, band ratios of water-leaving reflectance are often used (Gitelson 1992; Gitelson et al. 2008; O'Reilly et al. 1998). Here, I selected two band ratio indices for comparison: a two-band index ($R_{rs}(709)/R_{rs}(665)$) and a three-band index ($R_{rs}(753)/R_{rs}(665) - R_{rs}(753)/R_{rs}(709)$), which are widely used in turbid inland waters (Gitelson et al. 2008; Moses et al. 2009). The results are shown in Figures 2.4 and 2.5. Generally, the two band index provided better performance than the three-band index for all four atmospheric correction algorithms.

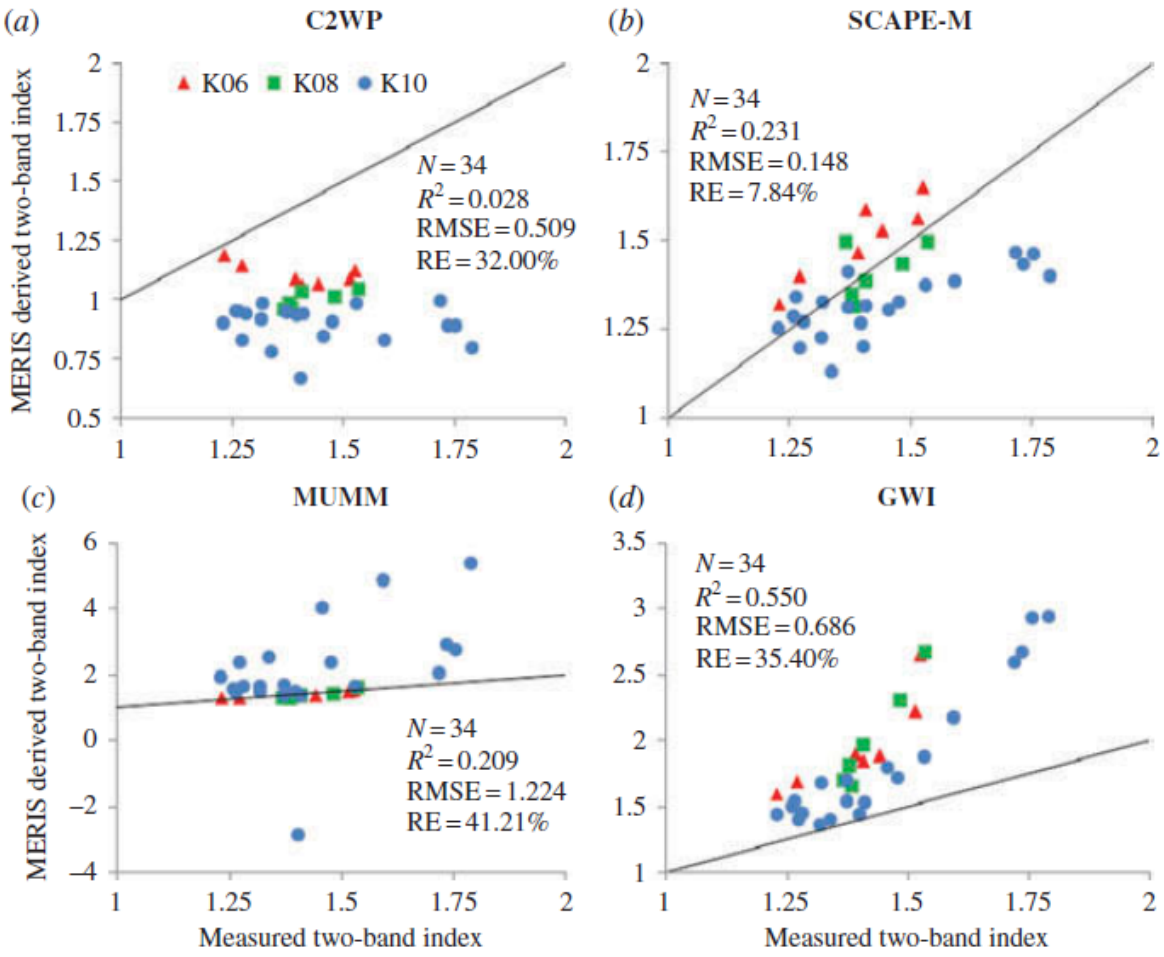

Figure 2.4. Scatterplots of MERIS-derived vs *in situ*-measured two-band index ($R_{rs}(709)/R_{rs}(665)$) by the algorithms: (*a*) C2WP, (*b*) SCAPE-M, (*c*) MUMM, and (*d*) GWI. The black line represents the 1:1 line.

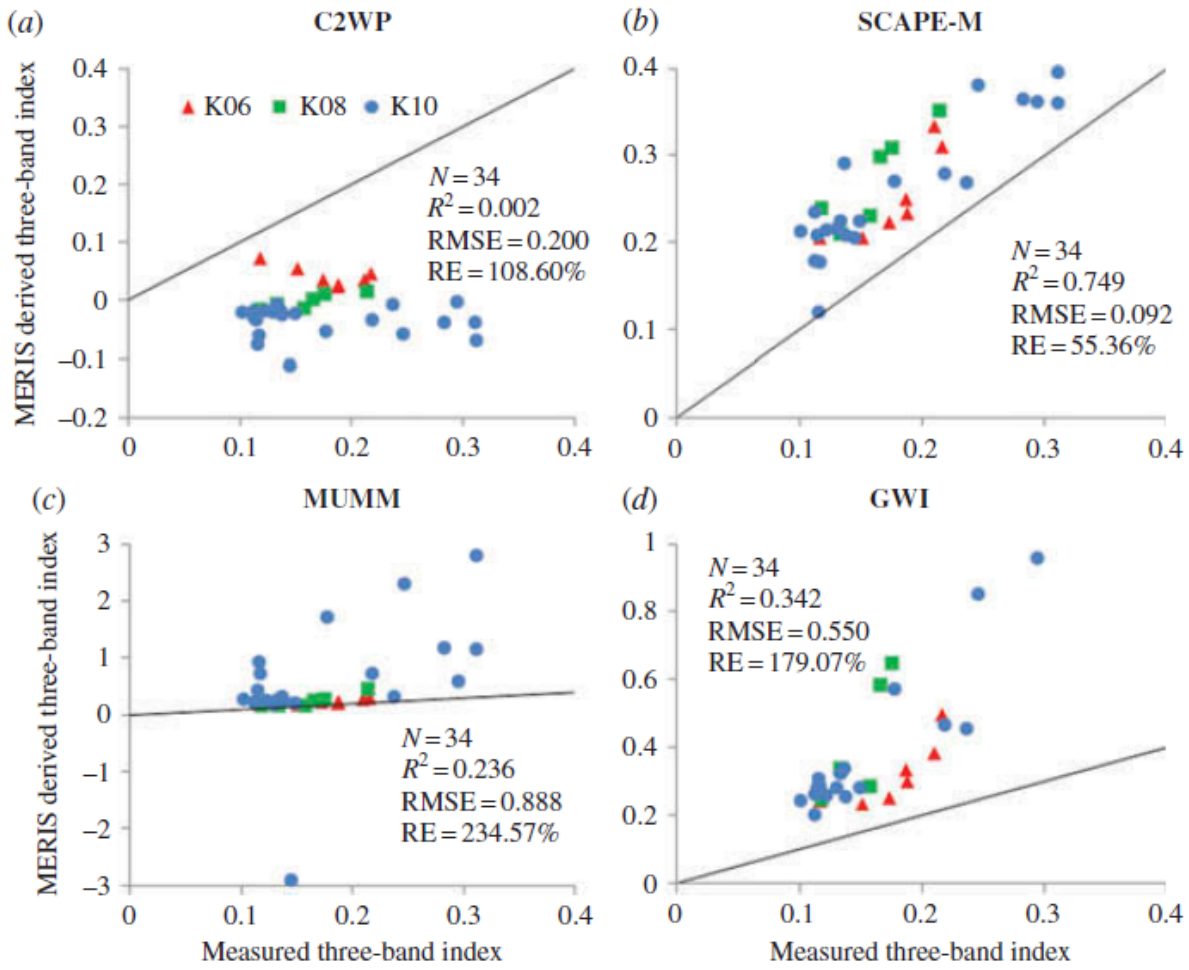

Figure 2.5. Scatterplots of the MERIS-derived vs *in situ*-measured three-band index ($R_{rs}(753)/R_{rs}(665) - R_{rs}(753)/R_{rs}(709)$) by the algorithms: (*a*) C2WP, (*b*) SCAPE-M, (*c*) MUMM, and (*d*) GWI. The black line represents the 1:1 line.

The SCAPE-M algorithm showed good performance (RE=7.84%) for the two-band index for all dates, although it gave a poor performance at each MERIS band for the 2010 data (Figures 2.2*(d)–(f)* and 2.3). The SCAPE-M algorithm produced overestimation for the three-band index for all dates. The MUMM algorithm showed acceptable performance for the 2006 and 2008 data for both band ratio indices, but poor performance for the 2010 data. The band ratio indices obtained from the GWI and C2WP algorithms showed relatively large errors.

2.4 Discussion

2.4.1 Performance of the C2WP algorithm

Compared with the other three algorithms, the C2WP algorithm showed lower atmospheric correction accuracies for all three dates, and even for all sampling sites with concentrations of three water constituents within the ranges of the training data (Figures 2.2*(a-c*) and 2.3). In addition, by comparing the averaged water-leaving reflectance spectra corrected by C2WP with those corrected by the other three atmospheric correction algorithms as well as *in situ* measurements for each date, I found that the C2WP algorithm changed the spectral shapes after atmospheric correction had been carried out, especially around the reflectance peak at the wavelength of 709 nm (Figure 2.6; the reflectance peak was smoothed by C2WP). The poor performance of the two-band and three-band indices also indicated that the C2WP algorithm could not reproduce actual spectral shapes well at the wavelength range 665–754 nm (Figures 2.4(*a*) and 2.5(*a*)).

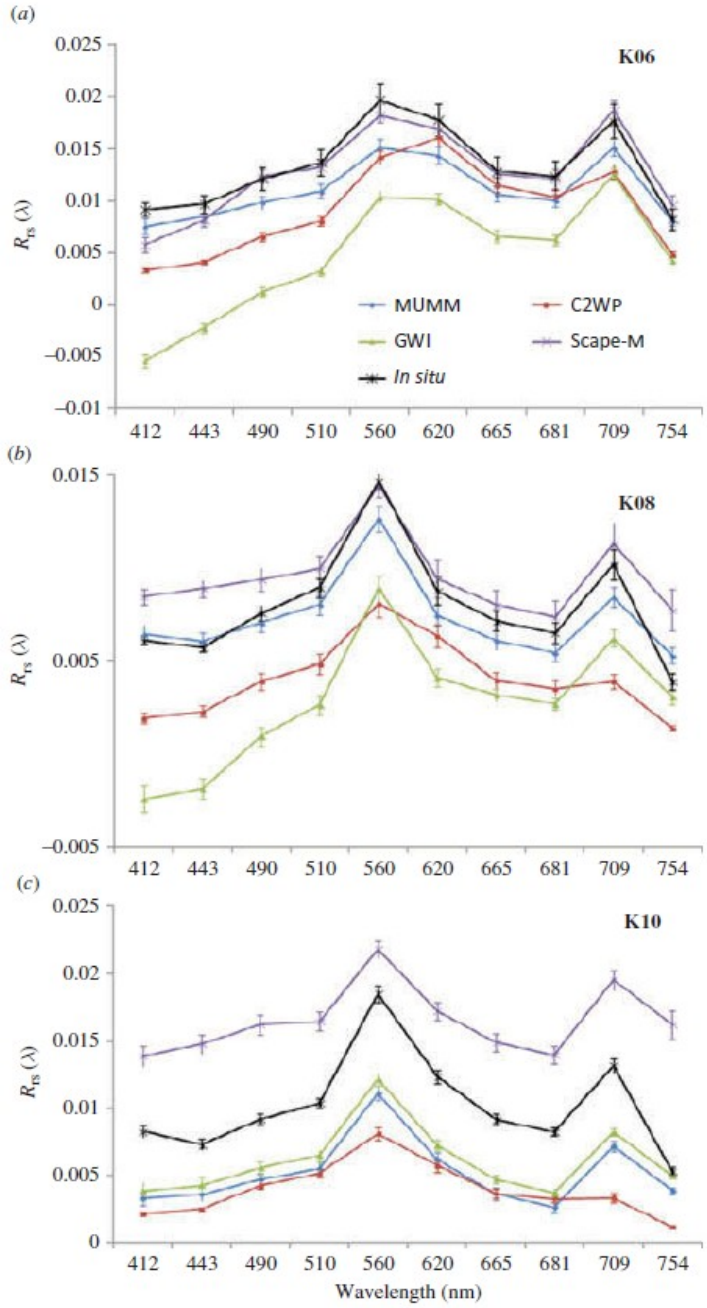

Figure 2.6. Comparison between *in situ*-measured and averaged MERIS-derived remote-sensing reflectance by the four atmospheric correction algorithms for each date. Error bars refer to the standard deviation calculated from all measurements available for a given date. (*a*) 18 February 2006; (*b*) 7 August 2008; (*c*) 18 May 2010.

This is probably because IOPs in Spanish lakes are different from those in Lake Kasumigaura (Yoshimura et al. 2012; Yang et al. 2013). These results strongly suggest that NN parameters should be retrained by a simulation data set on the basis of IOPs collected from target waters.

2.4.2 Performance of the SCAPE-M algorithm

The assumption in the SCAPE-M algorithm for aerosol retrieval is that the atmospheric state should be homogenous within an area of 30 km × 30 km (Guanter, Sanpedro, and Moreno 2007; Guanter et al. 2010). Figure 2.7 shows the average, standard deviation (SD), and coefficients of variation (CV) (CV = SD/average of parameter) of the Rayleigh scattering corrected remote-sensing reflectance at MERIS band 14 (885 nm) over Lake Kasumigaura. It can be seen that the Rayleigh scattering-corrected remote-sensing reflectance of 2006 (February 18) showed the least spatial variation (SD=0.001), followed by 2008 (August 7, SD=0.005), while that of 2010 (May 18) showed the largest spatial variation (SD=0.012, approximately 12-fold that of 2006 and 2.4-fold that of 2008). In addition, compared with the spatial variation in Rayleigh scattering-corrected remote-sensing reflectance, that of water-leaving reflectance at this band was low for all dates (SD=0.002 for 2006, 0.001 for 2008 and 2010).

These results indicate that the spatial variation in Rayleigh scattering-corrected remote-sensing reflectance at band 14 was mainly caused by the atmospheric status at that time.

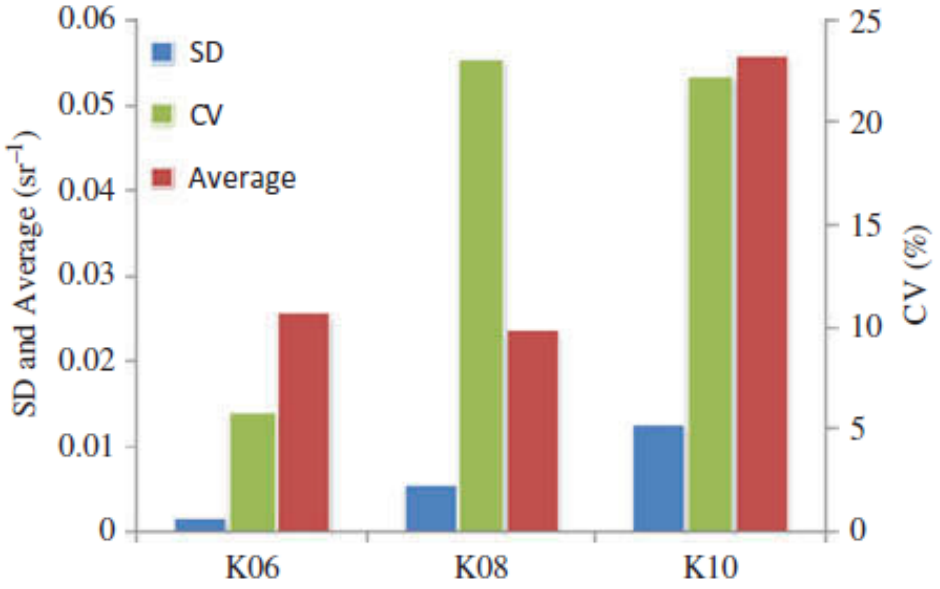

Figure 2.7. Average, Standard deviation (SD), and coefficients of variation (CV) of the Rayleigh scattering-corrected remote-sensing reflectance at MERIS band 14 (885 nm) over Lake Kasumigaura for each date.

Therefore, in Figure 2.7, it is clear that the atmospheric status on 18 May 2010 was the most heterogeneous, followed by 7 August 2008, while that on 18 February 2006 was the most homogeneous. This is the main reason why the SCAPE-M algorithm gave the best performance for the 2006 image, an acceptable atmospheric correction accuracy for the 2008 image, but failed for the 2010 image (Figures 2.2(*d*)–(*f*)). In addition, visibility at the times of satellite overpass (about 10:00 a.m., local time) was 35 km on 18 February 2006, 15 km on 7 August 2008, and 9 km on 18 May 2010, suggesting that aerosol loadings in the 2006, 2008, and 2010 data were low, moderate, and high, respectively.

It is surprising that the two-band index showed acceptable accuracy even for the 2010 image, when the SCAPE-M algorithm could not yield sufficient accuracy for all single bands (Figures 2.2(*f*), 2.3(*c*) and 2.4(*b*)). The three-band index obtained from SCAPE-M-corrected water-leaving reflectance also showed the best performance among the four atmospheric correction algorithms, even though RE for the four algorithms was low in each case (Figure 2.5(*b*)). These results indicate that the SCAPE-M algorithm can maintain the actual spectral shape of water-leaving reflectance because it avoided *a priori* assumptions regarding water composition and its spectral response by the use of neighbouring land pixels (Figure 2.6).

2.4.3 Performance of the MUMM algorithm

For the successful use of the MUMM algorithm, two assumptions must be valid (Ruddick, Ovidio, and Rijkeboer 2000). The first concerns the atmospheric status over

the target waters, which requires that the ratios of multiple-scattering aerosols and aerosol-Rayleigh reflectances at two NIR reference bands are spatially homogeneous over the sub-scene of interest (i.e. they can be assumed to be constant). Although there was a lack of atmospheric data to test this assumption over Lake Kasumigaura, the results shown in Figure 2.7, suggesting large spatial variation in atmospheric status in the 2010 image, probably make this assumption invalid. This invalid assumption for atmospheric status could be one reason why the MUMM algorithm performed poorly for the 2010 image (Figure 2.2(*i*)).

The second assumption concerns water composition and its spectral response, which requires that the ratios of water-leaving reflectances normalized by the sun–sea atmospheric transmittance at two NIR reference bands are spatially homogeneous over the subscene of interest (i.e. they can be assumed to be constant). *In situ* water-leaving reflectance values were used to test the validity of the second assumption following the method of Doron et al. (2011). Figure 2.8 shows the relationship between the ratio of $R_{rs}(779)$ and $R_{rs}(865)$ and single $R_{rs}(865)$. $R_{rs}(865)$ has been used as an indicator for water turbidity in previous studies (Ruddick et al. 2006; Doron et al. 2011). Generally, $R_{rs}(865)$ is lower than 10^{-4} for very clear waters, between 10^{-4} and 10^{-2} for moderately turbid to turbid waters, and between 10^{-2} and 10^{-1} for extremely turbid waters (Doron et al. 2011).

From Figure 2.8, it can be seen that the ratios were not constant as the second assumption required – they decreased with increasing turbidity. This result is similar to that reported by Doron et al. (2011). For MERIS data, the MUMM algorithm uses a constant ratio of 1.711.

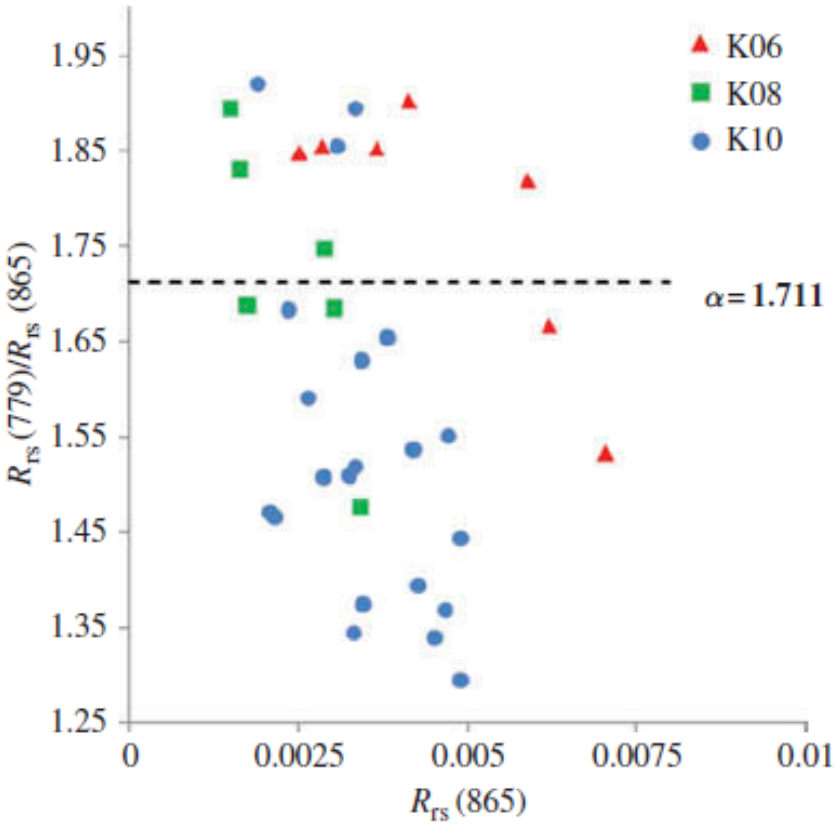

Figure 2.8. Scatterplots of $R_{rs}(779)/R_{rs}(865)$ vs $R_{rs}(865)$ for *in situ* measurements collected from three field campaigns. The constant value of the ratio $R_{rs}(779)/R_{rs}(865)$ used for MERIS data is 1.711 in SeaDAS, and is depicted as a straight line.

Compared with this constant value, the average bias of the ratios ($R_{rs}(779)/R_{rs}(865)$) estimated from *in situ* water-leaving reflectance was 8%, 6%, and 13% for 2006, 2008, and 2010, respectively.

Consequently, the performance of the MUMM algorithm for each image can be explained as follows: (*1*) the moderate performance for the 2006 image occurred because the data for this date met the first assumption (low and homogenous aerosol scattering), but failed for the second assumption (Figure 2.2(*g*)); (*2*) the best performance for the 2008 image occurred because the 2008 data met both assumptions relatively well (Figure 2.2(*h*)); and (*3*) the poor performance for the 2010 image occurred because both assumptions were not valid for that image (Figure 2.2(*i*)). These results indicate that limitations of the MUMM algorithm come not only from atmospheric status but also from water constituents and their spectral responses.

2.4.4 Performance of the GWI algorithm

The assumption in the GWI algorithm is that a bio-optical model can be used to accurately estimate water-leaving reflectance at two NIR reference bands (bands 12 and 13 of the MERIS) through an iterative procedure (Stumpf et al. 2003; Bailey, Franz, and Werdell 2010). Figure 2.9 shows comparisons between *in situ*-measured and estimated water-leaving reflectance at MERIS bands 12 and 13, respectively. It can be seen that the water-leaving reflectance at the two NIR reference bands were largely underestimated by the bio-optical model, especially for the 2006 and 2008 data (RE=56.0% for band 12, and RE= 59.0% for band 13).

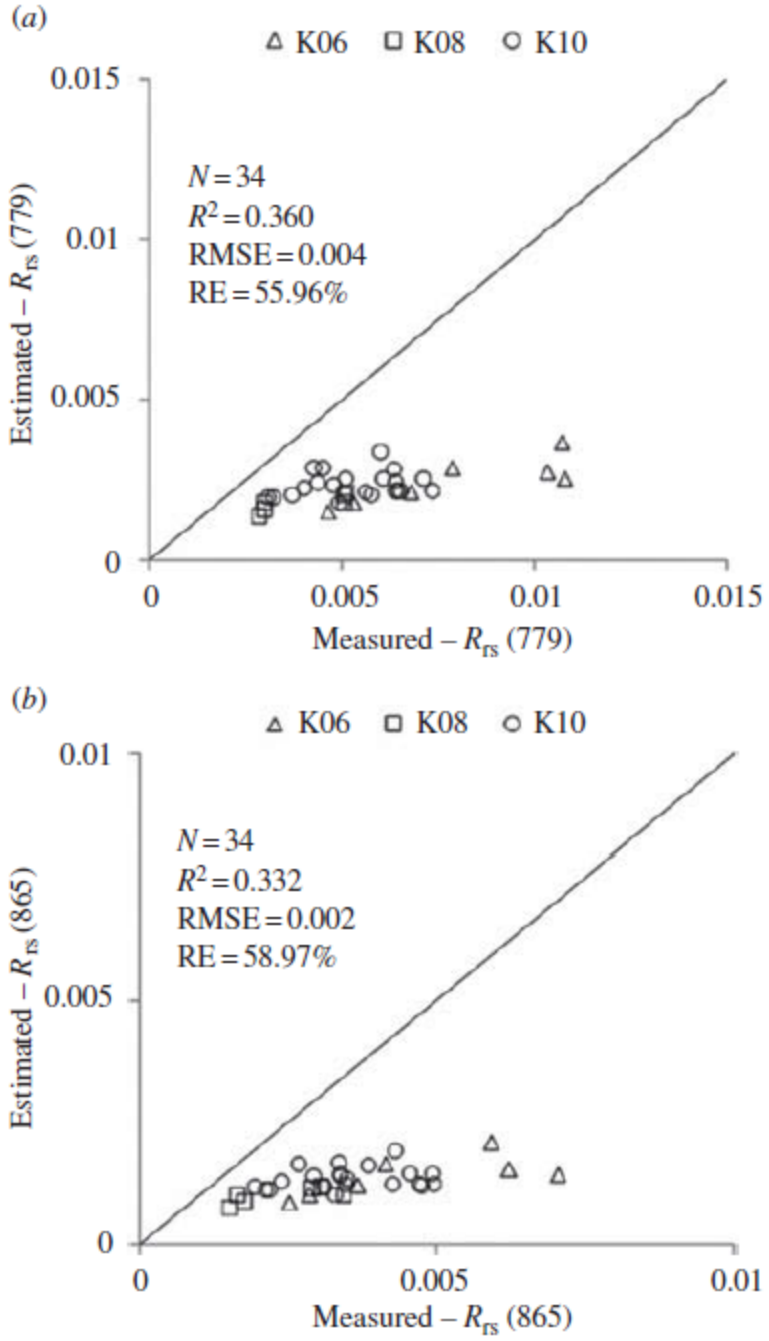

Figure 2.9. Comparison between *in situ*-measured and estimated water-leaving reflectance at two NIR reference bands. (*a*) MERIS band 12 (779 nm); (*b*) MERIS band 13 (865 nm).

These results indicate that the current bio-optical model used in the GWI algorithm is not able to provide sufficient accuracy for estimating water-leaving reflectance at the two NIR reference bands in Lake Kasumigaura. The underestimation of water-leaving reflectance at the two NIR reference bands will result in an overestimation of multiple-scattering aerosols and aerosol-Rayleigh reflectances at these bands, and then an overestimation of aerosol scattering at shorter bands. This is the reason why the atmospherically corrected water-leaving reflectances by the GWI algorithm were underestimated for all dates (Figures 2.2(*j*)–(*l*)).

2.4.5 Possibilities for improving atmospheric correction algorithm in Lake Kasumigaura

In the light of the above analyses, two possibilities can be considered towards improving the existing atmospheric correction algorithms in Lake Kasumigaura for future applications. The first is to improve the C2WP algorithm by retraining the parameters of NN using comprehensive simulation data. It is necessary to obtain the optical properties of water (e.g. IOPs and concentrations of water constituents) and atmosphere (e.g. amount and type of aerosol) in/over Lake Kasumigaura for accurate bio-optical and radiative transfer simulations.

Since Lake Kasumigaura is close to Tokyo, the largest city in Japan (only 60 km away), and several heavy industries are in operation along the Pacific coast, it is often difficult to assume a homogenous atmospheric status (especially for the amount and type of aerosol) over the lake (Figure 2.7). Therefore, attempts to improve the MUMM and SCAPE-M algorithms for atmospheric correction in Lake Kasumigaura will probably not

be successful. This is because both algorithms require the homogenous assumption regarding atmospheric status.

Consequently, the second possibility would be to improve the first type of approach (i.e. accurately estimating water-leaving reflectance at two NIR reference wavelengths using a more appropriate method). The bio-optical model used in the GWI algorithm has been shown to be inappropriate for Lake Kasumigaura, mainly because several empirical relationships for estimating absorption and backscattering coefficients were not valid (Figure 2.9). Extending the reference wavelength from visible to NIR domains can probably provide an opportunity to improve the performance of the bio-optical model (Yang et al. 2013), and thus more accurate atmospheric correction in Lake Kasumigaura.

2.5 Conclusions

Here, I evaluated four atmospheric correction algorithms using in situ water-leaving reflectance and concurrently acquired MERIS images collected from Lake Kasumigaura, Japan (turbid inland water). The validity of the assumptions in the four atmospheric correction algorithms was also investigated to understand both the advantages and limitations of each algorithm. The results show that all atmospheric correction algorithms evaluated have limitations in regard to Lake Kasumigaura, although the SCAPE-M and MUMM algorithms had acceptable accuracy for atmospheric correction in several cases (i.e. relative errors less than 30% for the 2006 and 2008 images). The performances of all four algorithms strongly depended on their assumptions (atmospheric status and/or

turbidity of water body), and each algorithm failed when its assumptions became invalid (e.g. for the 2010 image, the relative errors ranged from 42% to 83%).

These results indicate that further improvements are necessary to address the issue of atmospheric correction for turbid inland waters such as Lake Kasumigaura. By considering the features of atmosphere and water quality over/in Lake Kasumigaura, the NN technique with more suitable training data and the estimation of water-leaving reflectance at two NIR reference wavelengths using a more appropriate method may improve the existing atmospheric correction algorithms in the lake.

Chapter III Development of a new atmospheric correction algorithm for applying MERIS data to turbid inland waters I: implementation and performance

3.1 Introduction

The optical signal received by remote sensing sensor, which is called top of atmosphere (TOA) reflectance, is generally a mixture of signals from earth surface (lands or waters) and atmosphere as well as their interactions (Gordon and Wang 1994; Santer et al. 1999). In water areas, only 10% of signals recorded by the sensors originate from water bodies in the visible spectra (Huot et al. 2001; Siegel et al. 2000). Therefore, it is necessary to remove the atmospheric effects from remote sensing data before they were used for estimating water quality parameters.

Most of atmospheric correction (AC) algorithms for water color remote sensing originated from the basic scheme proposed by Gordon & Wang (1994), as follows :

$$\rho_{toa}(\lambda) = \rho_r(\lambda) + [\,\rho_a(\lambda) + \rho_{ra}(\lambda)] + t(\lambda)\rho_w(\lambda) \quad (3.1)$$

where $\rho_{toa}(\lambda)$ is the reflectance that recorded by satellite sensor, $\rho_r(\lambda)$ is the reflectance from Rayleigh scattering, $[\rho_a(\lambda)+ \rho_{ra}(\lambda)]$ is the reflectance from the sum of aerosol scattering and the interaction between Rayleigh and aerosol scattering (i.e. aerosol

multiple-scattering reflectance), $t(\lambda)$ is the diffuse transmittances of the atmospheric column, and $\rho_w(\lambda)$ is the water-leaving reflectance. In Equation 3.1, $\rho_r(\lambda)$ and $t(\lambda)$ can be calculated from radiative transfer model *a priori*, while variables $[\rho_a(\lambda) + \rho_{ra}(\lambda)]$ remains as the largest uncertainty that need to be solved for retrieving $\rho_w(\lambda)$ (Selby et al. 1978; Gordon et al. 1988; Gordon and Wang 1994).

In open oceans, the AC algorithm proposed by Gordon & Wang (1994) (denote as GW94 hereafter) is widely used by exploiting the fact that water-leaving reflectance at near infrared (NIR) wavelengths can be neglected in this kinds of clear waters. However, in most inland and coastal waters, the assumption of negligible water-leaving reflectances at the NIR wavelengths become invalid due to the higher water turbidity (Hu, Carder, and Muller-Karger 2000; Shi and Wang 2007; Shi and Wang 2009; Wang, Son, and Shi 2009).

There are many efforts have been made to solve this problem. My previous work summarized the existing AC algorithms for turbid waters and then evaluated four representative algorithms in Lake Kasumigaura, Japan (Jaelani et al. 2013). The results showed that all four AC algorithms have limitations in Lake Kasumigaura, Japan and further improvements are necessary to address the issue of atmospheric correction for turbid inland waters. Fortunately, from my previous work, I not only well understood the limitations of the evaluated AC algorithms, but also got two hints to improve the existing AC algorithms for turbid inland waters such as Lake Kasumigaura. The two hints are: (*1*) atmospheric status over a water body should be estimated pixel by pixel (i.e., considering heterogeneous atmospheric status, especially for the amount and type of aerosol); (*2*) water-leaving reflectance at two NIR reference wavelengths should be more accurately

estimated pixel by pixel.

Based on the above two hints, an existing AC algorithm, which was developed by Stumpf et al. (2003) and updated by Bailey, Franz, and Werdell (2010), shows a potential to be improved for turbid inland waters. This algorithm is based on the original AC scheme in the GW94 algorithm, but estimating water-leaving reflectance at two NIR reference bands by a bio-optical model rather than assuming them as zero. The two estimated water-leaving reflectance values were removed from corresponding remote-sensing reflectance at the TOA, and then inputted into the GW94 algorithm. This algorithm also adopted an iterative procedure to make the estimated water-leaving reflectance by the bio-optical model gradually close to actual water-leaving reflectance. For convenient, this algorithm was denoted as GWI (the standard Gordon and Wang algorithm with an iterative process and a bio-optical model) hereafter following my previous work.

The objectives of the present study were to (*1*) develop a new AC algorithm for turbid inland waters based on the scheme of the GWI algorithm; and (*2*) evaluate the performance of the developed algorithm using the *in situ*-measured remote-sensing reflectance collected from two turbid Asian lakes and four American sea waters (92 sites in total).

3.2 Methods

3.2.1 Dataset

3.2.1.1 In situ data collection

The *in situ* remote-sensing reflectance ($R_{rs}(\lambda)$) spectra were collected from two Asian lakes: Lake Kasumigaura, Japan and Lake Dianchi China. The Lake Kasumigaura (36^{o} 9'N; 140^{o} 14' E) is located in the eastern part of Japan's Kanto's plain and has a surface area of 171 km^2 (only for the western part), an average depth of 4.0 m, and a maximum depth of 7.3 m. It is the second largest lake in Japan (after Lake Biwa) and it is a eutrophic-turbid lake due to high loads of nutrients and resuspension of bottom sediments by wind (Matsushita et al. 2009). The Lake Dianchi (24^{o} 50'N; 102^{o} 41' E) is located in the Yungui plateau area of south-western China and has a surface area of 300 km^2, an average depth of 4.3 m, and a maximum depth of 11.3 m. This lake is also suffering from increasing eutrophication due to the large amount of industrial wastewater and municipal sewage (Gao et al. 2005).

In Lake Kasumigaura, three data collection campaigns were undertaken in 2006 (Feb. 18, 10 sites), 2008 (Aug. 7, 14 sites), and 2010 (May 18, 26 sites), and the campaigns were timed to coincide with the acquisitions of the MERIS images. The data collecting sites, which located less than one MERIS pixel away from the banks and corresponding MERIS pixels were contaminated by clouds were excluded from the analyses. Accordingly, 7, 6, and 21 sites remained for comparison in Feb. 2006, Aug. 2008 and May 2010, respectively (Figure 3.1). In Lake Dianchi, two data collection campaigns were undertaken in 2007 (Oct. 23, 3 sites) and 2009 (Mar. 12, 3 sites), and the both campaigns were 1 day before the acquisitions of the MERIS images.

All reflectance measurements were performed between 10:00 and 14:00 h local time over optically deep waters. The water-leaving radiance ($L_u(\lambda)$), the downward

irradiance ($E_d(\lambda)$), and the downward radiance of skylight ($L_{sky}(\lambda)$) were measured at each site using a FieldSpec HandHeld (or Pro VNIR) spectroradiometer (Analytical Spectral Devices, Boulder, CO) in the range of 325–1075 nm at 1-nm intervals. The above-water remote-sensing reflectance ($R_{rs}(\lambda)$) was calculated approximately using the following equation (Mobley 1999):

$$R_{rs}(\lambda) = \left(\frac{L_u(\lambda)}{E_d(\lambda)} - \frac{rL_{sky}(\lambda)}{E_d(\lambda)}\right) \times Cal\,(\lambda) \quad (3.2)$$

where $Cal(\lambda)$ is the spectral reflectance of the grey reference panel that has been accurately calibrated, and r represents a weighted surface reflectance for the correction of surface-reflected skylight and is determined as a function of wind speed (Mobley 1999).

Descriptive statistics of the optical water quality parameters are summarized in Table 3.1, in which it can be seen that the turbidity of Lakes Dianchi and Kasumigaura is very high.

3.2.1.2 Data collection from SeaBASS

As a comparative study, I also tested the performance of developed atmospheric correction algorithms using *in situ* dataset obtained from SeaBASS (The SeaWiFS Bio-optical Archive and Storage System), a project funded by NASA since 1997 (Werdell et al. 2003; Werdell and Bailey 2002). The SeaBASS database (http://seabass.gsfc.nasa.gov/) contains *in situ* ocean optical (e.g., ocean water-leaving radiance spectra), biological (e.g., chlorophyll-a concentration), and other related oceanographic and atmospheric data.

Table 3.1. Descriptive statistics of optical water quality parameters measured in Lake Kasumigaura, Japan and Lake Dianchi, China.

	Min.	Max.	Median	Average	SD	CV(%)	*N*
K060218							
Chl-a (mg m^{-3})	69.65	95.02	84.54	83.99	9.69	11.54	7
TSS (g m^{-3})	22.00	46.10	32.80	33.71	8.11	24.05	7
$a_{CDOM}(440)$ (m^{-1})	no data	no data	no data	no data	no data	no data	0
K080807							
Chl-a (mg m^{-3})	44.40	76.90	62.90	62.18	11.92	19.17	6
TSS (g m^{-3})	11.70	21.10	16.40	16.73	3.18	19.02	6
$a_{CDOM}(440)$ (m^{-1})	1.15	1.36	1.15	1.20	0.09	7.23	6
K100518							
Chl-a (mg m^{-3})	36.60	83.40	44.80	53.70	17.61	32.80	21
TSS (g m^{-3})	18.00	27.73	21.17	22.13	3.59	16.22	21
$a_{CDOM}(440)$ (m^{-1})	0.51	0.94	0.62	0.71	0.16	22.23	21
D071024							
Chl-a (mg m^{-3})	69.60	85.90	70.10	75.20	9.27	12.33	3
TSS (g m^{-3})	32.30	40.10	33.40	35.27	4.22	11.97	3
$a_{CDOM}(440)$ (m^{-1})	0.77	1.02	0.91	0.90	0.13	14.12	3
D090313							
Chl-a (mg m^{-3})	30.21	52.25	30.91	37.79	12.53	33.15	3
TSS (g m^{-3})	34.04	42.58	42.03	39.55	4.78	12.08	3
$a_{CDOM}(440)$ (m^{-1})	0.41	1.28	0.56	0.75	0.46	61.58	3

Note: Chl-a: chorophyll-a concentration; TSS: total suspended solids;
$a_{CDOM}(440)$: absorption coefficient of CDOM at 440 nm
SD: Standard deviation; CV: coefficient of variation (SD/average of parameter)
N: number of samples.

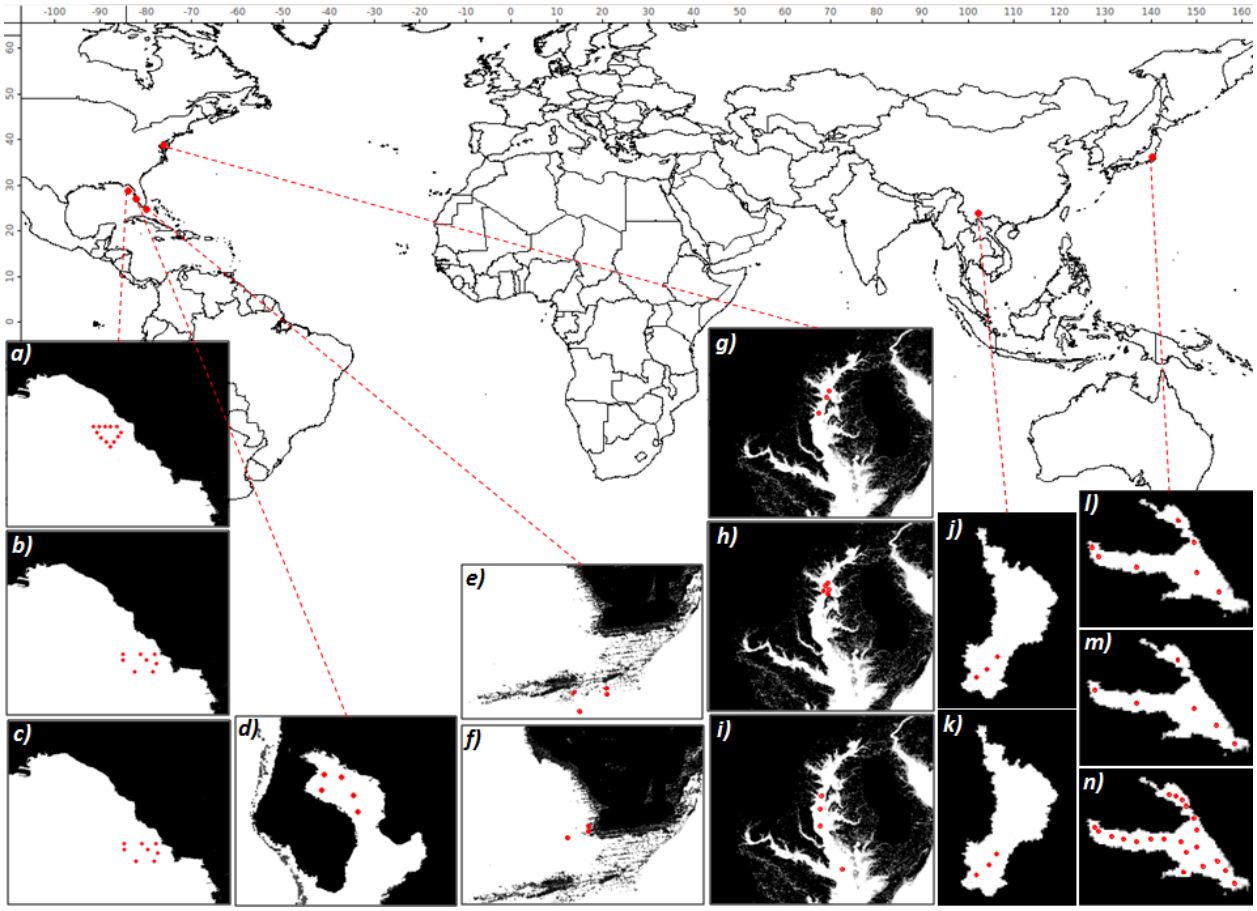

Figure 3.1. The location and spatial distribution of the sampling sites. Deadman Bay on (*a*) Mar. 13, 2011, 12 sites; (*b*) Sept. 25, 2011, 8 sites and (*c*) Nov. 21, 2011, 8 sites; Tampa Bay on (*d*) June 16, 2011, 5 sites; South Florida's sea on (*e*) Feb. 28, 2012, 4 sites; (*f*) Mar. 1, 2012; 3 sites; Chesapeake Bay on (*g*) Jul. 11, 2012, 3 sites; (*h*) Jul. 14, 2012, 5 sites; (*i*) Jul. 17, 2012; 4 sites; Lake Dianchi, China on (*j*) Oct. 24, 2007, 3 sites; (*k*) Mar. 13, 2009, 3 sites and Lake Kasumigaura, on (*l*) Feb. 18, 2006, 7 sites; (*m*) Aug. 07, 2008, 6 sites; (n) May 18, 2010, 21 sites. Red represent the sites location.

SeaBASS data were contributed by a variety of researchers from international ocean community, using various instrumentation with all measurements closely follow rigorous, community-defined deployment and data processing protocols (Mueller and Fargion 2002). In this study, I used one criterion, that the MERIS data is available at the same day when field campaigns were undertaken, for selecting *in situ*-measured $R_{rs}(\lambda)$ from the SeaBASS database. As the result, I obtained 52 *in situ*-measured $R_{rs}(\lambda)$ data that were collected in South Florida's sea (Feb. 28 and Mar. 1, 2012; 7 sites), Chesapeake Bay (Jul. 11, 14 and 17, 2012; 12 sites), Tampa Bay (June 16, 2011; 5 sites) and Deadman Bay (Mar. 13, Sept. 25 and Nov. 21, 2011; 28 sites). The location and spatial distribution of the sampling sites are shown in Figure 3.1.

3.2.1.3 MERIS data

According to the available *in situ* $R_{rs}(\lambda)$ data and matchup MERIS data, 14 full-resolution MERIS images (level-1b) were downloaded using EOLi (ESA's Link to Earth Observation, http://earth.esa.int/EOLi/EOLi.html), the European Space Agency's client for Earth Observation Catalogue and Ordering Services. Three images covering Lake Kasumigaura were acquired on February 18, 2006 (named as K060218 hereafter), August 7, 2008 (named as K080807 hereafter), and May 18, 2010 (named as K100518 hereafter). Two images covering Lake Dianchi, China were acquired on October 24, 2007 (named as D071024 hereafter) and March 13, 2009 (named as D090313 hereafter). Two images covering South Florida's sea were acquired on February 28, 2012 (named as SF120228 hereafter) and March 1, 2012 (named as SF120301 hereafter). Three images covering

Chesapeake Bay were acquired on July 11, 2011 (named as CB110711 hereafter), July 14, 2011 (named as CB110714 hereafter) and July 17, 2011 (named as CB110717 hereafter). One image covering Tampa Bay was acquired on June 16, 2011 (named as TB110616 hereafter). Three images covering Deadman Bay were acquired on March 13, 2011 (named as DB110313 hereafter), September 25, 2011 (named as DB110925 hereafter) and November 21, 2011 (named as DB111121 hereafter). All field campaigns were timed to coincide with acquisition of MERIS images, except for the field campaigns in Lake Dianchi (one day before). The orbital information of 14 MERIS images is summarized in Table 3.2.

All downloaded MERIS images were processed using SeaDAS software package (version 6.4, http://seadas.gsfc.nasa.gov/) and BEAM toolbox (version 4.11, http://www.brockmann-consult.de/beam/), with the outputs of above-water remote sensing reflectance $R_{rs}(\lambda)$ at center wavelengths of 620, 665, 681, 709 and 754 nm (corresponding to MERIS bands 6-10), which are directly comparable with *in situ*-measured $R_{rs}(\lambda)$. The average of 3-by-3 window was used to compare with *in situ*-measured $R_{rs}(\lambda)$ to avoid potential error in the geometric correction and dynamics of water bodies, as well as the potential error in spatial variability (Han and Jordan 2005).

Table 3.2. Orbital information for 14 MERIS images used in this study (UTC: Coordinated Universal Time).

	Orbit	Acquisition Date	Starting Time (UTC)	Ending Time (UTC)	Sun Zenith (°)	Sun Azimuth (°)	View Zenith (°)	View Azimuth (°)
K060218	20755	Feb 18, 2006	1:13:47	1:15:26	53.0986	150.0340	21.4847	285.5670
K080807	33652	Aug 07, 2008	0:56:48	0:58:26	31.0734	122.7615	12.5257	102.7238
K100518	42942	May 18, 2010	0:59:28	1:01:06	27.2518	121.5042	11.6660	102.7989
D071024	29531	Oct 24, 2007	3:32:08	3:33:46	40.8491	150.3395	22.1640	284.1296
D090313	36774	Mar 13, 2009	3:29:15	3:30:53	36.9181	133.6979	21.7139	284.0547
SF120228	52295	Feb 28, 2012	15:35:20	15:36:58	45.1531	136.2971	19.9833	101.8650
SF120301	52324	Mar 01, 2012	16:01:38	16:03:17	41.8361	142.6473	21.9487	284.3173
CB110711	48962	Jul 11, 2011	15:37:16	15:38:51	25.4221	120.8660	0.6930	237.2557
CB110714	49005	Jul 14, 2011	15:27:18	15:28:57	27.1980	118.1972	14.5994	102.5849
CB110717	49048	Jul 17, 2011	15:17:22	15:19:01	28.0588	117.3778	20.1237	102.0859
TB110616	48603	Jun 16, 2011	15:56:24	15:58:03	20.1394	95.6044	21.3363	284.2502
DB110313	47238	Mar 13, 2011	15:38:07	15:39:46	41.9180	132.4648	19.6077	101.9411
DB110925	50054	Sep 25, 2011	15:54:12	15:55:51	35.3106	140.7099	3.6382	283.2451
DB111121	50873	Nov 21, 2011	16:04:33	16:06:11	50.8573	158.7520	22.2738	284.4092

3.2.1.4 Synthetic dataset

The synthetic data was obtained from IOCCG (http://ioccg.org/groups/OCAG_data.html) containing absorption coefficient of phytoplankton pigments, colored dissolved organic matters (CDOM), detritus/mineral, and total absorption coefficient; backscattering of phytoplankton, detritus/mineral and total backscattering; remote-sensing reflectance (below and above surface) and irradiance reflectance (below and above surface) as well as down-welling diffuse attenuation coefficient. The IOP data were simulated based on extensive field measurements, whereas AOPs data were generated using Hidrolight (IOCCG 2006). This synthetic data was used for generating a new equation for calculating a spectral slope of particle backscattering (i.e., Y value) from $R_{rs}(\lambda)$.

3.2.2 Development of a new AC Algorithm based on the GWI scheme

The atmospheric correction for clear waters has been developed with sufficient accuracy (Gordon and Wang 1994). Therefore, in this study, I focused on the development of an AC algorithm that is applicable in turbid waters. In turbid waters, the most useful $R_{rs}(\lambda)$ are at longer wavelengths (i.e. in the range of 665-754 nm), because the shorter wavelengths (blue-green) are not suitable to be used for estimating water quality parameters (e.g., chlorophyll-*a*) (Gitelson 1992; Gitelson et al. 2008; Yang et al. 2011; Yu et al. 2014). Therefore, it can be considered that the users only have a strong concern for accuracy of AC at longer wavelengths if they are studying a turbid water body.

Accordingly, two principal policies for the development of a new AC algorithm are: (*1*) use of the GWI scheme to avoid the problem caused by spatial homogeneity

assumption; and (*2*) AC only for longer wavelengths (i.e., longer than 620 nm). This new AC algorithm was denoted as N-GWI hereafter for convenience. To ensure that the N-GWI algorithm is applicable in turbid inland waters, the improvements have been carried out in three aspects. The details are delineated hereafter.

a) Using a fixed aerosol model

In the GWI algorithm, aerosol multiple scatterings [$\rho_a(\lambda_{NIR}) + \rho_{ra}(\lambda_{NIR})$] at 779 and 865 nm were firstly estimated from TOA reflectance, Rayleigh scattering reflectance, and estimated water-leaving reflectance by the bio-optical model according to the Equation 3.1. The estimated aerosol multiple scatterings were then converted to aerosol single scatterings $\rho_{as}(\lambda_{NIR})$ at the same wavelengths through a look up table (LUT) as follows:

$$[\rho_a(779) + \rho_{ra}(779)] \underset{LUT}{\longrightarrow} \rho_{as}(779) \tag{3.3a}$$

$$[\rho_a(865) + \rho_{ra}(865)] \underset{LUT}{\longrightarrow} \rho_{as}(865) \tag{3.3b}$$

The AC parameter epsilon (i.e., ε(779,865)) is calculated from the ratio of the two aerosol single scatterings at 779 and 865 nm as follow:

$$\varepsilon(779,865) = \frac{\rho_{as}(779)}{\rho_{as}(865)} \tag{3.4}$$

The value of ε(779,865), which varies from 0.976 to 1.203, is corresponding to 80 prepared aerosol models with different ratios of fine particles (95, 80, 50, 30, 20, 10, 05,

02, 01 and 00 %) and relative humidity (30, 50, 70, 75, 80, 85, 90 and 95 %). For each value of ε(779,865), I can extrapolate it to other wavelengths using the following equation (also Figure 3.2):

$$\varepsilon(\lambda, 865) = \exp\left[\frac{\ln(\varepsilon(779,865))}{865-779}(865-\lambda)\right] \quad (3.5)$$

Aerosol single scattering reflectance at all wavelengths can be estimated from that at 865 nm ($\rho_{as}(865)$) and the epsilons at all wavelengths ($\varepsilon(\lambda,865)$):

$$\rho_{as}(\lambda) = \rho_{as}(865)\varepsilon(\lambda, 865) \quad (3.6)$$

Based on the values of aerosol single scattering reflectance, the values of aerosol multiple scattering reflectance can be estimated through the LUT provided in SeaDAS software:

$$\rho_{as}(\lambda) \underset{LUT}{\longrightarrow} \rho_a(\lambda) + \rho_{ra}(\lambda) \quad (3.7)$$

Finally, water-leaving reflectance ($\rho_w(\lambda)$) at all wavelengths can be derived as follow:

$$\rho_w(\lambda) = \frac{\rho_{toa}(\lambda) - \{\rho_r(\lambda) + [\rho_a(\lambda) + \rho_{ra}(\lambda)]\}}{t(\lambda)} \quad (3.8)$$

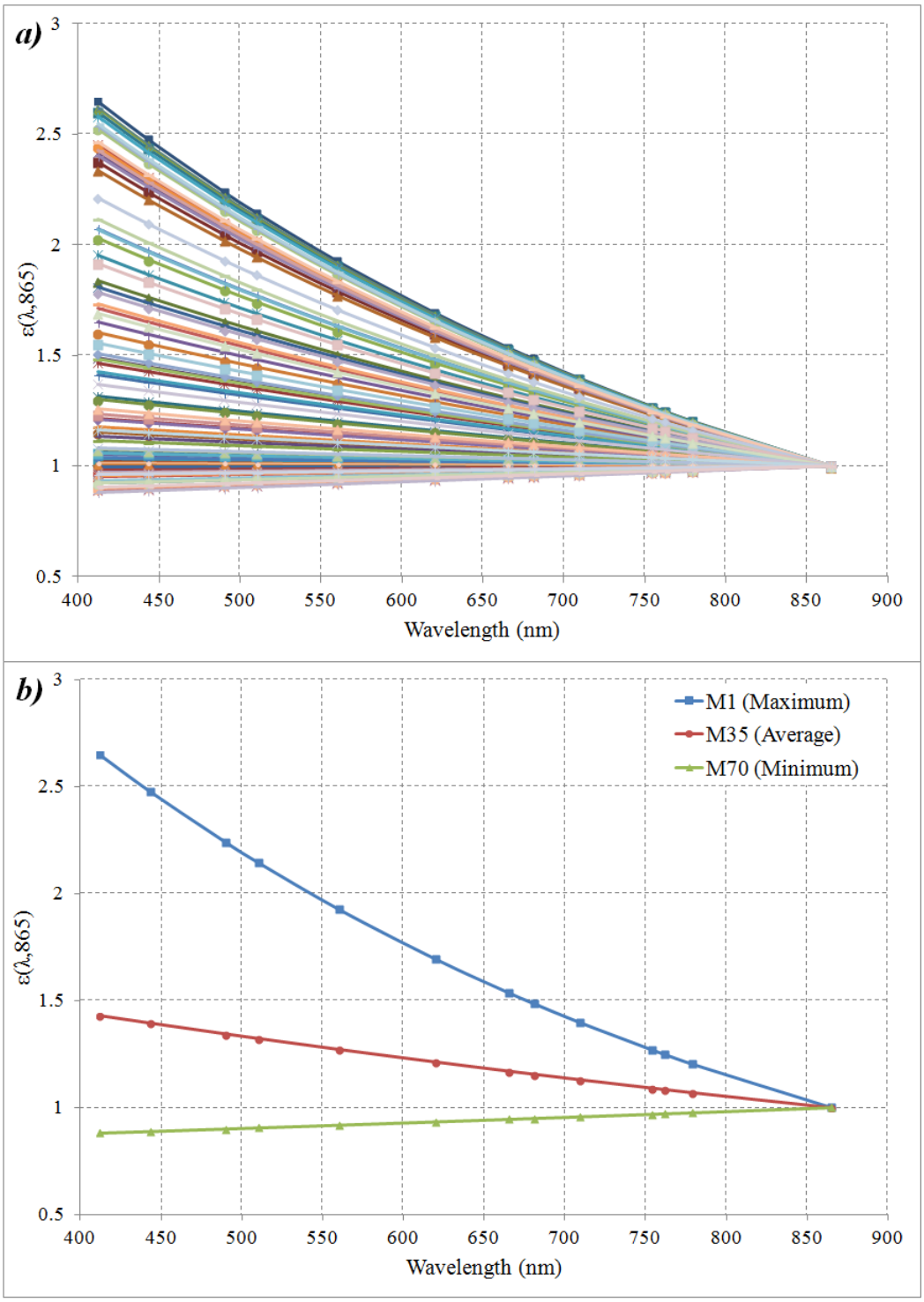

Figure 3.2. $\varepsilon(\lambda, 865)$ as a function of wavelength for 80 prepared aerosol models in SeaDAS. Based on $\varepsilon(779, 865)$ value, M35 is average which is corresponds to a Coastal aerosol model with relative humidity (RH) of 75% and fine particles ratio of 20%.

Therefore, it is clear that the value of $\varepsilon(779,865)$ plays an important role for selecting the most appropriate aerosol model for a pixel. However, in the waters with relatively high turbidities, the GWI algorithm usually could not provide accurate water-leaving reflectance at 779 and 865 nm due to several empirical relationships for estimating absorption and backscattering coefficients were not valid in these kinds of waters (Jaelani et al. 2013). Therefore, the GWI algorithm could not obtain a reasonable value of $\varepsilon(779,865)$ and thus an appropriate aerosol model.

From Figure 3.2, it can be seen that the $\varepsilon(779,865)$ values among all 80 aerosol models do not show larger variation if I just considered wavelengths longer than 620 nm. For the wavelength of 620 nm, the $\varepsilon(620,865)$ values varies from 0.933 to 1.693 with an average of 1.222. For the wavelength of 779 nm, the $\varepsilon(779,865)$ values varies from 0.976 to 1.203 with an average of 1.073. The $\varepsilon(779,865)$ value of 1.073 corresponds to a Coastal aerosol model with relative humidity (RH) of 75% and fine particles ratio of 20%. This finding indicates that the selection of aerosol model is not so important if I just consider AC for longer wavelengths. Therefore, it is possible to fix the $\varepsilon(779,865)$ values as the average of 1.073 in the N-GWI algorithm instead of estimating it every time. This improvement can not only avoid an inaccurate $\varepsilon(779,865)$ estimation from the ratio of aerosol scattering reflectance at two 779 and 865 nm, but also make the N-GWI algorithm only need to estimate aerosol scattering at 865 nm.

b) Shifting the reference band from visible to NIR

The GWI algorithm used a visible band around 670 nm as the reference for clear and less

turbid waters (Stumpf et al. 2003; Bailey, Franz, and Werdell 2010). The value of $a_t(670)$ was firstly calculated based on an empirical relationship derived from NOMAD (the NASA bio-Optical Marine Algorithm Dataset) (Werdell and Bailey 2005) as follow:

$$a_t(670) = exp[\ln(Chl_a) * 0.9389 - 3.7589] + a_w(670) \quad (3.9)$$

where Chl_a is the concentration of chlorophyll-*a*, and $a_w(670)$ is the absorption coefficient of pure water at the wavelength of 670 nm. Then, the backscattering coefficient of particles at 670 nm ($b_{bp}(670)$) was calculated using the following equation:

$$b_{bp}(670) = \frac{\mu(670)a_t(670)}{1-\mu(670)} - b_{bw}(670) \quad (3.10)$$

where $\mu(670)$ can be semi-analytically calculated from $R_{rs}(670)$ using a bio-optical model (Lee, Carder, and Arnone 2002; Yang et al. 2013).

In turbid inland waters, it is difficult to accurately predict chlorophyll-*a* concentration before an accurate AC was carried out, and thus the use of Equation 3.9 is limited. Yang et al. (2013) suggested the use of a longer wavelength at 754 nm instead of 555 nm or 670 nm as the reference band. At the wavelength of 754 nm, the assumption of total absorption (a_t) mostly come from pure water will be valid even for highly turbid waters (i.e., $a_t(754) \approx a_w(754)$). Therefore, the backscattering coefficient of particles at 754 nm ($b_{bp}(754)$) can be semi-analytically calculated as follow:

$$b_{bp}(754) \approx \frac{\mu(754)a_w(754)}{1-\mu(754)} - b_{bw}(754) \quad (3.11)$$

where $b_{bw}(754)$ is the backscattering coefficient of pure water, and $\mu(754)$ can be semi-analytically calculated from $R_{rs}(754)$ using a bio-optical model.

c) Generating a semi-analytical model for the estimation of spectral slope of particle backscattering

The following equation is used to obtain particle backscattering coefficients at a given wavelength (Yang et al. 2013) :

$$b_{bp}(\lambda) = b_{bp}(754)\left(\frac{754}{\lambda}\right)^{Y} \quad (3.12)$$

where λ is the given wavelength, and Y is the spectral slope of particle backscattering. In the GWI algorithm, the Y values are estimated using an empirical relationship proposed by (Lee, Carder, and Arnone 2002) :

$$Y = 2.0 * [1.0 - 1.2 * e^{\left(-0.9*\frac{Rrs(443)}{Rrs(555)}\right)}] \quad (3.13)$$

It can be considered that there are two limitations in the above equation (Equation 3.13). First, this relationship is an empirical one, and thus is probably a site- or time-specific one because the empirical relationship strongly depends on the data used.

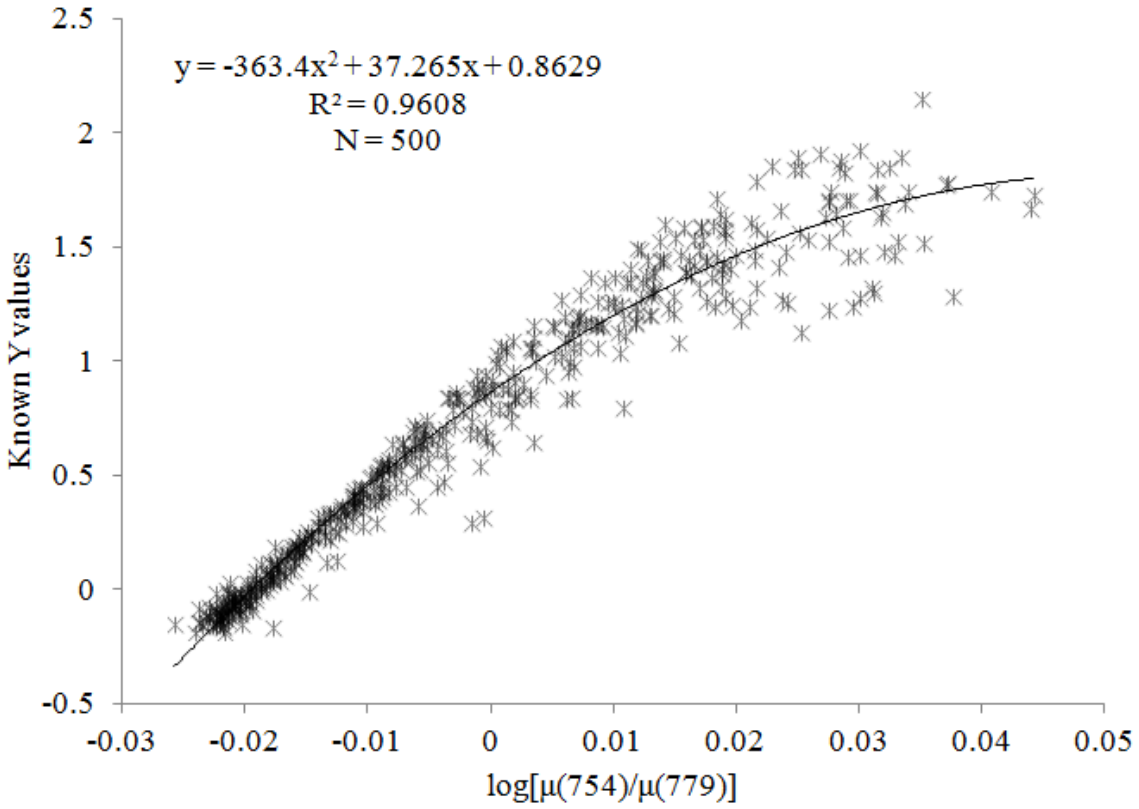

Figure 3.3. Scatter plot of log [μ(754)/μ(779)] vs. Y value derived from IOCCG synthetic dataset.

Second, the $R_{rs}(\lambda)$ at two shorter wavelengths were used in the equation. In turbid waters, the $R_{rs}(\lambda)$ at shorter wavelengths strongly suffers from not only interactions among water constituents but also imperfect atmospheric correction. In order to address the above two limitations, Yang et al. (2013) proposed a semi-analytical relationship for estimating Y values in turbid waters. The new relationship was generated using $R_{rs}(\lambda)$ at two longer wavelengths (754 and 779 nm) and corresponding IOPs data, which were obtained from IOCCG synthetic dataset (IOCCG 2006). In this study, I regenerated this relationship by using all 500 datasets according to the method proposed by Yang et al. (2013). In the original Yang et al. (2013), they only used 260 datasets because they used the remaining 240 dataset for validation. The new generated relationship is as follow (also Figure 3.3):

$$Y = -363.4 * \left[\log\left(\frac{\mu(754)}{\mu(779)}\right)\right]^2 + 37.265 * \log\left[\frac{\mu(754)}{\mu(779)}\right] + 0.8629 \quad (3.14)$$

where $\mu(754)$ and $\mu(779)$ can be estimated from $R_{rs}(754)$ and $R_{rs}(779)$ using a bio-optical model, respectively.

3.2.3 Accuracies Assessments

Two indices, root mean square error (RMSE) and normalize mean absolute error (NMAE), were used to assess the accuracy of atmospheric correction. These indices were defined as follows:

$$RMSE = \sqrt{\frac{\sum_{i=1}^{N}\left(x_{\mathrm{esti,i}} - x_{\mathrm{meas,i}}\right)^2}{N}} \quad (3.15)$$

$$NMAE = \frac{1}{N}\sum_{i=1}^{N}\left|\frac{x_{\text{esti,i}}-x_{\text{meas},i}}{x_{\text{meas}}}\right| 100\% \quad (3.16)$$

where $x_{\text{meas,i}}$ and $x_{\text{esti,i}}$ are the measured and estimated values, respectively, and N is the sample size. The RMSE gives the absolute scattering of the retrieved water-leaving reflectance, and the NMAE represents the uncertainty associated with satellite-derived distribution. The determination coefficient (R^2) between *in situ* measured $R_{\text{rs}}(\lambda)$ and estimated $R_{\text{rs}}(\lambda)$ from atmospherically corrected MERIS data was also calculated.

3.3 Results

3.3.1 Performance in Lake Kasumigaura

Figure 3.4 shows the comparison of *in situ* measured (x-axis) and atmospherically corrected (y-axis) $R_{\text{rs}}(\lambda)$ by the N-GWI algorithm as well as four previous AC algorithms (GWI, MUMM, C2WP and SCAPE-M) for MERIS bands 6–10 in Lake Kasumigaura.

For the data collected in 2006 (K060218, 7 stations), results show that the N-GWI and SCAPE-M algorithms achieved the best performance. The N-GWI produced root mean square error (RMSE) of 0.003, normalized mean average error (NMAE) of 18.33%, and the determination coefficient (R^2) of 0.767. While the SCAPE-M produced RMSE of 0.003, followed by the MUMM (RMSE=0.004), C2WP (RMSE=0.004) and GWI (RMSE=0.007).

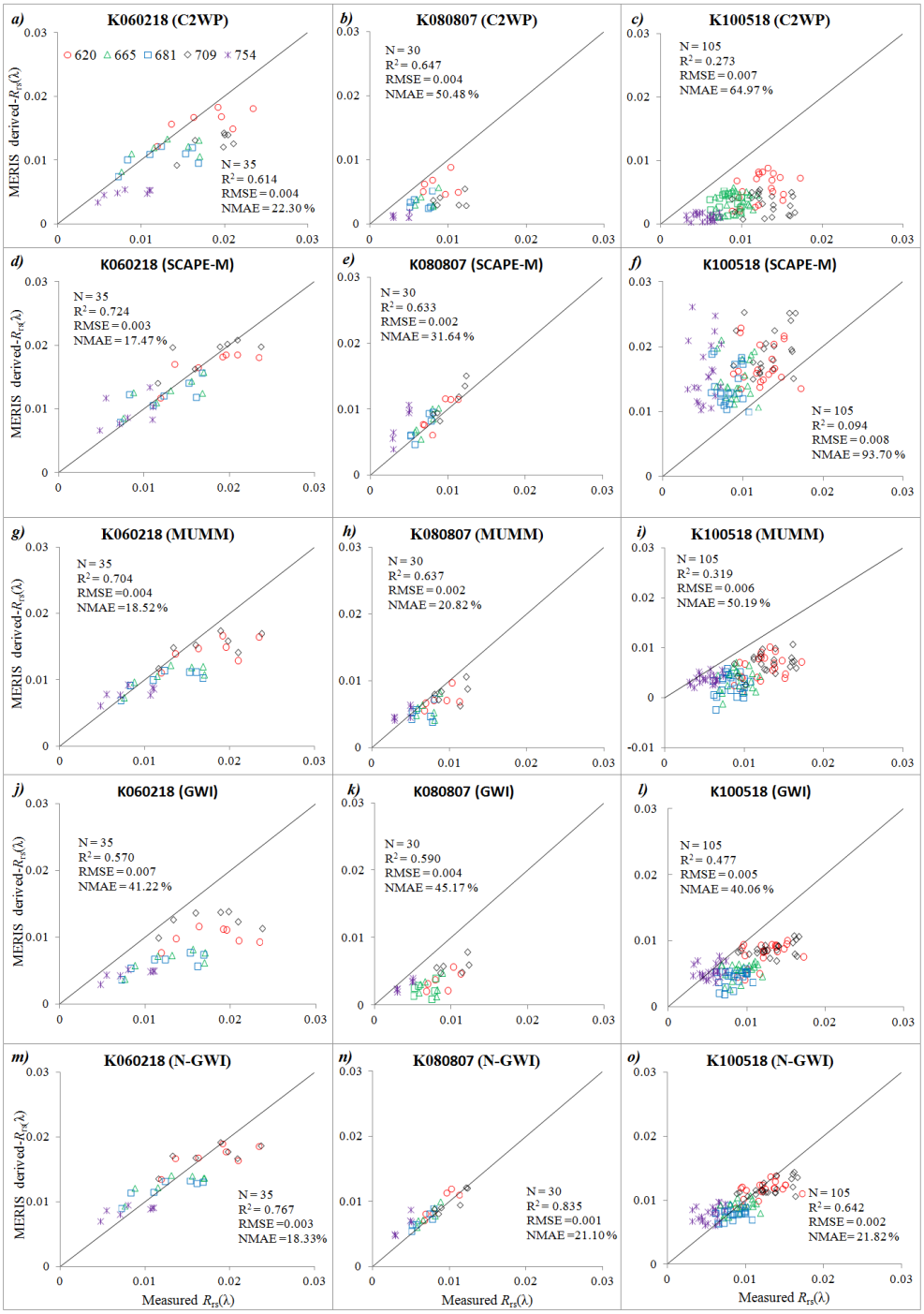

Figure 3.4. Comparisons between the *in situ*-measured and MERIS-derived water-leaving remote sensing reflectance by the N-GWI for MERIS bands 6–10 in Lake Kasumigaura: (*left*) K060218, (*middle*) K080807, (*right*) K100518. The center wavelength at each band is shown in the legend. The black line represents the 1:1 line.

For the data of 2008 (K080807, 6 stations), the N-GWI achieved the best performance (RMSE=0.001, NMAE=21.10%, R^2=0.835), followed by MUMM (RMSE=0.002), SCAPE-M (RMSE=0.002), C2WP (RMSE=0.004) and GWI (RMSE=0.004). Likewise for the data of 2010 (K100518, 21 stations), the N-GWI achieved the best performance (RMSE=0.002, NMAE=21.82%, R^2=0.642), followed by GWI (RMSE=0.004), MUMM (RMSE=0.006), C2WP (RMSE=0.007) and SCAPE-M (RMSE=0.008).

3.3.2 Performance in Lake Dianchi

The performances of N-GWI as well as three existing algorithms (GWI, C2WP and MUMM) were presented in Figure 3.5 and Table 3.3. Figure 3.5 show the performance of N-GWI for Lake Dianchi. In 2007 data (D071024, 3 stations) and 2009 data (D090313, 3 stations) N-GWI achieved the best performance with RMSE of 0.002 and 0.018, respectively. These performances followed by GWI with RMSE of 0.003 and 0.019, respectively; MUMM with RMSE of 0.003 and 0.026, respectively; and C2WP with RMSE of 0.006 and 0.027, respectively.

3.3.3 Performance in American sea waters

The performance of N-GWI in the tested American sea waters was different among the water bodies with NMAE in range of 83% to 1390%. The best retrieval achieved in Chesapeake Bay (CB110714, NMAE=83.56%) following with the data in Deadman Bay (DM111121, NMAE=219.90%) as presented in Figure 3.6.

Table 3.3. Performance of 4 atmospheric correction algorithms in 14 MERIS images. SCAPE-M is not included here.

No.	MERIS images	N-GWI			C2WP			GWI			MUMM		
		RMSE	*NMAE*	R^2	*RMSE*	*NMAE*	R^2	*RMSE*	*NMAE*	R^2	*RMSE*	*NMAE*	R^2
1	K060218	0.003	18.335	0.767	0.004	22.304	0.614	0.007	41.224	0.570	0.004	18.520	0.704
2	K080807	0.001	21.101	0.835	0.004	50.479	0.647	0.004	45.172	0.590	0.002	20.820	0.637
3	K100518	0.002	21.819	0.642	0.007	64.965	0.273	0.005	40.057	0.477	0.006	50.187	0.319
4	D071024	0.002	12.218	0.916	0.006	32.143	0.161	0.003	22.510	0.867	0.003	30.353	0.897
5	D090313	0.018	40.938	0.796	0.027	66.837	0.721	0.019	43.128	0.708	0.026	60.833	0.667
6	CB110711	0.006	343.490	0.861	0.001	44.724	0.610	0.002	75.810	0.450	0.002	129.956	0.837
7	CB110714	0.002	83.562	0.865	0.001	39.275	0.618	0.001	35.301	0.832	0.001	72.382	0.851
8	CB110717	0.003	312.292	0.840	0.001	33.634	0.686	0.001	37.157	0.813	0.002	166.783	0.847
9	DM110313	0.002	415.714	0.969	0.001	131.688	0.881	0.000	41.711	0.959	0.001	228.547	0.971
10	DM110925	0.002	862.259	0.739	0.001	231.482	0.727	0.000	53.757	0.880	0.001	440.839	0.847
11	DM111121	0.001	219.895	0.894	0.001	194.121	0.691	0.000	40.451	0.824	0.000	103.795	0.884
12	SF120228	0.006	1390.915	0.301	0.000	31.951	0.993	0.003	645.002	0.754	0.001	222.990	0.880
13	SF120301	0.005	298.787	0.914	0.001	59.335	0.911	0.001	39.251	0.912	0.001	75.886	0.858
14	TB110616	0.004	540.642	0.644	0.001	103.344	0.672	0.007	380.208	0.166	0.003	89.574	0.195

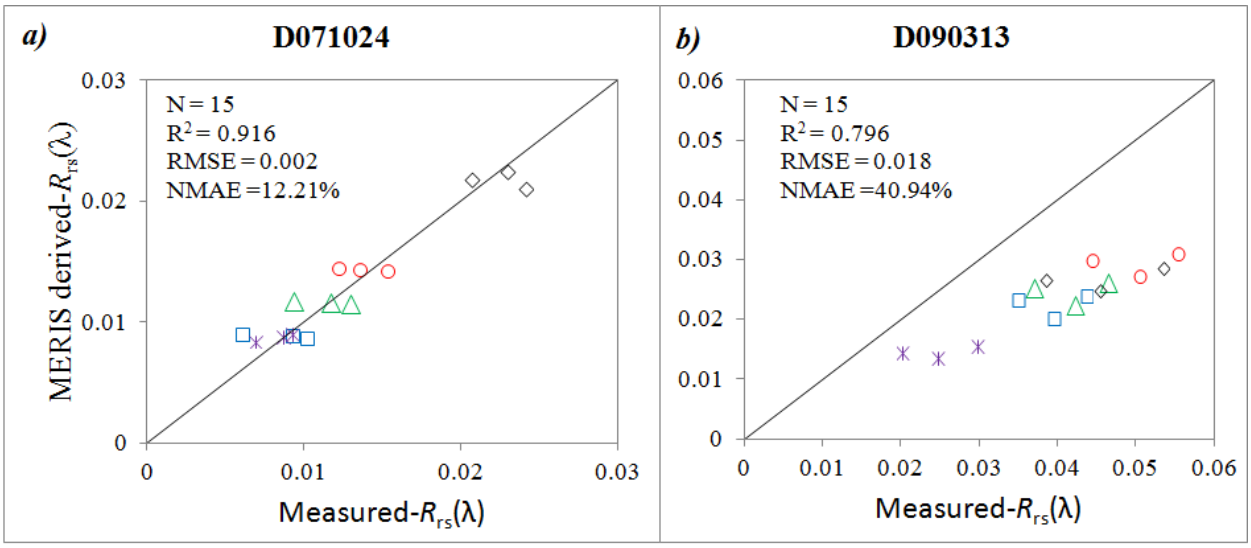

Figure 3.5. Comparisons between the *in situ*-measured and MERIS-derived water-leaving remote sensing reflectance by the N-GWI for MERIS bands 6–10 in Lake Dianchi: *(a)* D071024, *(b)* D090313. The center wavelength at each band is shown in the legend. The black line represents the 1:1 line.

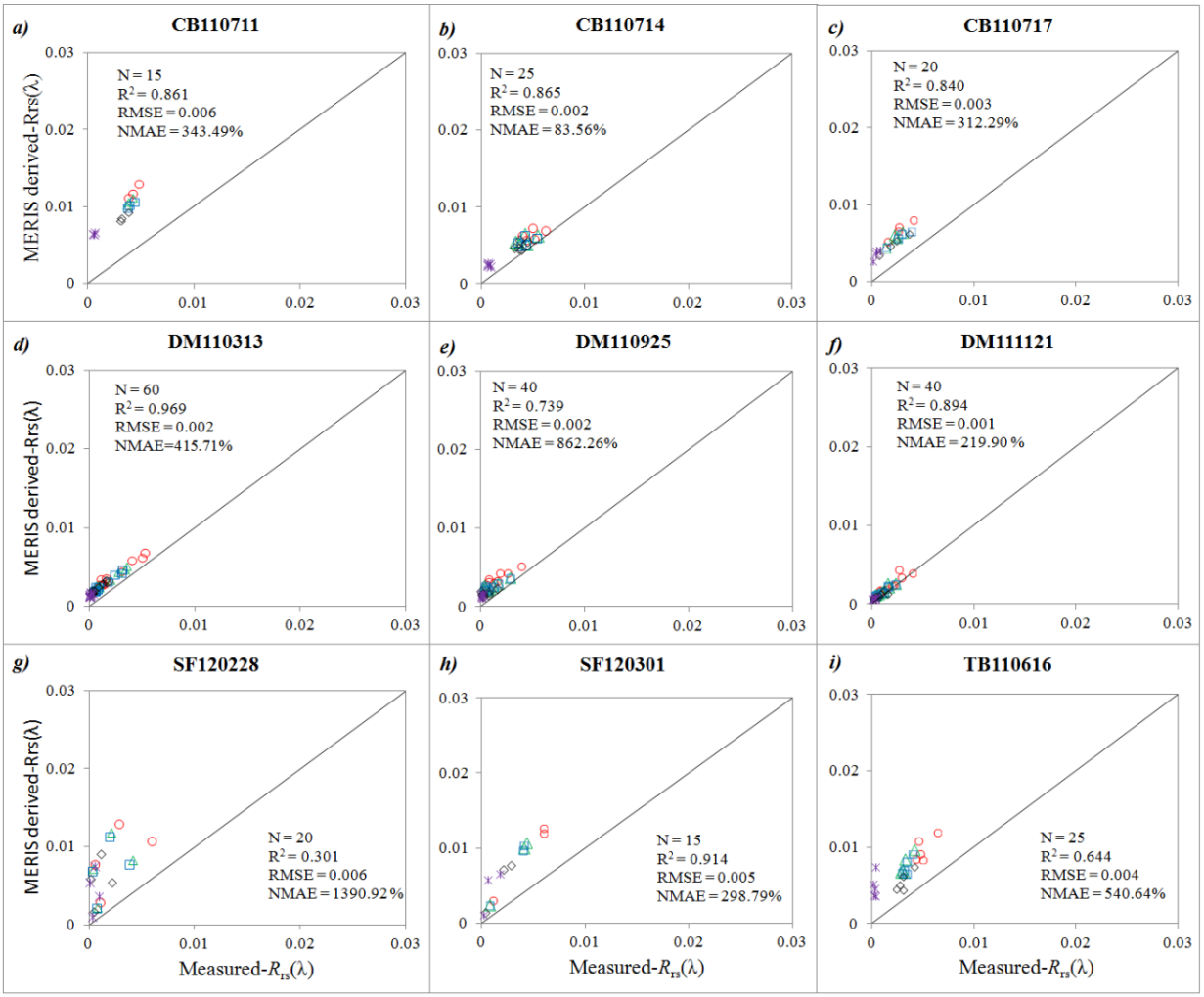

Figure 3.6. Comparisons between the *in situ*-measured and MERIS-derived water-leaving remote sensing reflectance by the N-GWI for MERIS bands 6–10 in American sea: *(a-c)* Chesapeake Bay; *(d-f)* Deadman Bay; *(g-h)* South Florida's Sea and *(i)* Tampa Bay. The center wavelength at each band is shown in the legend. The black line represents the 1:1 line.

The C2WP algorithm produced higher accuracy for all American sea waters: Chesapeake Bay data (CB110711, CB110714 and CB110717); Deadman Bay (DM110313, DM110925 and DM111121); South Florida's Sea (SF120228 and SF120301) and Tampa Bay (TB110616) with RMSE in range of 0.000 to 0.001. The similar performance achieved by GWI and MUMM algorithms, except in CB110711 (RMSE=0.002), SF120228 (RMSE=0.003) and TB110616 (RMSE=0.007) for GWI; and CB110711 (RMSE=0.002), CB110717 (RMSE=0.002) and TB110616 (RMSE=0.003) for MUMM. According to these results, C2WP algorithm is suitable for atmospheric correction in all American sea waters used in this study, whereas the developed algorithm achieved a lower accuracy than three existing algorithms.

3.4 Discussion

3.4.1 The performance of N-GWI

3.4.1.1 In turbid inland waters

In this study, all data collected in Asian turbid inland waters (K060218, K080807, K100518, D071024 and D090313) can be successfully processed by N-GWI with the NMAE less than 22% and RMSE less than 0.003 (except for D090313). As mentioned in Section 3.2.1.3, two field campaigns in Lake Dianchi, China were performed one day before satellite acquisition. The wind speed information in Lake Dianchi on the field campaign date as well as one day before and after was obtained from the closest meteorological station (Kunming Meteorological Station).

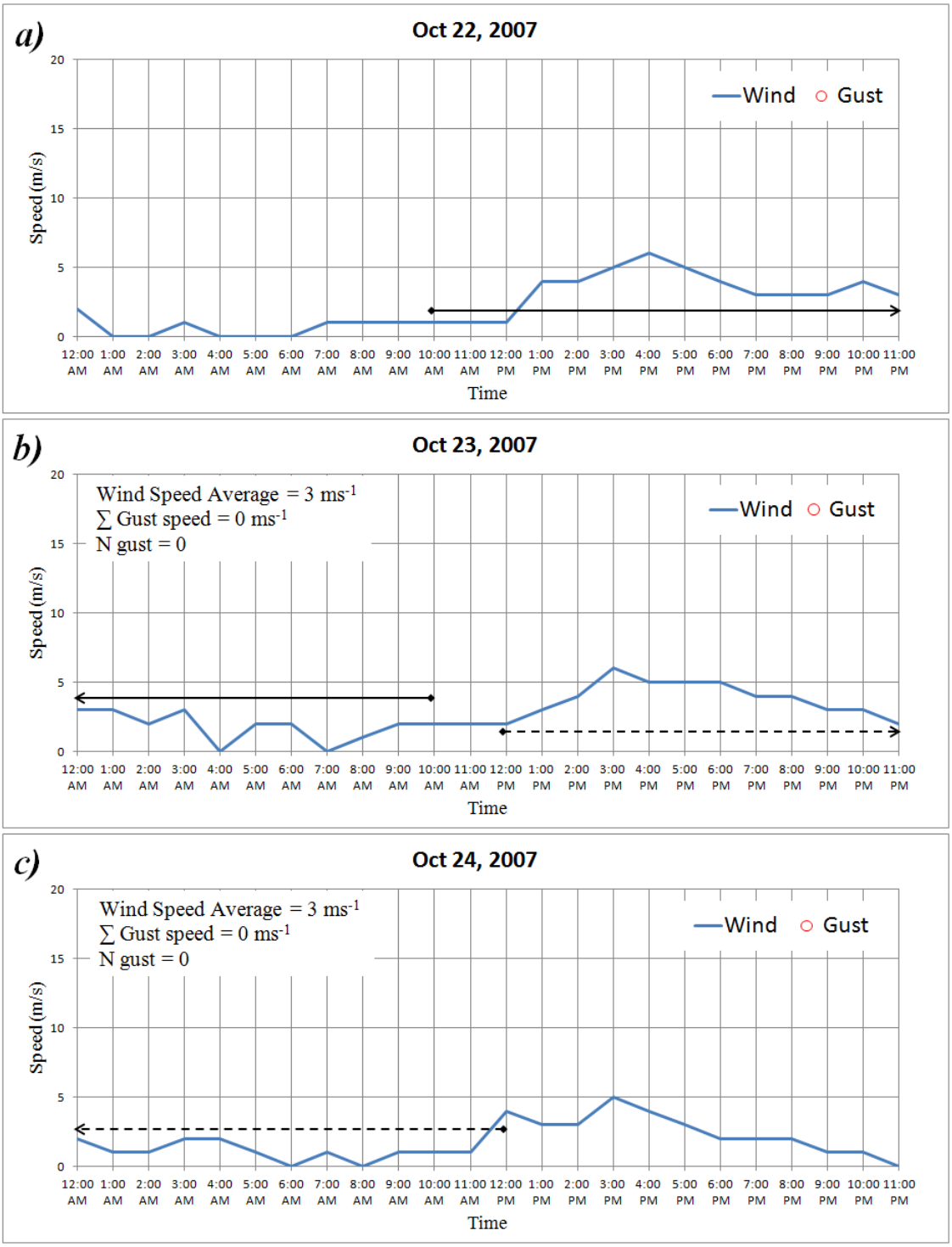
a)
Oct 22, 2007
Wind
Gust
Speed (m/s)
Time
b)
Oct 23, 2007
Wind Speed Average = 3 ms-1
∑ Gust speed = 0 ms-1
N gust = 0
Wind
Gust
Speed (m/s)
Time
c)
Oct 24, 2007
Wind Speed Average = 3 ms-1
∑ Gust speed = 0 ms-1
N gust = 0
Wind
Gust
Speed (m/s)
Time

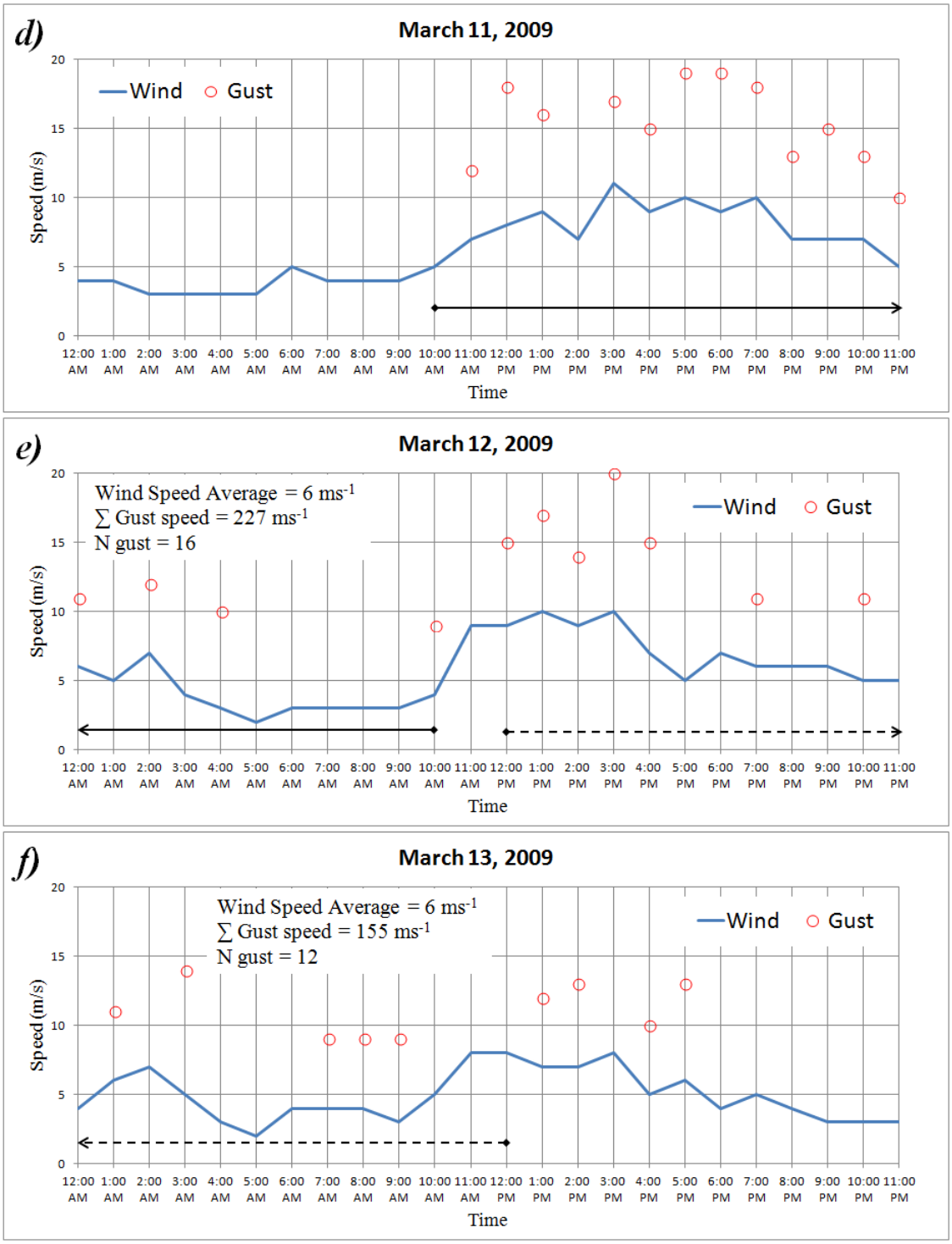

Figure 3.7. Wind speed data over Lake Dianchi recorded by Kunming Meteorological Station (obtained from wunderground.com). *In situ* measurement time at 10.00; satellite acquisition time at 11.30 CST.

The wind speed on October 22, 2007 (one day before field campaign), October 23, 2007 (field campaign date) and October 24, 2007 (image acquisition date) were slow and stable with averaged values of 2, 3, and 2 ms^{-1}, respectively and without gust blew (Figures 3.7(*a-c*). In contrast, the wind speed on March 11, 2009 (one day before field campaign), March 12, 2009 (field campaign date) and March 13, 2009 (image acquisition date) were strong and unstable with averaged values of 6, 6.16, and 5.92 ms^{-1}, respectively and a number of gusts blew (Figures 3.7(*d-f*)). These data indicated that water qualities in periods between field campaign and MERIS data acquisition were similar in 2007, whereas were very different in 2009 due to the sediment resuspentation by strong wind before field campaign. This is considered as the reason why an underestimation occurred in 2009 dataset of Lake Dianchi.

3.4.1.2 In less turbid sea's waters

All data obtained from SeaBASS database in this study (Deadman Bay, Tampa Bay, Chesapeake Bay and South Florida's Sea) were categorized as turbid water by Shi and Wang (2007). However, comparing with the two Asian lakes used in this study, their turbidities are still low. Therefore, I grouped the SeaBASS data into less turbid waters. Generally the N-GWI gave overestimations in these waters (Figure 3.6). This is probably because that the low turbidities and thus low backscattering from water column combined with strong water absorption at 754 nm resulted in very low reflectance at this reference wavelength and thus cannot provide enough signal-to-noise ratio (SNR) for accurate $b_{bp}(754)$ estimation by equation 3.11. These results indicate that the N-GWI algorithm is

not suitable to be applied in the clear and less turbid waters. On the other hand, the GWI, C2WP and MUMM produced higher accuracies in these American sea waters, indicating a potential to use these AC algorithm in less turbid waters.

3.4.2 Advantages and Limitation of the N-GWI

The N-GWI has four advantages. First, the N-GWI was developed to estimate water-leaving reflectance pixel by pixel, and then estimate aerosol contribution pixel by pixel. Therefore, it does not require to assume a spatial homogeneity for aerosol state over a water area as in SCAPE-M and MUMM, to assume a spatial homogeneity for the ratios of water-leaving reflectance at two NIR wavelengths as in MUMM, to need training data like the C2WP. Second, the N-GWI used a fixed aerosol model (i.e. fixed epsilon value) rather than selecting it every time. Figure 3.8 shows the performance of N-GWI in Lake Kasumigaura for three different epsilon values. Figures 3.8(*a-c)* are for using a minimum epsilon value among 80 aerosol models in SeaDAS, whereas Figures 3.8(*d-f)* and 3.8(*g-i*) are for using the average and maximum epsilon values, respectively. The performances of N-GWI were relatively similar in K060218 for all epsilon values (RMSE=0.003); comparable performances in K080807 with RMSE of 0.002, 0.002 and 0.001 for minimum, maximum and average epsilon values, respectively; and different performance in K100518 with RMSE of 0.003, 0.005 and 0.002 for minimum, maximum and average epsilon values, respectively. The use of average epsilon value could represent most cases of atmospheric status.

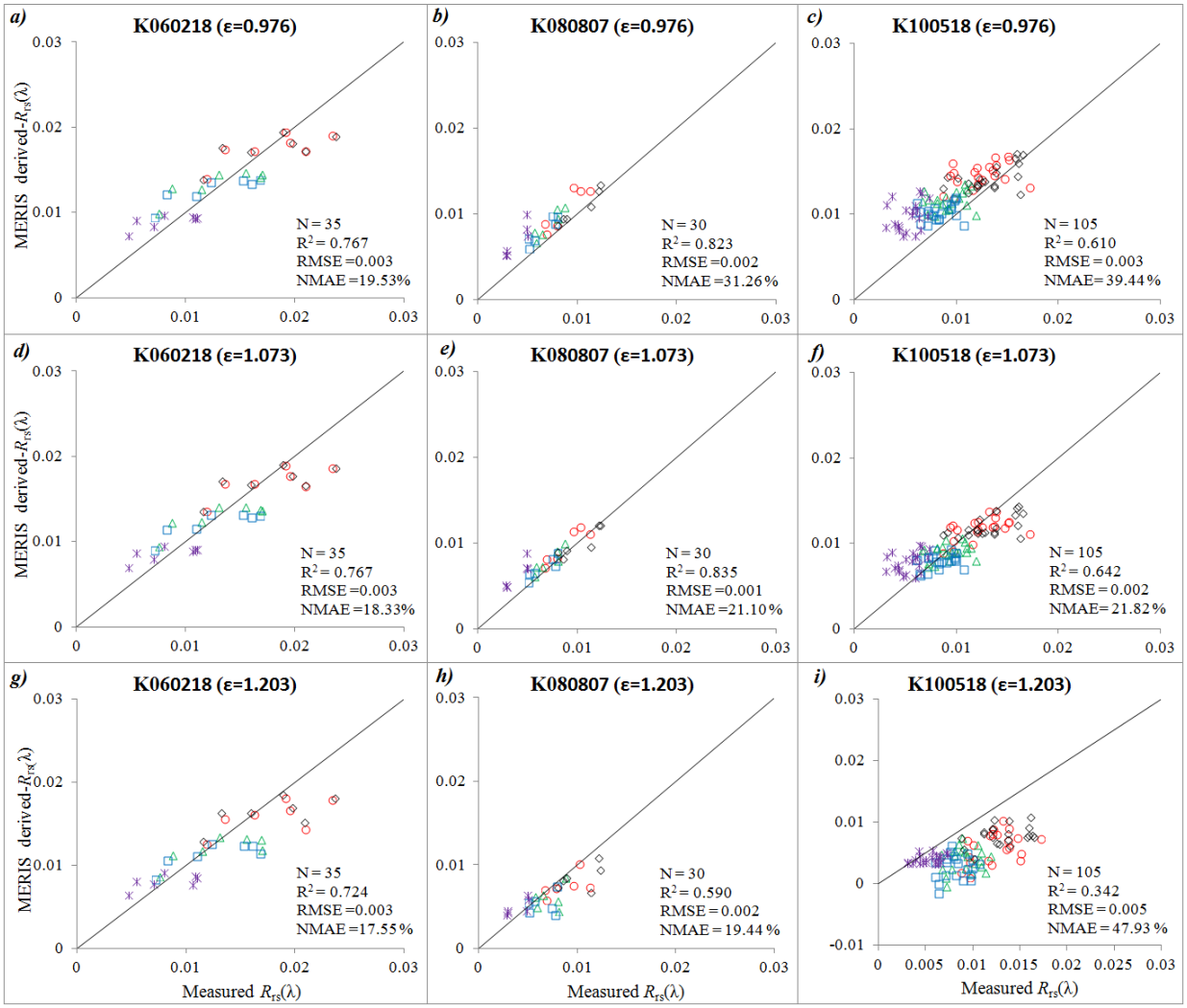

Figure 3.8. Comparisons between the in situ-measured and MERIS-derived water-leaving remote sensing reflectance by the N-GWI for MERIS bands 6–10 in Lake Kasumigaura. Epsilon (ε(779,865)) value: (*a-c*) minimum; (*d-f*) average and (*g-i*) maximum. The center wavelength at each band is shown in the legend. The black line represents the 1:1 line.

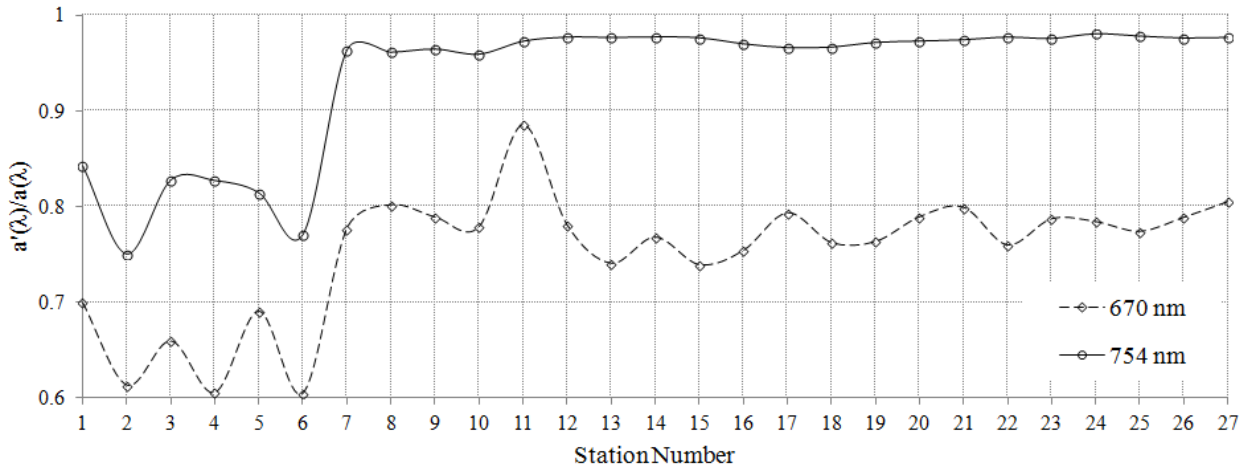

Figure 3.9. The ratio of estimated and measured total absorption (a'(λ)/a(λ)) at 27 sampling sites collected in Lake Kasumigaura for two reference band (670 nm and 754 nm). The estimated total absorption at 670 nm (a'(670)) is calculated from chlorophyll-a-based empirical equation used in GWI algorithm. The estimated total absorption at 754 nm (a'(754)) is assumed to be equal to the water absorption. Station number 1-6 from K080807 and 7-27 from K100518.

Third, the N-GWI used 754 nm as the reference band and thus makes the assumption for total absorption coefficient at this wavelength become valid even for turbid waters. Figure 3.9 shows the ratio of estimated and measured total absorption at 754 nm outperformed that at 670 nm. The averaged ratio at 754 nm are 0.8 and 0.98 in K080807 (station number 1-6) and in K100518 (station number 7-27), respectively. Even though the measured-chlorophyll-*a* concentration were used to calculate the estimated-absorption at 670 nm through an empirical equation (Equation 3.9), their performance are still poorer than that achieved by the use of 754 nm. Fourth, the N-GWI used a semi-analytical equation to calculate Y value for extrapolating a bio-optical parameter (i.e., b_{bp}) from reference to NIR wavelength (Equation 3.14) rather than the use of empirical equation (Equation 3.13) in the GWI.

Considering the basic assumptions used in the N-GWI, the algorithm has three critical limitations: (*1*) the N-GWI does not promise accuracy for shorter wavelengths; (*2*) in clear and less turbid water, the low signal at reference band (754 nm) make an invalid estimation of aerosol scattering reflectance, and (*3*) the N-GWI cannot produce a sufficient accuracy in extremely turbid water when the assumption of backscattering coefficient at 754 nm mostly comes from water is invalid. Further investigation of applicability of the developed algorithm should be carried out in future study.

3.4.2 Implementation to other remote sensing sensors

Although the N-GWI was designed for MERIS sensor, there is a possibility to extend its implementation to other sensors. Corresponding to the three improvements in the N-GWI,

I need to adjust its parameters and equations based the characteristic of sensor (e.g., wavelength availability, number of bands). For example, for using MODIS or SeaWIFS sensors, I need to: (*1*) change the reference band, because MODIS and SeaWIFS have not equipped by wavelength of 754 nm, the reference band should be shifted to 748 and 765 respectively; and (*2*) change the bands couple for Y estimation using two NIR bands in MODIS and SeaWIFS; and reproduce the semi-analytical equation using synthetic data.

3.5 Conclusions

I developed a new atmospheric correction algorithm (N-GWI) for inland turbid waters. The N-GWI was based on the scheme of the GWI that was implemented in SeaDAS for less turbid waters. The N-GWI includes three improvements: (*1*) using a fixed aerosol model; (*2*) shifting the reference band from visible to NIR; and (*3*) generating a semi-analytical model for the estimation of spectral slope of particle backscattering.

The N-GWI showed good performance for two turbid inland waters (Lakes Kasumigaura and Dianchi) with the RMSE less than 0.003 except for the data in Lake Dianchi in 2009, but poor performance for four less turbid sea waters in America. These results show the limitations of the N-GWI in less turbid waters. Considering the advantages as well as its limitations, the N-GWI gave a promising result for atmospheric correction in turbid waters.

Chapter IV Development of a new atmospheric correction algorithm for applying MERIS data to turbid inland waters II: further validation and an application for long-term chlorophyll-*a* monitoring in Lake Kasumigaura, Japan

4.1 Introduction

Monitoring water quality in inland waters is required to support the sustainable use of freshwater ecosystems. Considering the ability to provide routine data with a large area coverage and sufficient spatial resolution, remote-sensing approach is suitable for monitoring spatial and temporal heterogeneities of water bodies (Liu, Islam, and Gao 2003). One of the most important applications of water color remote-sensing is to estimate the chlorophyll-*a* concentration, which is a key parameter for assessing the water quality (Gons 1999; O'Reilly et al. 1998). However, the successful of chlorophyll-*a* retrieval from satellite remote-sensing data strongly depend on the accuracy of not only retrieval algorithm of the chlorophyll-*a* concentration but also atmospheric correction (Ruddick, Ovidio, and Rijkeboer 2000; Yang et al. 2011; Sathyendranath, Prieur, and Morel 1987).

In clear waters, both chlorophyll-*a* retrieval algorithms (e.g., O'Reilly et al. 1998) and atmospheric corrections algorithms (e.g., Gordon and Wang 1994) have been developed with sufficient accuracies. In contrast, although the algorithms for retrieving

chlorophyll-*a* have been well developed in turbid waters (e.g., Gitelson et al. 2008, 2011; Le et al. 2009; Yang et al. 2010, 2011), the atmospheric correction algorithms for these kinds of waters are still a challenge (Jaelani et al. 2013).

In Chapter III, I developed a new atmospheric correction algorithm for turbid waters, which is based on the scheme of Bailey, Franz, & Werdell (2010) and named as N-GWI (New- the standard Gordon and Wang algorithm with an Iterative process and a bio-optical model). Performance of the N-GWI algorithm was primarily evaluated by comparing atmospherically corrected remote sensing reflectance ($R_{rs}(\lambda)$) with *in situ*-measured $R_{rs}(\lambda)$ in two turbid Asian lakes and four American sea waters. Since the N-GWI algorithm was specifically developed for waters with higher turbidities, only the atmospherically corrected $R_{rs}(\lambda)$ at longer wavelengths (longer than 620 nm) would be required because the $R_{rs}(\lambda)$ at shorter wavelengths could not be used for retrieving water quality parameters in these waters (Gitelson 1992; Gitelson et al. 2008; Yang et al. 2011; Yu et al. 2014)

The objectives of this chapter were to (*1*) further validate the performance of the N-GWI algorithm by comparing the measured chlorophyll-*a* concentration with estimated one; and (*2)* demonstrate a possibility for long-term water quality monitoring by satellite data in Lake Kasumigaura, Japan. For these objectives, I firstly processed 215 MERIS images, which cover the Lake Kasumigaura, Japan and were acquired between 2003 and 2012, using the N-GWI algorithm as well as other four existing atmospheric correction algorithms to produce atmospheric corrected $R_{rs}(\lambda)$. I then inputted these

atmospherically corrected $R_{rs}(\lambda)$ to chlorophyll-*a* retrieval algorithm for chlorophyll-*a* estimation and compared the results with the measured chlorophyll-*a* collected in Lake Kasumigaura.

4.2 Methods

4.2.1 Study area

Lake Kasumigaura, Japan (36^{o} 9'N; 140^{o} 14' E) is located in the eastern part of Japan's Kanto's plain and has a surface area of 171 km^2 (only for the western part), an average depth of 4.0 m, and a maximum depth of 7.3 m. It is the second largest lake in Japan (after Lake Biwa) and it is a eutrophic-turbid lake due to high loads of nutrients and resuspension of bottom sediments by wind (Matsushita et al. 2009). During the last two or three decades, Lake Kasumigaura's average TSM concentration increased from 14.1 to 26.4 g m^{-3} (due mainly to the re-suspension of bottom sediments by wind), the chlorophyll-a concentration decreased from 87 to 61 mg m^{-3} (owing to the watershed management by the local government), and the Secchi disk depth decreased from 70 to 52 cm (CEBES 2011).

4.2.2 Measured chlorophyll-a

There are two measured chlorophyll-*a* datasets were used in this study. The first dataset is collected by Team of University of Tsukuba. Three data collection campaigns were undertaken in 2006 (Feb. 18, 10 sites), 2008 (Aug. 7, 14 sites), and 2010 (May 18, 26 sites), and the campaigns were timed to coincide with the acquisitions of the MERIS images. The data collecting sites, which located less than one MERIS pixel away from

the banks and corresponding MERIS pixels were contaminated by clouds were excluded from the analyses. Accordingly, 7, 6, and 21 sites remained for comparison in Feb. 2006 (denoted as K060218 hereafter), Aug. 2008 (denoted as K080807 hereafter) and May 2010 (denoted as K100518 hereafter), respectively (Figures 4.1(*b-d*)). The range of water quality parameters during these campaigns are presented in Table 4.1.

The second dataset is obtained from Lake Kasumigaura Database (CEBES 2011), which is a long term database maintained by Center for Environmental Biology and Ecosystem Studies (CEBES), National Institute of Environmental Sciences (NIES), Japan for monitoring water qualities in Lake Kasumigaura. Water samples were regularly collected by boat at 10 sites on the second Wednesday every month since 1977. This database contains weather data, water quality parameters (e.g., pH, water temperature, electric conductivity, DOC, Secchi depth, COD, pigments including chlorophyll-*a* concentration, SS), and biological data (e.g., bacteria, protozoa, phytoplankton, NPP). In which, chlorophyll-*a* concentration data collected from four sites (sites, 3, 7, 9, 12; Figure 4.1(*a*)) between 2004 and 2011 (corresponding to available MERIS data in Lake Kasumigaura) were used in this study, and denoted as NIES-dataset hereafter. Field survey dates during the above period are summarized in Table 4.2. The data after March 2011 are not available because they are still not yet opened for public use.

Water samples of K060218, K080807, and K100518 were collected from the water surface (0.2-0.5 m) using 4.0 liters polycarbonate bottles at each site. While water samples of NIES dataset were collected from 0.0 to 2.0 m depth by using a column water sampler of 2.0 m length and of 6.0 cm diameter.

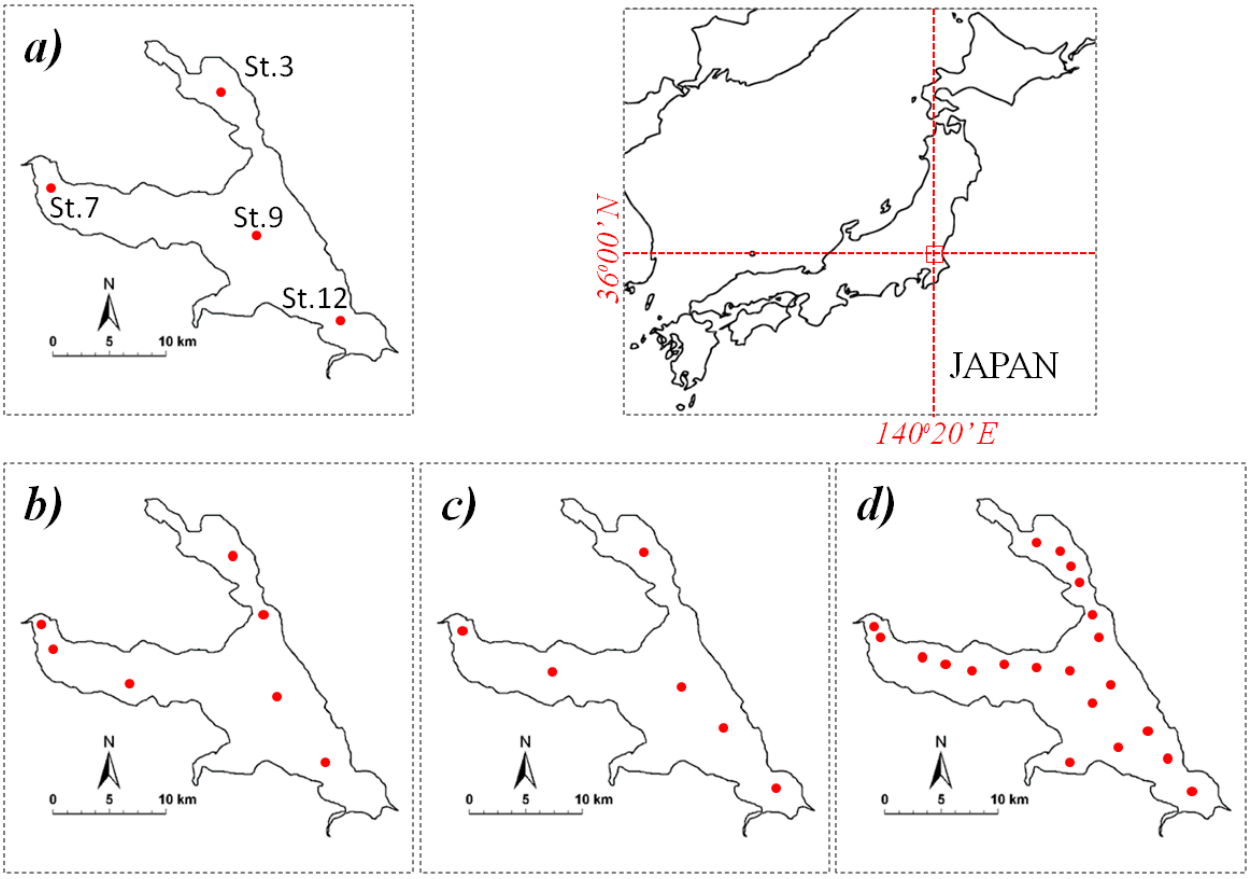

Figure 4.1. Location of sampling stations: (*a*) NIES-dataset regular stations for long-term monitoring; (*b*) K060218; (*c*) K080807; and (*d*) K100518

Table 4.1. Range of water quality data in Lake Kasumigaura, Japan

	Min.	Max.	Median	Average	SD	CV(%)	*N*
K060218							
Chl-a (mg m^{-3})	69.65	95.02	84.54	83.99	9.69	11.54	7
TSS (g m^{-3})	22.00	46.10	32.80	33.71	8.11	24.05	7
$a_{CDOM}(440)$ (m^{-1})	no data	no data	no data	no data	no data	no data	0
K080807							
Chl-a (mg m^{-3})	44.40	76.90	62.90	62.18	11.92	19.17	6
TSS (g m^{-3})	11.70	21.10	16.40	16.73	3.18	19.02	6
$a_{CDOM}(440)$ (m^{-1})	1.15	1.36	1.15	1.20	0.09	7.23	6
K100518							
Chl-a (mg m^{-3})	36.60	83.40	44.80	53.70	17.61	32.80	21
TSS (g m^{-3})	18.00	27.73	21.17	22.13	3.59	16.22	21
$a_{CDOM}(440)$ (m^{-1})	0.51	0.94	0.62	0.71	0.16	22.23	21

Note: Chl-a: chorophyll-a concentration; TSS: total suspended solids;
$a_{CDOM}(440)$: absorption coefficient of CDOM at 440 nm
SD: Standard deviation; CV: coefficient of variation (SD/average of parameter)
N: number of samples.

Table 4.2. Field measurement date

Year / Month	2004	2005	2006	2007	2008	2009	2010	2011
January	7	12	11	10	9	7	14	12
February	10	9	8	7	13	12	10	9
March	10	9	8	7	12	12	10	9
April	7	13	12	11	10	8	7	n/a
May	12	11	10	9	7	13	12	n/a
June	9	8	7	13	11	10	9	n/a
July	7	13	12	11	9	9	7	n/a
August	11	10	9	8	6	12	18	n/a
September	9	8	13	5	10	9	8	n/a
October	14	12	11	10	8	7	13	n/a
November	10	9	8	7	12	11	10	n/a
December	8	7	13	12	10	9	8	n/a

Except for water sampling method, other methods for keeping and processing water samples for chlorophyll-*a* measurement are all similar. The water samples were kept in ice boxes during the field survey, and taken to the laboratory within approximately 0.5 h after the field surveys. Then water samples were filtered by Whatman GF/F filter, and the filter paper was kept in a freezer under a temperature of -20^{o}C. Chlorophyll-*a* was extracted using methanol (100%) at 4°C under dark conditions for 24 h. The optical density of the extracted chlorophyll-*a* was measured at four wavelengths (750, 663, 645 and 630 nm) by absorption spectrum method, and the concentration was calculated according to SCOR-UNESCO equations (SCOR-UNESCO 1966).

4.2.3 MERIS data

I searched all available full-resolution MERIS data (level-1b) over Lake Kasumigara, Japan between 2003 and 2012 by using EOLi (ESA's Link to Earth Observation, http://earth.esa.int/EOLi/EOLi.html), the European Space Agency's client for Earth Observation Catalogue and Ordering Services. In total, 492 MERIS images were found covering whole or a part of Lake Kasumigaura. After screened images that were contaminated by cloud over Lake Kasumigaura using the preview images on EOLi, I downloaded 215 cloud-free MERIS images. The numbers of the available MERIS images for each month are presented in Table 4.3. In which, three MERIS images were acquired on February 18, 2006, August 7, 2008, and May 18, 2010, which are the same dates as my three field surveys; other 39 MERIS images were acquired with the maximum different time from NIES-dataset within 3 days (9, 12, 11 and 7 images with 0, 1, 2 and 3

days different, respectively). The time difference between field surveys and MERIS acquisitions are presented in Table 4.4.

4.2.4 Candidate Atmospheric Correction algorithms

The first candidate is the N-GWI algorithm, which was developed in my previous work and installed in SeaDAS software package (version 6.4, http://seadas.gsfc.nasa.gov/) by modifying the original code of GWI and recompiling the new code. There were three improvements in the N-GWI: (*a*) using a fixed aerosol model (relative humidity of 75% and ratio of fine particles of 20%). At the longer wavelengths, since the differences among different aerosol models are small, it is possible to just use a fixed aerosol model to carry out atmospheric correction for different pixels, and thus can avoid invalid epsilon estimation for selecting aerosol model in the original code; (*b*) shifting the reference band from 670 nm to 754 nm. At the wavelength of 754 nm, the total absorption coefficient can be assumed to approximately be equal to the pure water absorption coefficient, and thus can semi-analytically calculate backscattering coefficient of particles; and (*c*) using a semi-analytical model to replace empirical model in the original code for the estimation of spectral slope of particle backscattering.

For comparison, I also selected other four existing atmospheric correction algorithms developed for turbid waters. They are: (*1*) the GWI algorithm (Stumpf et al. 2003; Bailey, Franz, and Werdell 2010); (*2*) the MUMM algorithm (Management Unit of the North Sea Mathematical Models; Ruddick, Ovidio, and Rijkeboer [2000]); (*3*) the C2WP algorithm (Case-2 water Processor; Doerffer and Schiller [2008]); and (*4*) the

SCAPE-M algorithm (Self-Contained Atmospheric Parameters Estimation for MERIS data; Guanter, Sanpedro, and Moreno [2007]; Guanter et al. [2010]). The first and second algorithms are available in SeaDAS software; the third algorithm is available in BEAM toolbox (version 4.11, http://www.brockmann-consult.de/beam/). Since the SCAPE-M algorithm is not yet available for public use now, I asked algorithm's author (Dr. Luis Guanter) to process three MERIS images (Feb. 18, 2006; Aug. 7, 2008; May 18, 2010; corresponding to my own field surveys) using the SCAPE-M algorithm.

All downloaded MERIS images were processed using SeaDAS software package or BEAM toolbox to produce the atmospherically corrected $R_{rs}(\lambda)$ by N-GWI, GWI, MUMM, and C2WP algorithms at center wavelengths of 620, 665, 681, 709 and 754 nm (five longer wavelengths, corresponding to MERIS band 6-10). To evaluate the performance of the N-GWI, I extracted the average $R_{rs}(\lambda)$ of the pixels nearest the sampling locations along with the eight surrounding pixels (3 X 3 window) from the atmospherically corrected MERIS images, and compared estimated chlorophyll-*a* with measured chlorophyll-*a* to avoid potential error in the geometric correction and dynamics of water bodies, as well as the potential error in spatial variability (Han and Jordan 2005).

Table 4.3. The number of MERIS images

Month \ Year	2003	2004	2005	2006	2007	2008	2009	2010	2011	2012
January	0	0	1	0	5	0	4	6	2	0
February	0	0	0	1	4	7	1	4	3	0
March	0	0	2	4	7	3	4	4	1	1
April	0	3	1	5	5	3	8	4	0	0
May	0	2	1	3	4	5	5	1	0	0
June	0	1	0	3	4	3	2	0	0	0
July	0	8	0	1	1	0	2	1	0	0
August	0	4	0	2	2	2	0	2	0	0
September	0	0	0	1	3	1	5	2	0	0
October	0	1	1	1	4	8	5	1	0	0
November	0	0	0	1	0	6	3	3	0	0
December	1	0	1	3	2	3	1	2	4	0

Table 4.4. MERIS and Lake Kasumigaura database match-up data

Month	2004	2005	2006	2007	2008	2009	2010	2011
January	n/a	-1	n/a	-1	n/a	-1	-1	n/a
February	n/a	n/a	n/a	-1	0	n/a	-2	-2
March	n/a	n/a	-2	0	n/a	n/a	+2	n/a
April	-2	n/a	+2	n/a	n/a	0	-1	n/a
May	+2	n/a	n/a	0	n/a	+1	n/a	n/a
June	n/a	n/a	-1	0	+2	n/a	n/a	n/a
July	0	n/a	n/a	n/a	n/a	n/a	n/a	n/a
August	-3	n/a	-3	-1	0	n/a	n/a	n/a
September	n/a	n/a	n/a	-1	-3	0	+1	n/a
October	+3	n/a	-3	0	+2	-3	-2	n/a
November	n/a	n/a	n/a	n/a	n/a	-3	-1	n/a
December	n/a	n/a	-2	n/a	n/a	n/a	n/a	n/a

+(-)D = Meris acquisition time was D days after (before) field survey

4.2.5 Estimation of Chlorophyll-a concentration using SAMO-LUT

To estimate chlorophyll-*a* concentration, the SAMO-LUT algorithm (semi-analytical model optimizing and look-up tables) proposed by Yang et al. (2011) was used. Atmospherically corrected reflectance $R_{rs}(\lambda)$ by the N-GWI as well as the GWI, C2WP, MUMM and SCAPE-M algorithms were used as inputs of the SAMO-LUT.

The SAMO-LUT algorithm is originally proposed for simultaneously retrieving concentrations of the three water constituents (i.e., phytoplankton, NAP, and CDOM). The basic idea of the SAMO-LUT involves the use of an imaginary Case-2 water body, in which only one constituent changes while the other two are controlled as constants. A comprehensive synthetic dataset was used for model calibration, rather than the use of in situ data. In this way, I hoped to obtain not only a large sample size without a sampling bias for model calibration, but also a series of special cases to avoid effects from other constituents and thus improve model performance (e.g., a dataset only with various Chl-a while concentrations of NAP and CDOM are constants).

The main procedures of the SAMO-LUT are summarized as follows (Yu et al. 2014):

Step 1: Generation of simulation dataset. The $R_{rs}(\lambda)$ spectra were generated based on the SIOPs from target water and a bio-optical model. In the present study, only the SIOPs collected from Lake Dianchi were used due to the lack of complete SIOPs data for other lakes. The concentrations of Chl-a and NAP (i.e., tripton in the original paper), as well as the absorption coefficient of CDOM at 440 nm were varied in a wide range of 1-300 mg m^{-3} (31 values), 1-250 g m^{-3} (28 values) and 0.1-10 m^{-1} (23 values), respectively.

In all, 19,964 sample spectra were generated.

Step 2: Computation of selected semi-analytical indices. Three semi-analytical indices were selected for the estimation of Chl-a, NAP and CDOM, based on their reasonableness and performance. The selected indices were: a 3-band index ([1/R_{rs}(665)-1/R_{rs}(709)]*R_{rs}(754)) for Chl-a, remote-sensing reflectance for the band centered 754 nm (R_{rs}(754)) for NAP, and the band-ratio R_{rs}(560)/R_{rs}(665) for CDOM. The synthetic reflectances were resampled to the bandwidths of the MERIS (Medium Resolution Imaging Spectrometer) sensor based on its spectral response function, and then the selected indices were calculated.

Step 3: Construction of look-up tables. I constructed three 2-dimensional look-up tables containing the coefficients of the estimation model for one constituent of interest, determined by the concentrations of the other two constituents. For instance, for the estimation of Chl-a, increments of 1 g m^{-3} for NAP and of 0.1 m^{-1} for CDOM were respectively used in the ranges of 1-250 g m^{-3} and 0.1-10 m^{-1}, and the regression coefficients corresponding to different combinations of NAP and CDOM were stored in the LUT.

Step 4: Initial estimations of Chl-a and NAP. I derived initial values of Chl-a and NAP using two general estimation models obtained through regression analysis between the simulated reflectance and corresponding Chl-a and NAP. The two general estimation models were:

$$Chl-a = 223.86\left({}^{1}/_{R_{rs}(665)} - {}^{1}/_{R_{rs}(709)}\right)R_{rs}(754) + 23.95 \qquad (4.1)$$

$$NAP = 49909R_{rs}^2(754) - 61.38R_{rs}(754) + 4.74 \quad (4.2)$$

The calculated initial Chl-a and NAP were then used to estimate initial CDOM through a prepared LUT in step 3.

Step 5: Iteration to select more appropriate model coefficients. The estimation models were improved according to the initial Chl-a, NAP, and CDOM. After that, the refined Chl-a, NAP, and CDOM were obtained by using the improved estimation models.

Step 6: End of iteration. I found a more appropriate estimation model from the LUTs for each water constituent through the iterative use of the newly obtained Chl-a, NAP and CDOM. The iteration was stopped when the difference between the current and last output was sufficiently small. Generally, the differences become stable after the 10*th* iteration.

4.2.6 Accuracies Assessments

Two indices, root mean square error (RMSE) and normalized mean absolute error (NMAE), were used to assess the accuracy of atmospheric correction. These indices were defined as follows:

$$RMSE = \sqrt{\frac{\sum_{i=1}^{N}\left(x_{\mathrm{esti,i}} - x_{\mathrm{meas,i}}\right)^2}{N}} \quad (4.3)$$

$$NMAE = \frac{1}{N}\sum_{i=1}^{N}\left|\frac{x_{\mathrm{esti,i}} - x_{\mathrm{meas},i}}{x_{\mathrm{meas}}}\right| 100\% \quad (4.4)$$

where $x_{meas,i}$ and $x_{esti,i}$ are the measured and estimated values, respectively, and N is the sample size. The RMSE gives the absolute scattering of the retrieved water-leaving reflectance, and the NMAE represents the uncertainty associated with satellite-derived distribution. The determination coefficient (R^2) between *in situ* measured $R_{rs}(\lambda)$ and estimated $R_{rs}(\lambda)$ from atmospherically corrected MERIS data was also calculated.

4.3 Results

4.3.1 Validation using my dataset

Figure 4.2 shows a comparison of measured (*x*-axis) and estimated (*y*-axis) chlorophyll-*a* concentration by using my own dataset in Lake Kasumigaura. The estimated chlorophyll-*a* concentrations were derived from atmospherically corrected MERIS data by different atmospheric correction algorithms (the GWI: Figures 4.2(*a*-*c*); the MUMM: Figures 4.2(*d*-*f*); the C2WP: Figures 4.2(*g*-*i*); the SCAPE-M: Figures 4.2(*j*-*l*); and the N-GWI: Figures 4.2(*m*-*o*)) and the SAMO-LUT algorithm. Chlorophyll-*a* concentration estimated from the *in situ*-measured remote-sensing reflectance and the SAMO-LUT were also shown in Figures 4.2(*p*-*r*) for comparison. For the dataset of K060218, the SCAPE-M algorithm achieved the best performance with RMSE of 10.27 mg m^{-3}, followed by the GWI (RMSE=12.13 mg m^{-3}), the MUMM (RMSE=14.56 mg m^{-3}), the N-GWI (RMSE=24.98 mg m^{-3}) and the C2WP (RMSE= 56.59 mg m^{-3}).

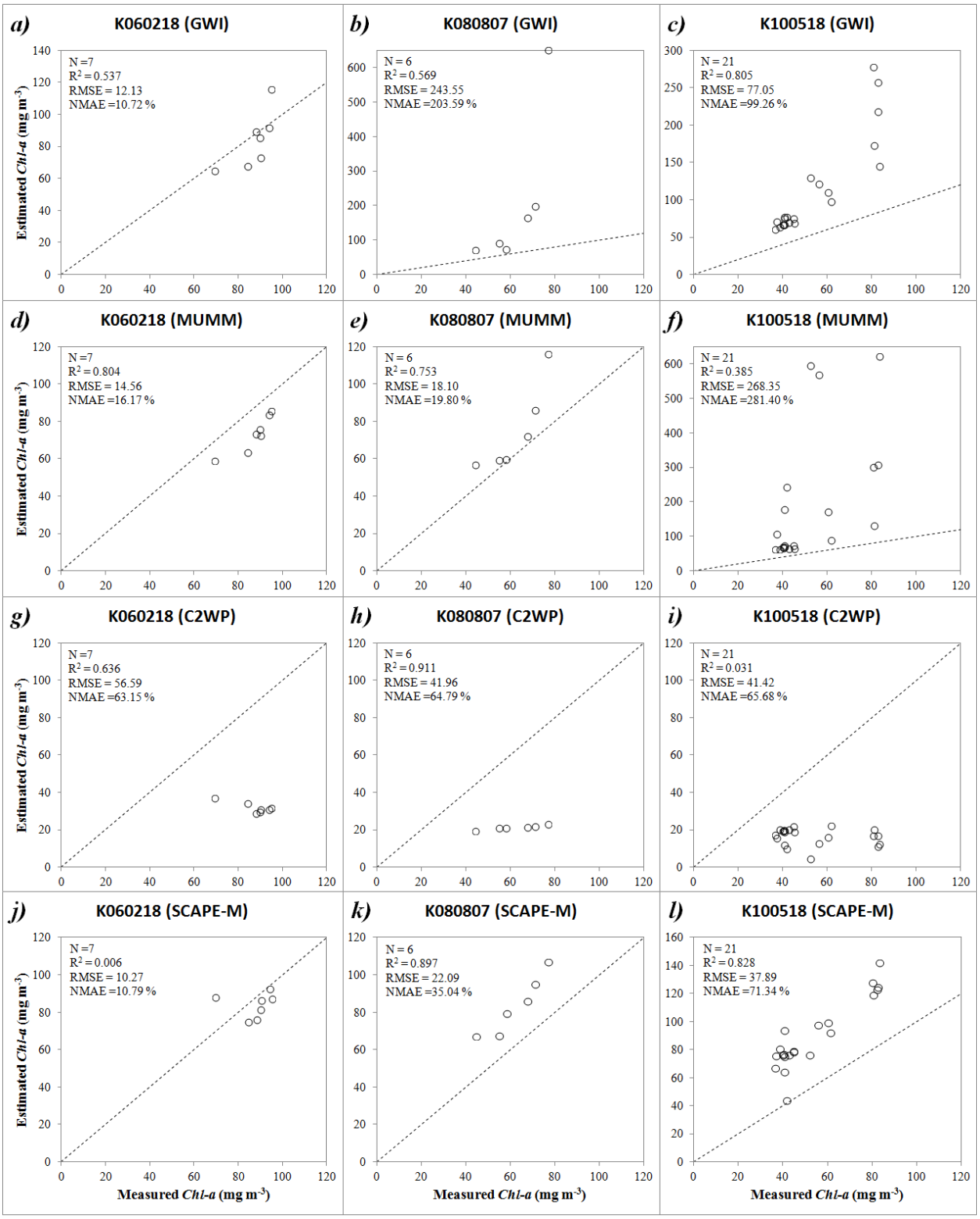
a) K060218 (GWI)
N =7
R² = 0.537
RMSE = 12.13
NMAE =10.72 %
b) K080807 (GWI)
N = 6
R² = 0.569
RMSE = 243.55
NMAE =203.59 %
c) K100518 (GWI)
N = 21
R² = 0.805
RMSE = 77.05
NMAE =99.26 %
d) K060218 (MUMM)
N =7
R² = 0.804
RMSE = 14.56
NMAE =16.17 %
e) K080807 (MUMM)
N = 6
R² = 0.753
RMSE = 18.10
NMAE =19.80 %
f) K100518 (MUMM)
N = 21
R² = 0.385
RMSE = 268.35
NMAE =281.40 %
g) K060218 (C2WP)
N =7
R² = 0.636
RMSE = 56.59
NMAE =63.15 %
h) K080807 (C2WP)
N = 6
R² = 0.911
RMSE = 41.96
NMAE =64.79 %
i) K100518 (C2WP)
N = 21
R² = 0.031
RMSE = 41.42
NMAE =65.68 %
j) K060218 (SCAPE-M)
N =7
R² = 0.006
RMSE = 10.27
NMAE =10.79 %
k) K080807 (SCAPE-M)
N = 6
R² = 0.897
RMSE = 22.09
NMAE =35.04 %
l) K100518 (SCAPE-M)
N = 21
R² = 0.828
RMSE = 37.89
NMAE =71.34 %
Estimated Chl-a (mg m-3)
Measured Chl-a (mg m-3)

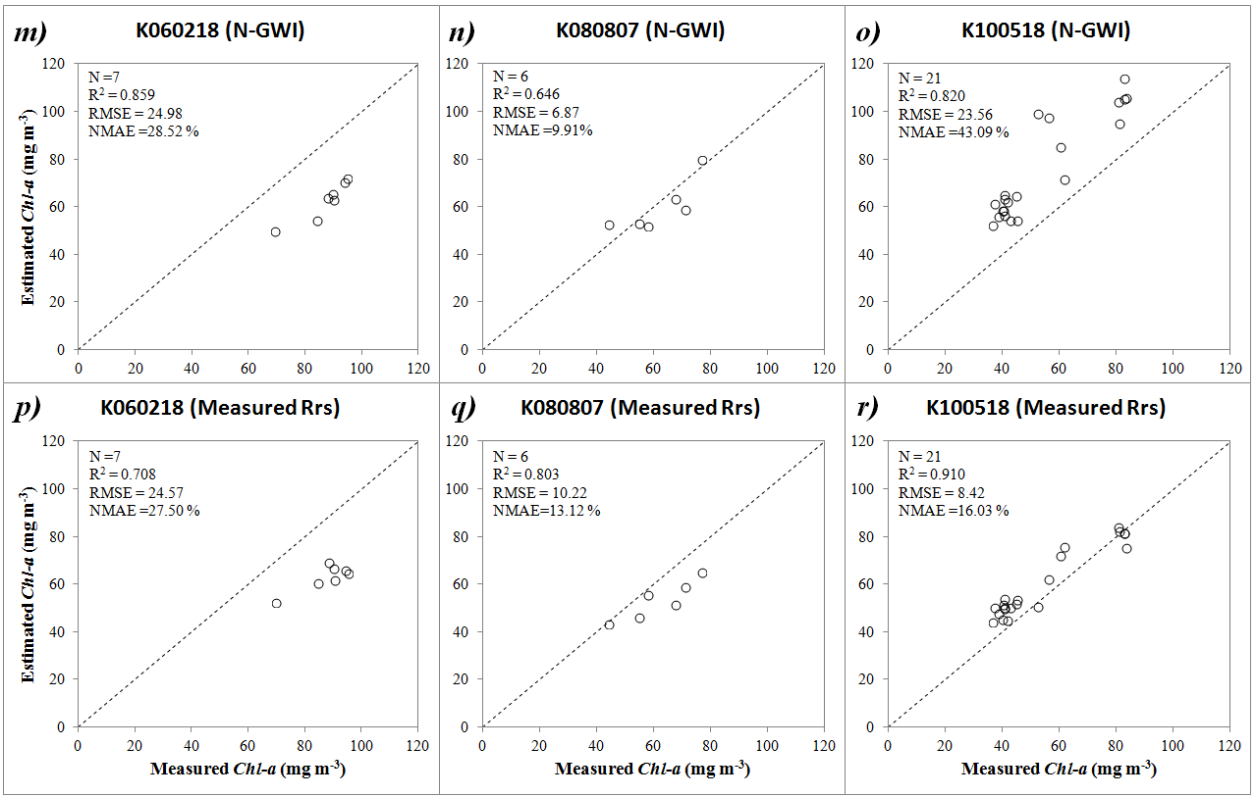

Figure 4.2. Comparisons between the *in situ*-measured and MERIS-derived chlorophyll-*a* concentration by four existing algorithms (GWI, MUMM, C2WP and SCAPE-M), the developed algorithm (N-GWI) and *in situ* measured $R_{rs}(\lambda)$ through SAMO-LUT model in Lake Kasumigaura, Japan. The black line represents the 1:1 line. Left column: February 18, 2006; middle: August 7, 2008; right: May 18, 2010.

However, the SCAPE-M could not catch the spatial variation of chlorophyll-*a* with very low determination coefficient (R^2=0.006). Although the N-GWI shows the poorer performance than the GWI, MUMM, and SCAPE-M, it shows the similar performance with using in situ-measured $R_{rs}(\lambda)$.

For the dataset of K080807, the chlorophyll-*a* retrieval by N-GWI achieved the highest accuracy (RMSE=6.87 mg m^{-3}) followed by MUMM, SCAPE-M, C2WP and GWI with RMSE of 18.10 mg m^{-3}, 22.09 mg m^{-3}, 41.96 mg m^{-3}, and 243.55 mg m^{-3}, respectively. For the dataset of K1005018, the N-GWI also achieved the highest accuracy (RMSE=23.56 mg m^{-3}), followed by the SCAPE-M, C2WP, GWI and MUMM with the RMSE of 37.89 mg m^{-3}, 41.42 mg m^{-3}, 77.05 mg m^{-3} and 268.35 mg m^{-3}, respectively. Overall, it can be considered that the N-GWI achieved its best performance for all three tested MERIS images compared to other atmospheric correction algorithms.

4.3.2 Validation using matchup NIES-dataset

In Figure 4.3, I compared the measured and estimated chlorophyll-*a* concentration using different dataset as in Figure 4.2. The measured chlorophyll-*a* concentration were obtained from NIES-dataset at four regular monitoring stations (i.e., Station 3, 7, 9 and 12), and the estimated chlorophyll-*a* concentration were obtained from corresponding atmospherically corrected matchup MERIS data and the SAMO-LUT.

At Stations 3, 7, and 12 (the first, second, and fourth row in Figure 4.3), the N-GWI achieved the best performance with the smallest RMSE (17.16-31.30 mg m^{-3}), NMAE (24.41%-34.04%), and the highest determination coefficients (0.533-0.603).

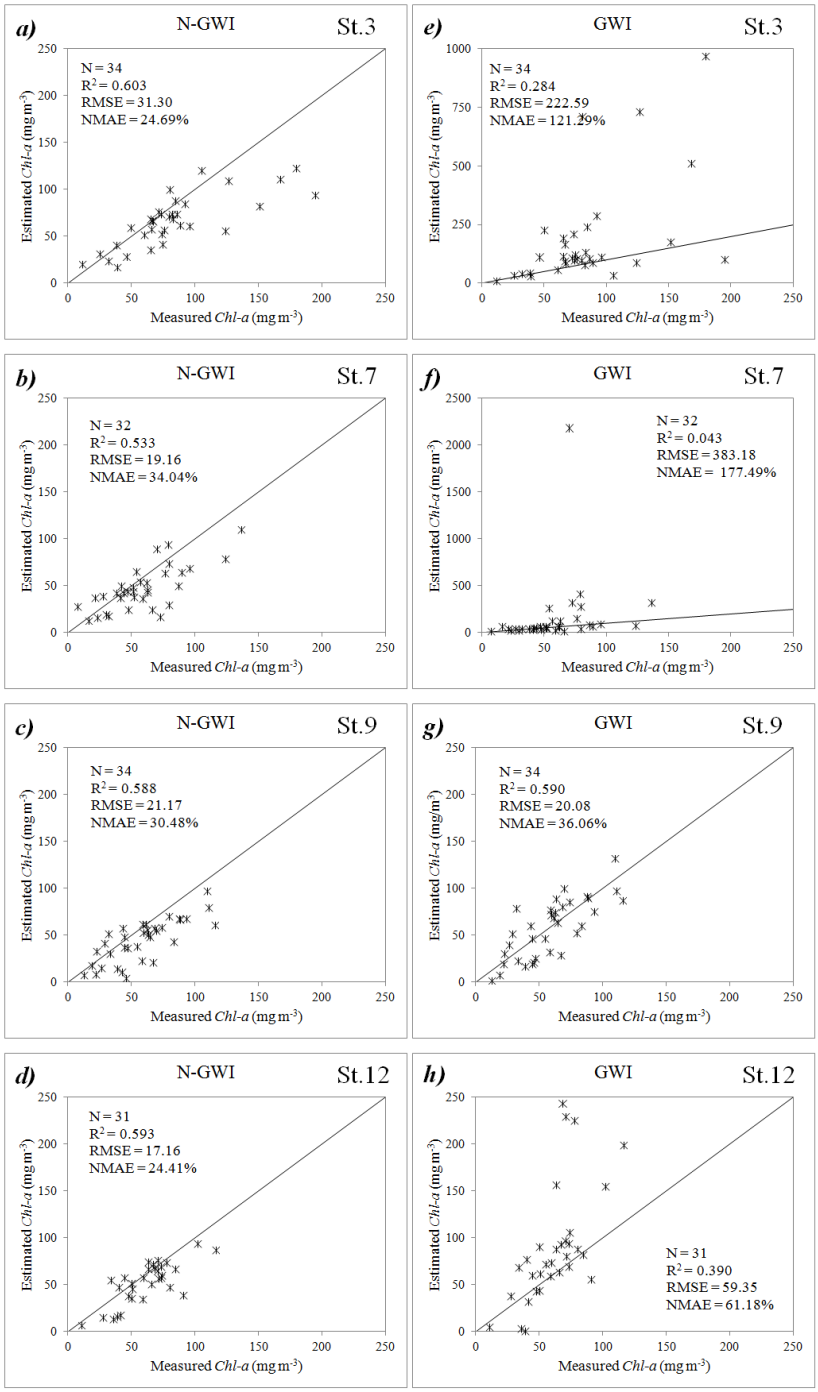
a)
N-GWI
St.3
N = 34
R² = 0.603
RMSE = 31.30
NMAE = 24.69%
e)
GWI
St.3
N = 34
R² = 0.284
RMSE = 222.59
NMAE = 121.29%
b)
N-GWI
St.7
N = 32
R² = 0.533
RMSE = 19.16
NMAE = 34.04%
f)
GWI
St.7
N = 32
R² = 0.043
RMSE = 383.18
NMAE = 177.49%
c)
N-GWI
St.9
N = 34
R² = 0.588
RMSE = 21.17
NMAE = 30.48%
g)
GWI
St.9
N = 34
R² = 0.590
RMSE = 20.08
NMAE = 36.06%
d)
N-GWI
St.12
N = 31
R² = 0.593
RMSE = 17.16
NMAE = 24.41%
h)
GWI
St.12
N = 31
R² = 0.390
RMSE = 59.35
NMAE = 61.18%
Estimated Chl-a (mg m-3)
Measured Chl-a (mg m-3)

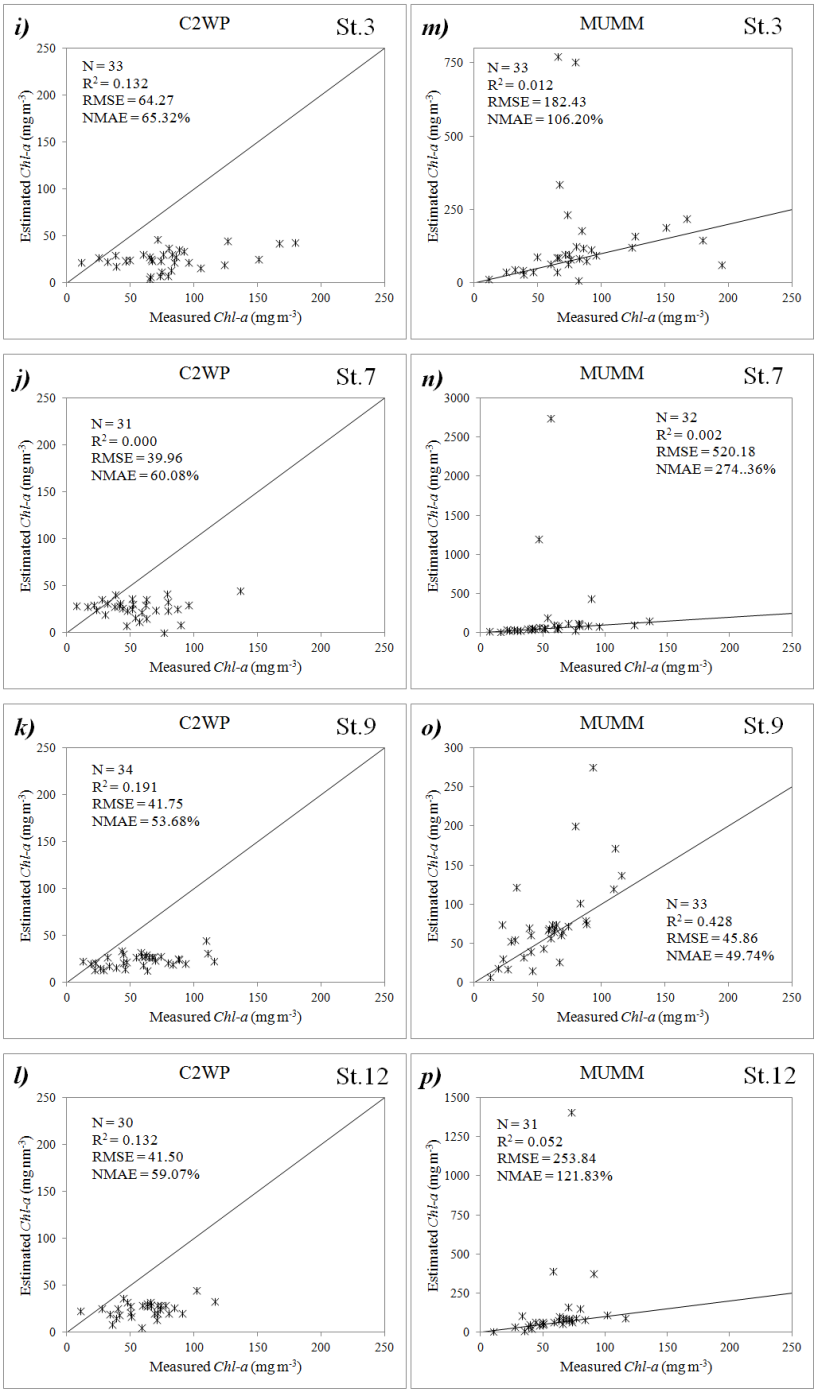

Figure 4.3. Comparisons between the *in situ*-measured and MERIS-derived chlorophyll-*a* concentration by three existing algorithms (GWI, MUMM and C2WP) and the developed algorithm (N-GWI) through SAMO-LUT model in Lake Kasumigaura, Japan. The black line represents the 1:1 line.

In contrast, the other three atmospheric correction algorithms (GWI, C2WP, and MUMM) showed poor performance for chlorophyll-*a* estimation, with the RMSE ranged from 39.96 to 520.18 mg m^{-3}, NMAE ranged from 59.07% to 274.36%, and determination coefficients ranged from 0.000 to 0.390.

At station 9 (center of the lake, the third row in Figure 4.3), the N-GWI algorithm yielded similar accuracy (RMSE of 21.17 mg m^{-3}, NMAE of 30.48%, R^2 of 0.588) with the GWI (RMSE of 20.08 mg m^{-3}, NMAE of 36.06%, R^2 of 0.590), but was superior to the C2WP (RMSE of 41.75 mg m^{-3}, NMAE of 53.68%, R^2 of 0.191) and the MUMM (RMSE of 45.86 mg m^{-3}, NMAE of 49.74%, R^2 of 0.428) for chlorophyll-*a* estimation. Overall, the N-GWI achieved the best performance for all four stations compared to other atmospheric correction algorithms.

4.3.2 Applicability of using MERIS data for long-term chlorophyll-a monitoring in Lake Kasumigaura

Figure 4.4 shows a comparison of the measured and estimated chlorophyll-*a* concentration for a long-term from 2003 to 2011. The measured chlorophyll-*a* concentrations were obtained from NIES-dataset, and the estimated chlorophyll-*a* concentrations were obtained from available MERIS data between 2003 and 2012. In total, I obtained 215 MERIS images; however, because some stations were covered by cloud and/or not covered by MERIS images (i.e., in the case of the Lake Kasumigaura was partly covered by one MERIS image), there are 179, 185, 190, and 176 available MERIS images for stations 3, 7, 9, and 12, respectively.

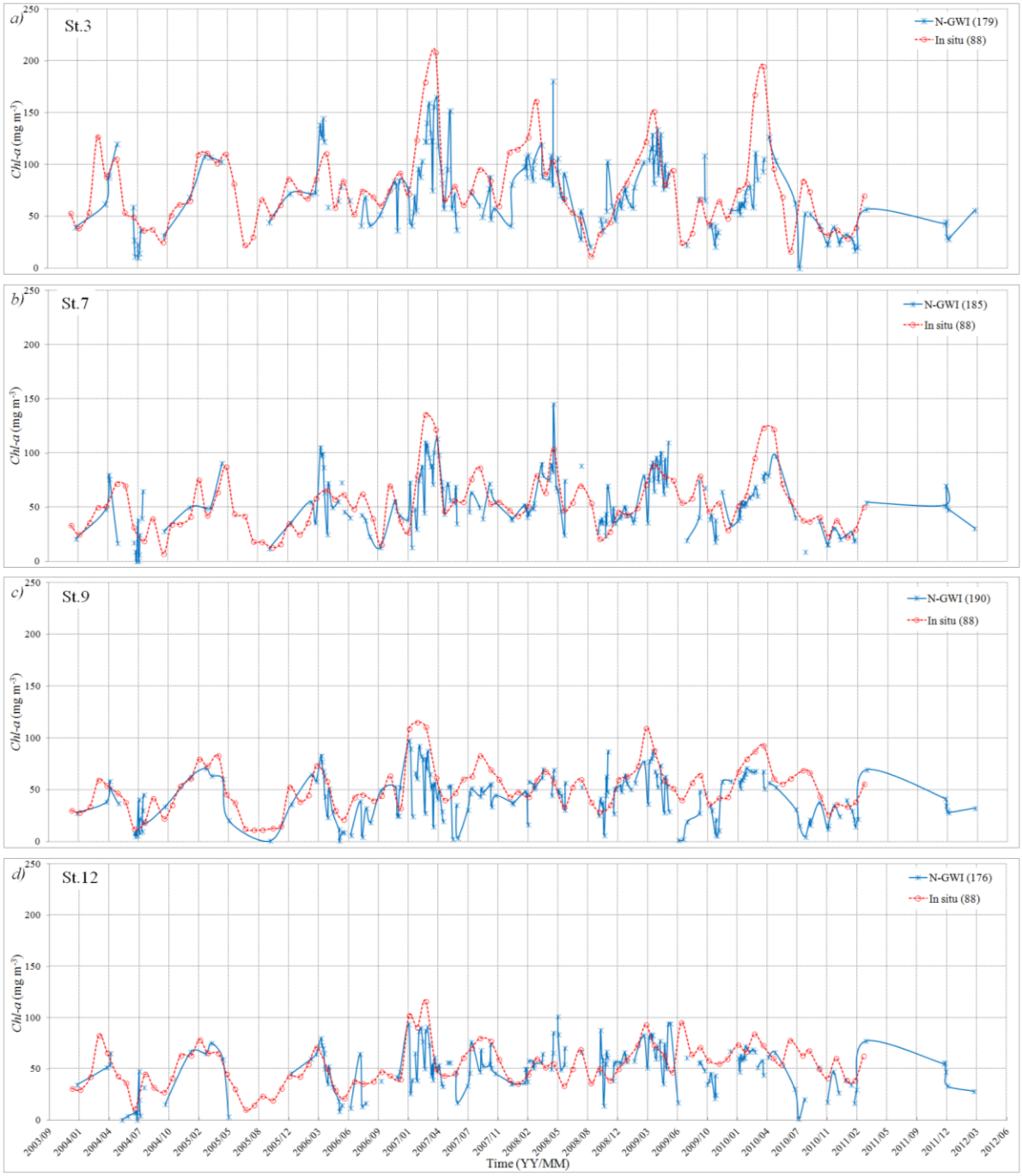

Figure 4.4. Temporal variation of *in situ*-measured and MERIS-derived chlorophyll-*a* concentration by N-GWI algorithm at St.3, St. 7, St.9 and St.12 in Lake Kasumigaura.

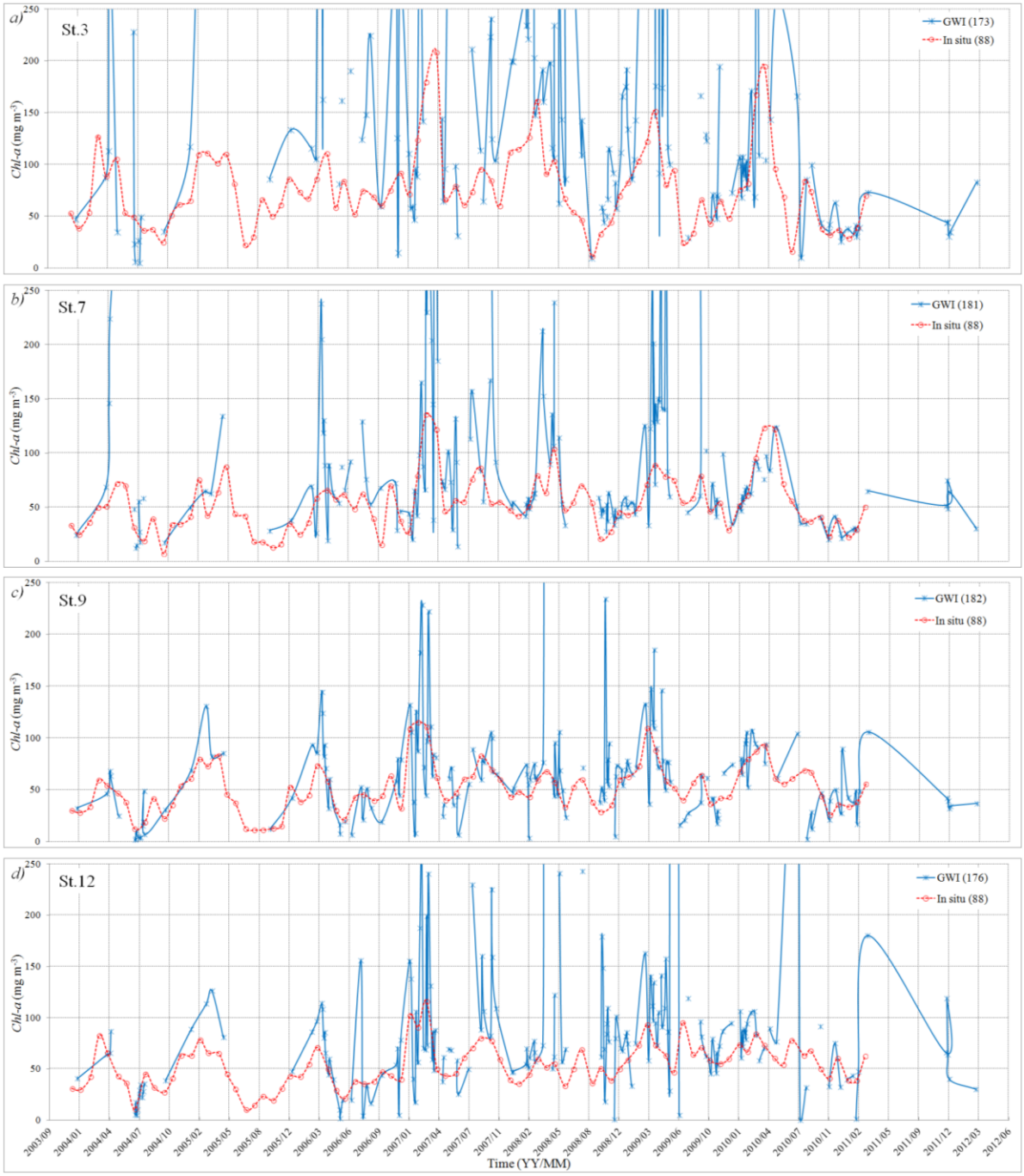

Figure 4.5. Temporal variation of *in situ*-measured and MERIS-derived chlorophyll-*a* concentration by GWI algorithm at St.3, St. 7, St.9 and St.12 in Lake Kasumigaura.

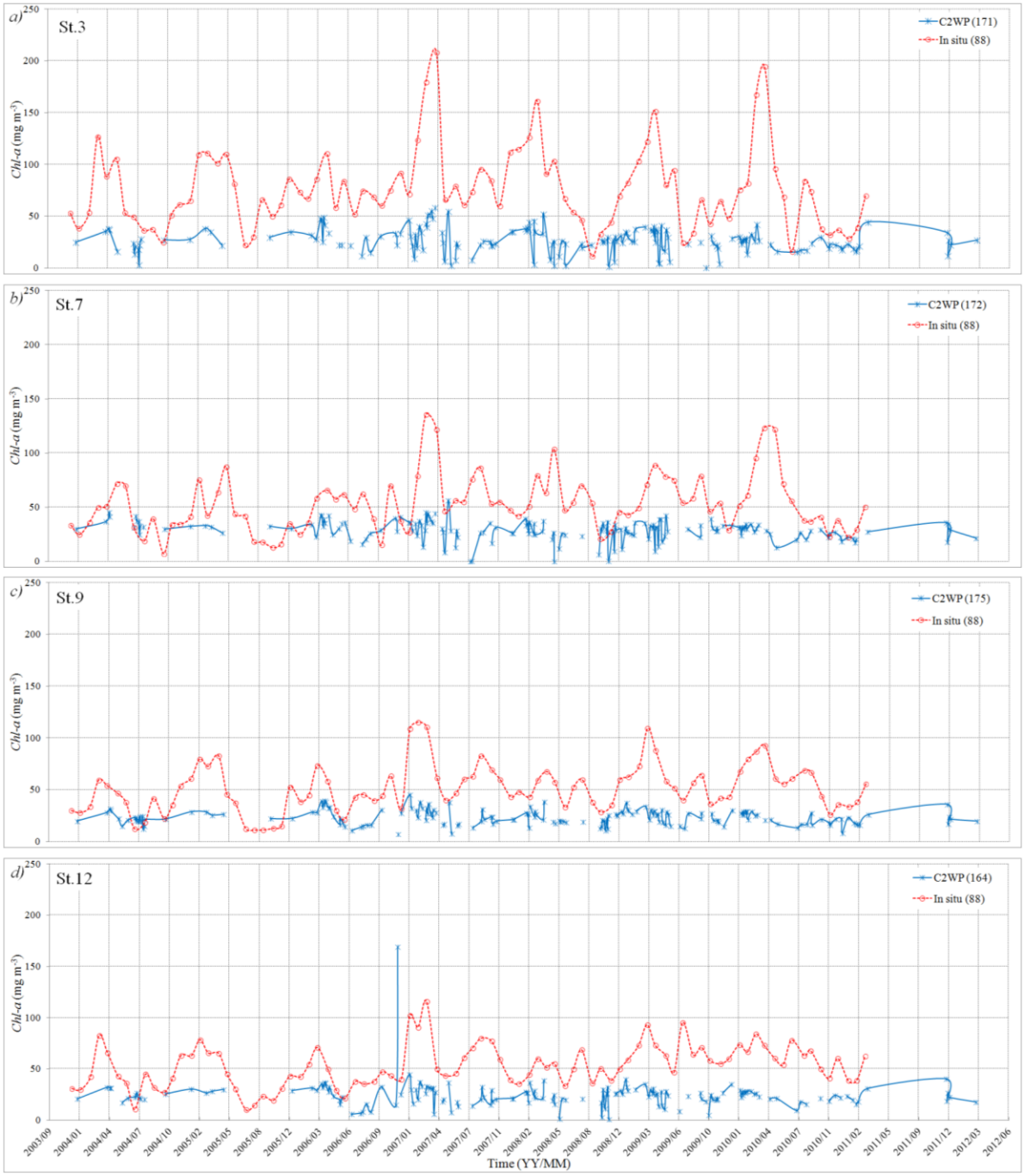

Figure 4.6. Temporal variation of *in situ*-measured and MERIS-derived chlorophyll-*a* concentration by C2WP algorithm at St.3, St. 7, St.9 and St.12 in Lake Kasumigaura.

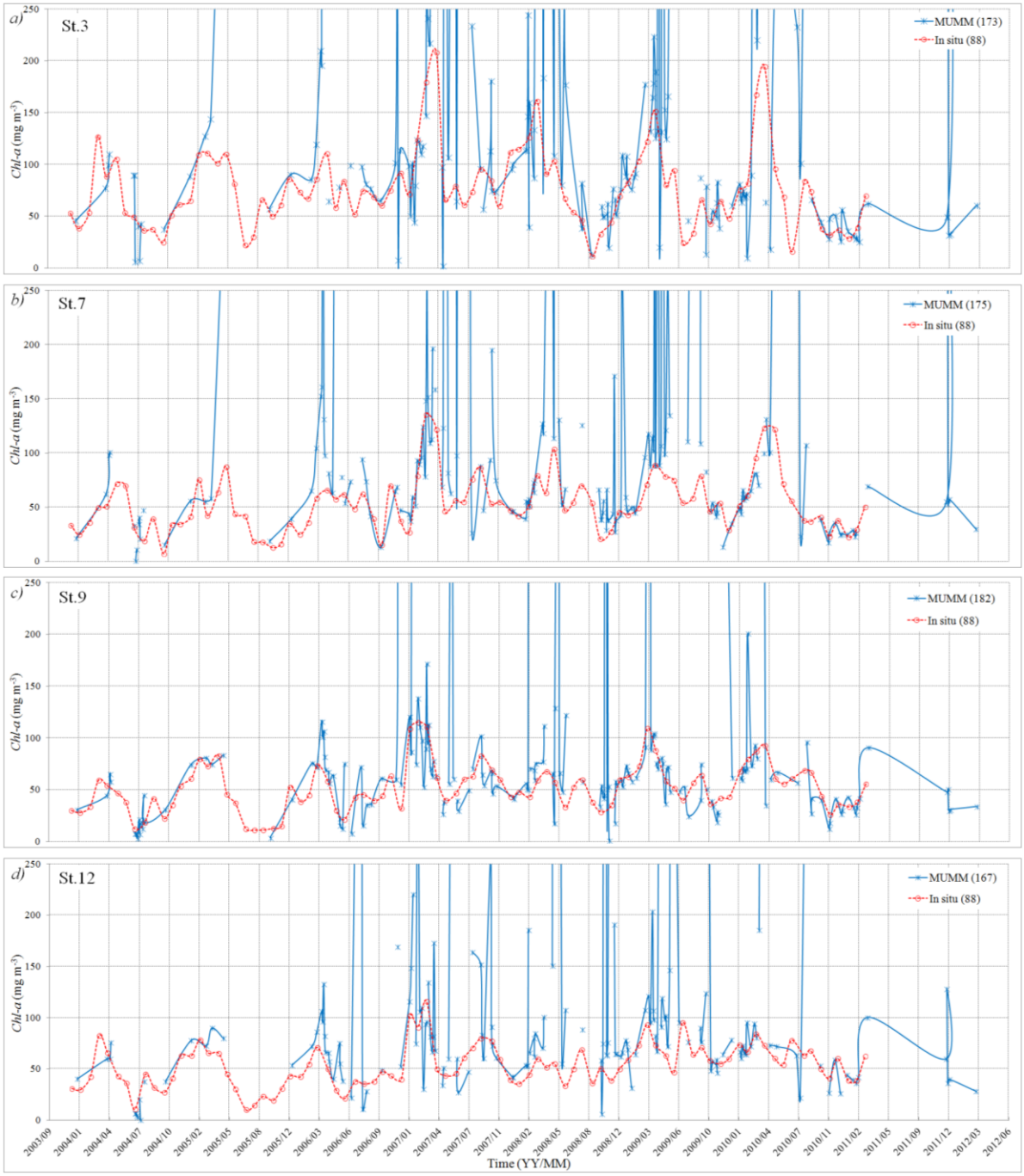

Figure 4.7. Temporal variation of *in situ*-measured and MERIS-derived chlorophyll-*a* concentration by MUMM algorithm at St.3, St. 7, St.9 and St.12 in Lake Kasumigaura.

In addition, since the GWI, C2WP, and MUMM algorithms could not process all pixels due to their assumptions, the GWI processed 173, 182, 182 and 176 data for Stations 3, 7, 9 and 12, respectively; the C2WP processed 171, 172, 175 and 164 data for Stations 3, 7, 9 and 12, respectively; the MUMM processed 173, 175, 182 and 167 data for Stations 3, 7, 9 and 12, respectively. It should note that some estimated chlorophyll-*a* by using atmospherically corrected $R_{rs}(\lambda)$ from the GWI and the MUMM algorithms were higher than 250 mg m^{-3}, those data were not showed in Figures 4.5 and 4.7.

From Figure 4.4, it can be seen that the estimated chlorophyll-*a* by using atmospherically corrected $R_{rs}(\lambda)$ from the N-GWI agreed well with measured chlorophyll-*a*. This result provides a strong case to show the potential for using satellite data instead of field measurements for water quality monitoring. In contrast, if other three atmospheric correction algorithms were used, the estimated chlorophyll-*a* would not agree with the measured ones in a lot of cases (Figures 4.5-4.7).

4.4 Discussion

Generally, the N-GWI algorithm is superior to other test atmospheric correction algorithms at all stations. At Station 9 (Figure 3.3(*g*)), the GWI algorithm also gave a similar accuracy with the N-GWI (RE=30.48%, RMSE=21.17 and R^2=0.588) (Figure 3.3(*c*)). This is probably because that the turbidity at Station 9 is less than those at other three stations. The Station 9 is located at the center of the Lake Kasumigaura, and thus is far away from banks and two dominant inflow rivers. This characteristic of location makes the water quality parameters around this station are less influenced by suspended

sediments carried by the inflow rivers. In addition, the water depth at the station 9 reached the maximum value (7.0 m) of the whole water body, and thus the possibility of re-suspended sediments by wind is low. The average suspended sediment (SS) at four stations are 29.6 g m^{-3}, 34.6 g m^{-3}, 23.7 g m^{-3} and 24.6 g m^{-3} for Stations 3, 7, 9 and 12, respectively.

Considering the validation methods used in this study, there are four possible error sources in the estimated chlorophyll-*a* concentration. The first error source is the accuracy of atmospheric correction algorithm itself. In this study, I fixed the aerosol model for all MERIS images. For longer wavelengths (longer than 620 nm), the error due to the use of fixed aerosol model should be acceptable (Jaelani et al., in submitting). If the actual aerosol data is available, accuracy of the N-GWI will be increased. In addition, the lacks of long-term *in situ* $R_{rs}(\lambda)$ make a direct comparison impossible, even though this comparison is an ideal way for validating atmospheric correction algorithm.

The second error source is come from chlorophyll-*a* retrieval algorithm (i.e., SAMO-LUT). The SAMO-LUT used *Cynobacteria*-dominated water to build its look up table (Yang et al. 2011). The accuracy of SAMO-LUT will slightly decrease when it was used to different phytoplankton's species (Yu et al. 2014). The underestimation both for the use of *in situ*-measured $R_{rs}(\lambda)$ and atmospherically corrected MERIS data of Feb. 18, 2006 by the N-GWI are probably because this reason. During the field survey on Feb. 18, 2006, the dominant phytoplankton species was diatom (*Bacillariophyceae,* Oyama et al. [2009]). In addition, several points with larger underestimation (measured chlorophyll-a larger than 125 mg m^{-3}) in Figure 3.3(*a*) were also dominant by diatom. If I excluded

these points, the RMSE and NMAE will be reduced from 31.30 mg m^{-3} to 15.97 mg m^{-3} and from 24.69% to 21.73%, respectively.

The third error source is from the measurement method of chlorophyll-*a*. The water samples by NIES were collected from 0.0 to 2.0 m depth in Lake Kasumigaura. The estimated chlorophyll-*a* from remote-sensing data generally represents the value from water surface to 0.5 m depth because the transparencies in Lake Kasumigaura are usually less than 1.0 m.

The last error source is the time different between *in situ* water sampling and MERIS acquisition. In the 39 matchup data from NIES dataset, 18%, 28%, 31% and 23% of data have 3, 2, 1, and 0 days different, respectively. These differences could make an error if there were water quality changes between *in situ* water sampling and image acquisition time.

4.5 Conclusions

In this study, I further validated the performance of the N-GWI algorithm by using an indirect comparison. Long-term MERIS images were processed by the N-GWI to produce atmospherically corrected $R_{rs}(\lambda)$, which are inputs of chlorophyll-*a* retrieval algorithm (SAMO-LUT). For my own dataset, the estimated chlorophyll-*a* by the use of N-GWI and SAMO-LUT produced acceptable accuracy with normalized mean absolute error (NMAE) in the range of 10 to 43%, root mean squared error (RMSE) in the range of 7 mg m^{-3} to 25 mg m^{-3} and determination coefficient (R^2) of 0.6 to 0.9. For the matchup data from NIES dataset, the estimated chlorophyll-*a* by the use of N-GWI and SAMO-

LUT also produced acceptable accuracy with the NMAE in the range of 24% to 34%, the RMSE in the range of 17 mg m^{-3} to 31 mg m^{-3} and R^2 of 0.5 to 0.6. The good agreements between long-term measured and estimated chlorophyll-*a* provided a strong case to show the potential for using satellite data instead of field measurements for water quality monitoring.

Chapter V General Conclusions

I evaluated four atmospheric correction algorithms using *in situ* water-leaving reflectance and concurrently acquired MERIS images collected from Lake Kasumigaura, Japan (turbid inland water). The validity of the assumptions in the four atmospheric correction algorithms was also investigated to understand both the advantages and limitations of each algorithm. The results show that all atmospheric correction algorithms evaluated have limitations in regard to Lake Kasumigaura, although the SCAPE-M and MUMM algorithms had acceptable accuracy for atmospheric correction in several cases (i.e. relative errors less than 30% for the 2006 and 2008 images). The performances of all four algorithms strongly depended on their assumptions (atmospheric status and/or turbidity of water body), and each algorithm failed when its assumptions became invalid (e.g. for the 2010 image, the relative errors ranged from 42% to 83%). These results indicate that further improvements are necessary to address the issue of atmospheric correction for turbid inland waters such as Lake Kasumigaura.

In order to overcome some limitations of existing atmospheric correction algorithm in Lake Kasumigaura, I developed a new atmospheric correction algorithm (N-GWI) which was designed to be applicable in inland turbid waters. N-GWI was based on the algorithm of GWI that implemented in SeaDAS with sufficient accuracy in less turbid waters. The limitation of GWI that cannot be used in very turbid waters have been overcome by (*1*) using a fixed aerosol model; (*2*) shifting the reference band from visible to NIR; and (*3*) generating a semi-analytical model for the estimation of spectral slope of

particle backscattering.

To validate the performance of N-GWI I did three validations, firstly I compared the atmospheric corrected $R_{rs}(\lambda)$ by the developed algorithms as well as four existing algorithms (GWI, SCAPE-M, MUMM and C2WP) with *in situ*-measured $R_{rs}(\lambda)$ collected in Lake Kasumigaura. The N-GWI achieved the best performance for data collected in K080807 (RMSE=0.001) and K100518 (RMSE=0.002), and similar performance with SCAPE-M in K060218 (RMSE=0.003). The second validation was performed by comparing atmospheric corrected reflectance of N-GWI and three existing algorithms (GWI, MUMM and C2WP) with *in situ*-measured $R_{rs}(\lambda)$ collected in Lake Dianchi. The N-GWI produced the best retrieval in D071024 (RMSE=0.002) and D090313 (RMSE=0.018) followed by GWI with RMSE of 0.003 and 0.019 respectively. The last validation was performed (same method with second validation) using remote-sensing data collected in four less turbid sea waters in America. Here, the N-GWI produced poor performance with NMAE ranged from 83% -1391%. Whereas, the existing algorithms (GWI and C2WP) produced better accuracy with NMAE ranged from 35%-645% and 31%-231% respectively. These data show the limitation of N-GWI in less turbid waters.

Further validation using long-term MERIS images and chlorophyll-*a* concentration was performed to evaluate the applicability of N-GWI. Long term MERIS images were processed by N-GWI to produce atmospheric corrected reflectance which was an input of SAMO-LUT model to estimate chlorophyll-*a* concentration. Two set of data were used to validate the MERIS-derived chlorophyll-*a* concentration, they were Lake Kasumigaura *in situ* dataset which was collected by the team of University of

Tsukuba (my own dataset) and Lake Kasumigaura database (NIES-dataset) which was collected and managed by CEBES-NIES, Japan. The match-up data of *in situ* measured chlorophyll-*a* and MERIS images were 34 and 39 for my own dataset and NIES-dataset, respectively. In my own dataset, the estimated chlorophyll-*a* by N-GWI produced acceptable accuracy with normalized mean absolute error (NMAE) in range of 10 to 43%, root mean squared error (RMSE) in range of 7 to 25 mg m^{-3} and determination coefficient (R^2) of 0.6 to 0.9. Whereas in NIES-dataset, the estimated chlorophyll-a by N-GWI produced acceptable accuracy with NMAE in range of 24% to 34%, RMSE in range of 17 to 31 mg m^{-3} and R^2 of 0.5 to 0.6. The good agreements between long-term measured and estimated chlorophyll-*a* provided a strong case to show the potential for using satellite data instead of field measurements for water quality monitoring.

There are three future studies that have to be carried out to improve the advantages of N-GWI algorithm. They are (*1*) implementing the N-GWI to other sensors by adjusting the parameters and equations based on the characteristic of those sensors (e.g., number of bands and wavelength availabilities); (*2*) making an algorithm for selecting the appropriate atmospheric correction algorithms in case of heterogeneous water turbidity; and (*3*) developing a new atmospheric correction for extremely turbid water (e.g., Lake Tonlesap in Cambodia) based on the N-GWI algorithm..

References

Aschbacher, Josef, and Maria Pilar Milagro-Pérez. 2012. “The European Earth Monitoring (GMES) Programme: Status and Perspectives.” *Remote Sensing of Environment* 120 (2012) (May): 3–8. doi:10.1016/j.rse.2011.08.028. http://linkinghub.elsevier.com/retrieve/pii/S0034425712000612.

Ayres, W., A. Busia, A. Dinar, R. Hirji, S. Lintner, A. McCalla, and R. Robelus. 1996. *Integrated Lake and Reservoir Management: World Bank Approach and Experience*. *Wordbank Technical Paper*. Vol. 358. World Bank Technical Paper. Washington, DC.

Bailey, Sean W, Bryan A Franz, and P Jeremy Werdell. 2010. “Estimation of near-Infrared Water-Leaving Reflectance for Satellite Ocean Color Data Processing.” *Optics Express* 18 (7) (March 29): 7521–7. doi:10.1364/OE.18.007521. http://www.ncbi.nlm.nih.gov/pubmed/20389774.

CEBES. 2011. “Lake Kasumigaura Database”. National Institute for Environmental Studies, Japan. http://db.cger.nies.go.jp/gem/moni-e/inter/GEMS/database/kasumi/contents/database/datalist.html.

Doerffer, R., and H. Schiller. 2007. “The MERIS Case 2 Water Algorithm.” *International Journal of Remote Sensing* 28 (3-4) (February): 517–535. doi:10.1080/01431160600821127. http://www.tandfonline.com/doi/abs/10.1080/01431160600821127.

———. 2008. “MERIS Regional Coastal and Lake Case 2 Water Project - Atmospheric Correction ATBD”. GKSS Research Center 21502 Geesthacht Version 1.0 18. May 2008.

Doron, Maéva, Simon Bélanger, David Doxaran, and Marcel Babin. 2011. “Spectral Variations in the near-Infrared Ocean Reflectance.” *Remote Sensing of Environment* 115 (7) (July): 1617–1631. doi:10.1016/j.rse.2011.01.015. http://linkinghub.elsevier.com/retrieve/pii/S0034425711000356.

Duan, Hongtao, Ronghua Ma, Stefan G. H. Simis, and Yuanzhi Zhang. 2012. “Validation of MERIS Case-2 Water Products in Lake Taihu, China.” *GIScience & Remote Sensing* 49 (6) (November 1): 873–894. doi:10.2747/1548-1603.49.6.873. http://bellwether.metapress.com/openurl.asp?genre=article&id=doi:10.2747/1548-1603.49.6.873.

Fukushima, Takehiko, Je-chul Park, Akio Imai, and Kazuo Matsushige. 1996. “Dissolved Organic Carbon in a Eutrophic Lake; Dynamics, Biodegradability and Origin.” *Aquatic Sciences* 58 (2): 139–157. doi:10.1007/BF00877112. http://link.springer.com/10.1007/BF00877112.

Gao, Li, Jianmin M. Zhou, Hao Yang, and Jie Chen. 2005. “Phosphorus Fractions in Sediment Profiles and Their Potential Contributions to Eutrophication in Dianchi Lake.” *Environmental Geology* 48 (7) (December 29): 835–844. doi:10.1007/s00254-005-0005-3. http://www.springerlink.com/index/10.1007/s00254-005-0005-3.

Giardino, Claudia, Monica Pepe, Pietro Alessandro Brivio, Paolo Ghezzi, and Eugenio Zilioli. 2001. “Detecting Chlorophyll, Secchi Disk Depth and Surface Temperature in a Sub-Alpine Lake Using Landsat Imagery.” *Science of The Total Environment* 268 (1-3) (March 14): 19–29. doi:10.1016/S0048-9697(00)00692-6. http://www.ncbi.nlm.nih.gov/pubmed/11315741.

Gitelson, Anatoly a, Bo-Cai Gao, Rong-Rong Li, Sergey Berdnikov, and Vladislav Saprygin. 2011. “Estimation of Chlorophyll-a Concentration in Productive Turbid Waters Using a Hyperspectral

Imager for the Coastal Ocean—the Azov Sea Case Study." *Environmental Research Letters* 6 (2) (April 1): 024023. doi:10.1088/1748-9326/6/2/024023. http://stacks.iop.org/1748-9326/6/i=2/a=024023?key=crossref.533b7023d5901ca90fe4a659f3f4334f.

Gitelson, Anatoly A. 1992. "The Peak near 700 Nm on Reflectance Spectra of Algae and Water: Relationships of Its Magnitude and Position with Chl. Concentration." *International Journal of Remote Sensing* 13 (17): 3367–3373.

Gitelson, Anatoly A., Giorgio Dall'Olmo, Wesley Moses, Donald C. Rundquist, Tadd Barrow, Thomas R. Fisher, Daniela Gurlin, and John Holz. 2008. "A Simple Semi-Analytical Model for Remote Estimation of Chlorophyll-a in Turbid Waters: Validation." *Remote Sensing of Environment* 112 (9) (September): 3582–3593. doi:10.1016/j.rse.2008.04.015. http://linkinghub.elsevier.com/retrieve/pii/S0034425708001569.

Gons, Herman J. 1999. "Optical Teledetection of Chlorophyll a in Turbid Inland Waters." *Environmental Science & Technology* 33 (7) (April): 1127–1132. doi:10.1021/es9809657. http://pubs.acs.org/doi/abs/10.1021/es9809657.

Gordon, Howard R., Otis B. Brown, Robert H Evans, James W Brown, Raymond C Smith, Karen S Baker, and Dennis K Clark. 1988. "A Semianalytic Radiance Model of Ocean Color." *Journal of Geophysical Research* 93 (D9): 10909. doi:10.1029/JD093iD09p10909. http://doi.wiley.com/10.1029/JD093iD09p10909.

Gordon, Howard R., and Menghua Wang. 1994. "Retrieval of Water-Leaving Radiance and Aerosol Optical Thickness over the Oceans with SeaWiFS: A Preliminary Algorithm." *Applied Optics* 33 (3) (January 20): 443–52. http://www.ncbi.nlm.nih.gov/pubmed/20862036.

Guanter, Luis, M. Del Carmen González- Sanpedro, and J. Moreno. 2007. "A Method for the Atmospheric Correction of ENVISAT/MERIS Data over Land Targets." *International Journal of Remote Sensing* 28 (3-4) (February): 709–728. doi:10.1080/01431160600815525. http://www.tandfonline.com/doi/abs/10.1080/01431160600815525.

Guanter, Luis, Antonio Ruiz-Verdú, Daniel Odermatt, Claudia Giardino, Stefan Simis, Víctor Estellés, Thomas Heege, Jose Antonio Domínguez-Gómez, and Jose Moreno. 2010. "Atmospheric Correction of ENVISAT/MERIS Data over Inland Waters: Validation for European Lakes." *Remote Sensing of Environment* 114 (3) (March 15): 467–480. doi:10.1016/j.rse.2009.10.004. http://linkinghub.elsevier.com/retrieve/pii/S0034425709003137.

Han, Luoheng, and Karen J. Jordan. 2005. "Estimating and Mapping Chlorophyll- a Concentration in Pensacola Bay, Florida Using Landsat ETM+ Data." *International Journal of Remote Sensing* 26 (23) (December 10): 5245–5254. doi:10.1080/01431160500219182. http://www.tandfonline.com/doi/abs/10.1080/01431160500219182.

Hu, Chuanmin, Kendall L Carder, and Frank E Muller-Karger. 2000. "Atmospheric Correction of SeaWiFS Imagery over Turbid Coastal Waters." *Remote Sensing of Environment* 74 (2) (November): 195–206. doi:10.1016/S0034-4257(00)00080-8. http://linkinghub.elsevier.com/retrieve/pii/S0034425700000808.

Huot, J.-P., H Tait, M Rast, S. Delwart, J.-L. Bézy, and G. Levrini. 2001. "The Optical Imaging Instruments and Their Applications: AATSR and MERIS." *ESA Bulletin* 106 (june): 56–66.

IOCCG. 2006. “Remote Sensing of Inherent Optical Properties: Fundamentals, Tests of Algorithms, and Applications. Lee, Z.-P. (ed.), Reports of the International Ocean-Colour Coordinating Group, No. 5”. Dartmouth, Canada.

———. 2010. “Atmospheric Correction for Remotely-Sensed Ocean-Colour Products. Wang, M. (ed.), Reports of the International Ocean-Colour Coordinating Group, No. 10”. Dartmouth, Canada.

Jaelani, Lalu Muhamad, Bunkei Matsushita, Wei Yang, and Takehiko Fukushima. 2013. “Evaluation of Four MERIS Atmospheric Correction Algorithms in Lake Kasumigaura, Japan.” *International Journal of Remote Sensing* 34 (24) (December 20): 8967–8985. doi:10.1080/01431161.2013.860660. http://dx.doi.org/10.1080/01431161.2013.860660.

Jamet, Cédric, Hubert Loisel, Christopher P. Kuchinke, Kevin Ruddick, Giuseppe Zibordi, and Hui Feng. 2011. “Comparison of Three SeaWiFS Atmospheric Correction Algorithms for Turbid Waters Using AERONET-OC Measurements.” *Remote Sensing of Environment* 115 (8) (August): 1955–1965. doi:10.1016/j.rse.2011.03.018. http://linkinghub.elsevier.com/retrieve/pii/S0034425711000952.

Kuchinke, C. P., Howard R. Gordon, and Bryan A. Franz. 2009. “Spectral Optimization for Constituent Retrieval in Case 2 Waters I: Implementation and Performance.” *Remote Sensing of Environment* 113 (3) (March): 571–587. doi:10.1016/j.rse.2008.11.001. http://linkinghub.elsevier.com/retrieve/pii/S0034425708003301.

Kuchinke, C.P., H.R. Gordon, L.W. Harding, and K.J. Voss. 2009. “Spectral Optimization for Constituent Retrieval in Case 2 Waters II: Validation Study in the Chesapeake Bay.” *Remote Sensing of Environment* 113 (3) (March): 610–621. doi:10.1016/j.rse.2008.11.002. http://linkinghub.elsevier.com/retrieve/pii/S0034425708003295.

Le, Chengfeng, Yunmei Li, Yong Zha, Deyong Sun, Changchun Huang, and Heng Lu. 2009. “A Four-Band Semi-Analytical Model for Estimating Chlorophyll a in Highly Turbid Lakes: The Case of Taihu Lake, China.” *Remote Sensing of Environment* 113 (6) (June 15): 1175–1182. doi:10.1016/j.rse.2009.02.005. http://linkinghub.elsevier.com/retrieve/pii/S0034425709000327.

Lee, ZhongPing, Kendall L Carder, and Robert a Arnone. 2002. “Deriving Inherent Optical Properties from Water Color: A Multiband Quasi-Analytical Algorithm for Optically Deep Waters.” *Applied Optics* 41 (27) (September 20): 5755–72. http://www.ncbi.nlm.nih.gov/pubmed/12269575.

Liu, Yansui, Md Anisul Islam, and Jay Gao. 2003. “Quantification of Shallow Water Quality Parameters by Means of Remote Sensing.” *Progress in Physical Geography* 27 (1) (March 1): 24–43. doi:10.1191/0309133303pp357ra. http://ppg.sagepub.com/cgi/doi/10.1191/0309133303pp357ra.

Matsushita, Bunkei, Wei Yang, Jin Chen, and Takehiko Fukushima. 2009. “Possibility of Improving Three-Band Model for Different Phytoplankton Species in Case II Water ：Evidences from Three Experiments.” *Journal of The Remote Sensing Society of Japan* 29 (5): 653–664.

Mobley, Curtis D. 1999. “Estimation of the Remote-Sensing Reflectance from above-Surface Measurements.” *Applied Optics* 38 (36) (December 20): 7442–55. http://www.opticsinfobase.org/abstract.cfm?URI=ao-38-36-7442.

Moses, W. J., A A Gitelson, S Berdnikov, and V Povazhnyy. 2009. "Estimation of Chlorophyll- a Concentration in Case II Waters Using MODIS and MERIS Data—successes and Challenges." *Environmental Research Letters* 4 (4) (October 15): 045005. doi:10.1088/1748-9326/4/4/045005. http://stacks.iop.org/1748-9326/4/i=4/a=045005?key=crossref.c3c6cfaf8da1186e3f3db4700ff27de0.

Mueller, J. M., and G. S. Fargion. 2002. *Ocean Optics Protocols for Satellite Ocean Color Sensor Validation. Revision 3, Part I & II,NASA Tech. Memo. 2002–210004*. Vol. 1. Greenbelt, Maryland: NASA Goddard Space Flight Center.

O'Reilly, John E., Stéphane Maritorena, B. Greg Mitchell, David A. Siegel, Kendall L. Carder, Sara A. Garver, Mati Kahru, and Charles McClain. 1998. "Ocean Color Chlorophyll Algorithms for SeaWiFS." *Journal of Geophysical Research* 103 (C11): 24937. doi:10.1029/98JC02160. http://doi.wiley.com/10.1029/98JC02160.

Oyama, Youichi, Bunkei Matsushita, Takehiko Fukushima, Kazuo Matsushige, and Akio Imai. 2009. "Application of Spectral Decomposition Algorithm for Mapping Water Quality in a Turbid Lake (Lake Kasumigaura, Japan) from Landsat TM Data." *ISPRS Journal of Photogrammetry and Remote Sensing* 64 (1) (January): 73–85. doi:10.1016/j.isprsjprs.2008.04.005. http://linkinghub.elsevier.com/retrieve/pii/S0924271608000592.

Ramon, D., and R. Santer. 2005. "Aerosol over Land with MERIS, Present and Future." In *Proceeding of the MERIS and AATSR Workshop 2005, ESA SP-597, 26–30 September 2005, ESRIN, Frascati, Italy*.

Ruddick, Kevin George, Vera De Cauwer, Young-Je Park, and Gerald Moore. 2006. "Seaborne Measurements of near Infrared Water-Leaving Reflectance: The Similarity Spectrum for Turbid Waters." *Limnology and Oceanography* 51 (2): 1167–1179. doi:10.4319/lo.2006.51.2.1167. http://www.aslo.org/lo/toc/vol_51/issue_2/1167.html.

Ruddick, Kevin George, Fabrice Ovidio, and Machteld Rijkeboer. 2000. "Atmospheric Correction of SeaWiFS Imagery for Turbid Coastal and Inland Waters." *Applied Optics* 39 (6) (February 20): 897–912. http://www.opticsinfobase.org/abstract.cfm?URI=ao-39-6-897.

Santer, R, V Carrere, P Dubuisson, and J C Roger. 1999. "Atmospheric Correction over Land for MERIS." *International Journal of Remote Sensing* 20 (9) (January): 1819–1840. doi:10.1080/014311699212506. http://www.tandfonline.com/doi/abs/10.1080/014311699212506.

Santer, R., J. Vidot, and O. Aznay. 2005. "Standard Aerosol Model Families Used for Atmospheric Correction: How Comparable Are They? How Valid Are They?" In *Proceeding of the MERIS and AATSRWorkshop 2005, ESA SP-597, 26–30 September 2005, ESRIN, Frascati, Italy*, edited by H. Lacoste. Frascati, Italy: European Space Agency. http://adsabs.harvard.edu/cgi-bin/nph-data_query?bibcode=2005ESASP.597E..56S&link_type=GIF.

Sathyendranath, S., L. Prieur, and A. Morel. 1987. "An Evaluation of the Problems of Chlorophyll Retrieval from Ocean Colour, for Case 2 Waters." *Advances in Space Research* 7 (2) (January): 27–30. doi:10.1016/0273-1177(87)90160-8. http://linkinghub.elsevier.com/retrieve/pii/0273117787901608.

Schroeder, T.H., I. Behnert, M. Schaale, J. Fischer, and R. Doerffer. 2007. "Atmospheric Correction Algorithm for MERIS above case- 2 Waters." *International Journal of Remote Sensing* 28 (7) (April): 1469–1486. doi:10.1080/01431160600962574. http://www.tandfonline.com/doi/abs/10.1080/01431160600962574.

Schroeder, T.H., M. Schaale, and J. Fischer. 2007. “Retrieval of Atmospheric and Oceanic Properties from MERIS Measurements: A New Case- 2 Water Processor for BEAM.” *International Journal of Remote Sensing* 28 (24) (December 20): 5627–5632. doi:10.1080/01431160701601774. http://www.tandfonline.com/doi/abs/10.1080/01431160701601774.

SCOR-UNESCO. 1966. *Determination of Photosynthetic Pigment in Seawater, Monographs on Oceanographic Methodology*. Paris: SCOR-UNESCO. http://unesdoc.unesco.org/images/0007/000716/071612eo.pdf.

Selby, J. E. A., F. X. Kneizys, Jr. J.H. Chetwynd, and R. A. McClatchey. 1978. “Atmospheric Transmittance / Radiance ：Computer Code LOWTRAN 4. AFGL-TR-78-0053.” *Air Force Geophysics Laboratory*. Hanscom AFB, MA.

Shi, Wei, and Menghua Wang. 2007. “Detection of Turbid Waters and Absorbing Aerosols for the MODIS Ocean Color Data Processing.” *Remote Sensing of Environment* 110 (2) (September): 149–161. doi:10.1016/j.rse.2007.02.013. http://linkinghub.elsevier.com/retrieve/pii/S0034425707000880.

———. 2009. “An Assessment of the Black Ocean Pixel Assumption for MODIS SWIR Bands.” *Remote Sensing of Environment* 113 (8) (August): 1587–1597. doi:10.1016/j.rse.2009.03.011. http://linkinghub.elsevier.com/retrieve/pii/S0034425709000911.

Siegel, D. A, M Wang, S Maritorena, and W Robinson. 2000. “Atmospheric Correction of Satellite Ocean Color Imagery: The Black Pixel Assumption.” *Applied Optics* 39 (21) (July 20): 3582–91. http://www.ncbi.nlm.nih.gov/pubmed/18349929.

Stumpf, R. P., R. A. Arnone, R. W. Gould, P.M. Martinolich, and V. Ransibrahmanakul. 2003. “A Partially Coupled Ocean-Atmosphere Model for Retrieval of Water-Leaving Radiance from SeaWiFS in Coastal Waters. NASA Technical Memorandum 2003-206892(22).” *Nasa Technical Memorandum*. Vol. 22. Greenbelt, Maryland.

Wang, Menghua, and Wei Shi. 2007. “The NIR-SWIR Combined Atmospheric Correction Approach for MODIS Ocean Color Data Processing.” *Optics Express* 15 (24): 15722. doi:10.1364/OE.15.015722. http://www.opticsinfobase.org/abstract.cfm?URI=oe-15-24-15722.

Wang, Menghua, Wei Shi, and Lide Jiang. 2012. “Atmospheric Correction Using near-Infrared Bands for Satellite Ocean Color Data Processing in the Turbid Western Pacific Region.” *Optics Express* 20 (2) (January 16): 741–53. doi:10.1364/OE.20.000741. http://www.opticsinfobase.org/abstract.cfm?URI=oe-20-2-741.

Wang, Menghua, Wei Shi, and Junwu Tang. 2011. “Water Property Monitoring and Assessment for China’s Inland Lake Taihu from MODIS-Aqua Measurements.” *Remote Sensing of Environment* 115 (3) (March): 841–854. doi:10.1016/j.rse.2010.11.012. http://linkinghub.elsevier.com/retrieve/pii/S0034425710003317.

Wang, Menghua, SeungHyun Son, and Wei Shi. 2009. “Evaluation of MODIS SWIR and NIR-SWIR Atmospheric Correction Algorithms Using SeaBASS Data.” *Remote Sensing of Environment* 113 (3) (March): 635–644. doi:10.1016/j.rse.2008.11.005. http://linkinghub.elsevier.com/retrieve/pii/S0034425708003349.

Werdell, P Jeremy, and Sean W Bailey. 2002. *The SeaWiFS Bio-Optical Archive and Storage System (SeaBASS): Current Architecture and Implementation*. Edited by Giulietta S. Fargion and Charles R. McClain. Greenbelt, Maryland: Goddard Space Flight Center.

Werdell, P. Jeremy, Sean Bailey, Giulietta Fargion, Christophe Pietras, Kirk Knobelspiesse, Gene Feldman, and Charles McClain. 2003. "Unique Data Repository Facilitates Ocean Color Satellite Validation." *Eos, Transactions American Geophysical Union* 84 (38): 377. doi:10.1029/2003EO380001. http://www.agu.org/pubs/crossref/2003/2003EO380001.shtml.

Werdell, P. Jeremy, and Sean W. Bailey. 2005. "An Improved in-Situ Bio-Optical Data Set for Ocean Color Algorithm Development and Satellite Data Product Validation." *Remote Sensing of Environment* 98 (1) (September): 122–140. doi:10.1016/j.rse.2005.07.001. http://linkinghub.elsevier.com/retrieve/pii/S0034425705002208.

Yang, Wei, Bunkei Matsushita, Jin Chen, and Takehiko Fukushima. 2011. "Estimating Constituent Concentrations in Case II Waters from MERIS Satellite Data by Semi-Analytical Model Optimizing and Look-up Tables." *Remote Sensing of Environment* 115 (5) (May 15): 1247–1259. doi:10.1016/j.rse.2011.01.007. http://linkinghub.elsevier.com/retrieve/pii/S0034425711000204.

Yang, Wei, Bunkei Matsushita, Jin Chen, Takehiko Fukushima, and Ronghua Ma. 2010. "An Enhanced Three-Band Index for Estimating Chlorophyll-a in Turbid Case-II Waters: Case Studies of Lake Kasumigaura, Japan, and Lake Dianchi, China." *IEEE Geoscience and Remote Sensing Letters* 7 (4) (October): 655–659. doi:10.1109/LGRS.2010.2044364. http://ieeexplore.ieee.org/lpdocs/epic03/wrapper.htm?arnumber=5446366.

Yang, Wei, Bunkei Matsushita, Jin Chen, Kazuya Yoshimura, and Takehiko Fukushima. 2013. "Retrieval of Inherent Optical Properties for Turbid Inland Waters From Remote-Sensing Reflectance." *IEEE Transactions on Geoscience and Remote Sensing* 51 (6) (June): 3761–3773. doi:10.1109/TGRS.2012.2220147. http://ieeexplore.ieee.org/lpdocs/epic03/wrapper.htm?arnumber=6392257.

Yoshimura, Kazuya, Nobuhiro Zaitsu, Yuta Sekimura, Bunkei Matsushita, Takehiko Fukushima, and Akio Imai. 2012. "Parameterization of Chlorophyll a-Specific Absorption Coefficients and Effects of Their Variations in a Highly Eutrophic Lake: A Case Study at Lake Kasumigaura, Japan." *Hydrobiologia* 691 (1) (March 27): 157–169. doi:10.1007/s10750-012-1066-4. http://cat.inist.fr/?aModele=afficheN&cpsidt=25829054.

Yu, Gongliang, Wei Yang, Bunkei Matsushita, Renhui Li, Yoichi Oyama, and Takehiko Fukushima. 2014. "Remote Estimation of Chlorophyll-a in Inland Waters by a NIR-Red-Based Algorithm: Validation in Asian Lakes." *Remote Sensing* 6 (4) (April 22): 3492–3510. doi:10.3390/rs6043492. http://www.mdpi.com/2072-4292/6/4/3492/.